



Publicly Accessible Penn Dissertations


Summer 8-12-2011

An an Vitro and in Silico Investigation of the Role of Nmda Receptor Subtypes Following Mechanical injury

Pallab Singh

University of Pennsylvania, psingh@seas.upenn.edu

Follow this and additional works at: <http://repository.upenn.edu/edissertations>

 Part of the [Biomedical Engineering and Bioengineering Commons](#), [Computational Neuroscience Commons](#), and the [Molecular and Cellular Neuroscience Commons](#)

Recommended Citation

Singh, Pallab, "An an Vitro and in Silico Investigation of the Role of Nmda Receptor Subtypes Following Mechanical injury" (2011). *Publicly Accessible Penn Dissertations*. 374.
<http://repository.upenn.edu/edissertations/374>

This paper is posted at Scholarly Commons. <http://repository.upenn.edu/edissertations/374>
For more information, please contact libraryrepository@pobox.upenn.edu.

An an Vitro and in Silico Investigation of the Role of Nmda Receptor Subtypes Following Mechanical injury

Abstract

The N-methyl D-aspartate receptor (NMDAR), a common glutamate receptor found throughout the brain, has long been implicated as the major mediator of the pathology seen after traumatic brain injury (TBI). However, given their critical role in physiologic function of neural networks, complete inhibition of these receptors is an unsuitable therapeutic strategy. Thus, further investigation into how these receptors respond to injury is required to identify more directed therapeutic targets. Here, we aimed to use two unique experimental models to further investigate the role of NMDARs in the neuronal response to TBI, with specific emphasis on the contribution of different NMDAR subtypes. TBI produces a unique disease paradigm containing mechanical and biochemical components, which can both affect NMDAR activity. We sought to isolate the effects of both these components and then to examine how they combine to create a unique injury response.

We utilized a recombinant system expressing known NMDAR subtypes to first examine the action of mechanical stretch on specific subtypes. We demonstrated that mechanosensitivity of the NMDAR is indeed dependent on its subunit composition, with the NR2B subunit conferring stretch sensitivity. Further, we were able to investigate the regulation of NR2B mechanosensitivity and found that a single PKC phosphorylation site on the NR2B C-terminal tail can critically control stretch sensitivity.

We next developed a computational model of a single dendritic spine to evaluate the patterns of activation among NMDAR subtypes in both physiologic and pathologic glutamatergic signaling. We demonstrate that the presence of multiple NMDAR subtypes on the dendritic spine enables the ability for a single synapse to produce unique responses to different glutamate inputs. Importantly, we discovered that injury induced release of synaptic glutamate vesicles results in enhanced contribution of NR2B containing receptors. Finally, we have shown that the collective effects of TBI can drastically enhance the calcium influx from synaptic and extrasynaptic NR1/NR2B-NMDARs, an NMDAR subtype known to mediate pro-death signaling. Together, our data demonstrates that the NR2B subunit represents a unique pathologic sensor for TBI, and could represent an intriguing target of manipulation in the development of improved TBI therapeutics.

Degree Type

Dissertation

Degree Name

Doctor of Philosophy (PhD)

Graduate Group

Bioengineering

First Advisor

Dr. David F. Meaney

Keywords

NMDA receptor, traumatic brain injury, computational model, NR2B

Subject Categories

Biomedical Engineering and Bioengineering | Computational Neuroscience | Molecular and Cellular Neuroscience

**AN *IN VITRO* AND *IN SILICO* INVESTIGATION OF THE ROLE OF NMDA
RECEPTOR SUBTYPES FOLLOWING MECHANICAL INJURY**

Pallab Singh

A DISSERTATION

in

Bioengineering

Presented to the Faculties of the University of Pennsylvania

in

Partial Fulfillment of the Requirements for the

Degree of Doctor of Philosophy

2011

David F. Meaney, PhD
Solomon R. Pollack Professor and Chair, Dept. of Bioengineering
Supervisor of Dissertation

Beth A. Winkelstein PhD
Professor, Dept. of Bioengineering
Graduate Group Chairperson

Dissertation Committee

Ravi Radhakrishnan, PhD, Associate Professor, Dept. of Bioengineering
David Lynch, MD, PhD, Professor, Dept. of Neurology, School of Medicine
Beth Winkelstein, PhD, Professor, Dept. of Bioengineering

AN *IN VITRO* AND *IN SILICO* INVESTIGATION OF THE ROLE OF NMDA
RECEPTOR SUBTYPES FOLLOWING MECHANICAL INJURY

COPYRIGHT

PALLAB SINGH

2011

ACKNOWLEDGEMENTS

There are many people who have been absolutely instrumental in this work and in my growth as both a scientist and as a person in my years at Penn. I'd first like to thank my thesis advisor, Dr. Dave Meaney, for all of his support and advice. Dave has taught me much over the years, on how to ask and answer the right questions, and importantly has worked with me to define what my strengths are as a scientist. Also, I thank my committee members, Dr. Ravi Radhakrishnan, Dr. Beth Winkelstein, and Dr. Dave Lynch for their contributions and advice. Further, a special thank you is needed for Dave Lynch and his lab for their help in our use of NMDAR plasmids in this work.

I would like to thank all the past and present members of the Meaney Lab including, Dr. Mike DeRidder, Dr. Bill Miller, Dr. Donna Geddes-Klein, Dr. Anthony Choo, Dr. Rosie Mott, Dr. Katie von Reyn, Dr. Jennifer Singh, Mahlet Mesfin, Yung Chia Chen, Tapan Patel, Steve Bernstein, Vineet Tiruvadi, Kim Schiffman, David Scarsella, Adam Hockenberry, Phil Nibley, Emory Kuo, Brittainy Wierzbicki, Kelly McManus, and Linda Le for all of their help, support, advice, and shared knowledge. As importantly, I thank them all for being good friends, which is essential in making a good lab environment. I'd also like to thank members of the Margulies Lab, Dr. Brittany Coats, Dr. Nicole Ibrahim, Dr. Stephanie Eucker, Dr. Taylor Cohen, Dr. Brian DiPaolo, Jill Ralston, and Gladys Gray Lawrence for their friendship, support, and necessary distractions.

As most people who know me realize, my friends are one the most important things in my life, and I have been blessed with a group of friends that have been loyal supporters and cheerleaders for me. Friends I will never forget: Nathan Clark, Nithin

Raikar, Jehu Mathew, DJ Mishel, Bill Palin, David Scarsella, Adam Hockenberry, Katie von Reyn, Nicole Ibrahim, Joe Foderaro, Danny Miller, Scott Mencer, Richard Capparell, and Mike Klein.

To my parents, I owe absolutely everything that I am. They are an absolute inspiration on how to take calculated risks and how to work for what you believe in. I thank them for giving me a passion for science and for their unyielding support over the years. Also, a sincere thank you to John, Martha, and Laura Spaethling for their support and for quickly adopting me into their family.

Finally, to my wife, Dr. Jennifer Singh, thank you. You are my best friend, my companion, and my calming influence. Words cannot express how lucky I am to have found you, and you are without a doubt my most important discovery in graduate school. I thank you for being a fantastic lab mate, friend, and wife. You have taught me how to be a better scientist and your presence makes me a better person. We have gotten through graduate school side by side, and I am eager to move on to experience the rest of my life with you next to me.

ABSTRACT

AN *IN VITRO* AND *IN SILICO* INVESTIGATION OF THE ROLE OF NMDAR SUBTYPES FOLLOWING MECHANICAL INJURY

Pallab Singh

David F. Meaney

The N-methyl D-aspartate receptor (NMDAR), a common glutamate receptor found throughout the brain, has long been implicated as the major mediator of the pathology seen after traumatic brain injury (TBI). However, given their critical role in physiologic function of neural networks, complete inhibition of these receptors is an unsuitable therapeutic strategy. Thus, further investigation into how these receptors respond to injury is required to identify more directed therapeutic targets. Here, we aimed to use two unique experimental models to further investigate the role of NMDARs in the neuronal response to TBI, with specific emphasis on the contribution of different NMDAR subtypes. TBI produces a unique disease paradigm containing mechanical and biochemical components, which can both affect NMDAR activity. We sought to isolate the effects of both these components and then to examine how they combine to create a unique injury response.

We utilized a recombinant system expressing known NMDAR subtypes to first examine the action of mechanical stretch on specific subtypes. We demonstrated that mechanosensitivity of the NMDAR is indeed dependent on its subunit composition, with

the NR2B subunit conferring stretch sensitivity. Further, we were able to investigate the regulation of NR2B mechanosensitivity and found that a single PKC phosphorylation site on the NR2B C-terminal tail can critically control stretch sensitivity.

We next developed a computational model of a single dendritic spine to evaluate the patterns of activation among NMDAR subtypes in both physiologic and pathologic glutamatergic signaling. We demonstrate that the presence of multiple NMDAR subtypes on the dendritic spine enables the ability for a single synapse to produce unique responses to different glutamate inputs. Importantly, we discovered that injury induced release of synaptic glutamate vesicles results in enhanced contribution of NR2B containing receptors. Finally, we have shown that the collective effects of TBI can drastically enhance the calcium influx from synaptic and extrasynaptic NR1/NR2B-NMDARs, an NMDAR subtype known to mediate pro-death signaling. Together, our data demonstrates that the NR2B subunit represents a unique pathologic sensor for TBI, and could represent an intriguing target of manipulation in the development of improved TBI therapeutics.

Table of Contents

Abstract.....	iv
Table of Contents	vi
List of Figures.....	viii
List of Tables	ix
<i>Chapter 1: Background and Significance</i>	1
INTRODUCTION.....	1
TBI	2
NMDARS	3
SUMMARY OF CHAPTERS	5
<i>Chapter 2: NMDA receptor mechanosensitivity is governed by the C-terminus of the NR2B subunit</i>	12
ABSTRACT.....	12
INTRODUCTION.....	13
METHODS	16
Cell Culture	16
Plasmids	17
Transfection.....	17
<i>In vitro</i> stretch injury.....	18
Data analysis.....	19
RESULTS	20
Subunit composition of the NMDAR influences mechanosensitivity.....	20
NR2B C-terminal tail confers mechanosensitivity.....	27
Regulation of NR2B mechanosensitivity by PKC phosphorylation site on NR2B.....	29
DISCUSSION	32
Models used to evaluate NMDAR mechanosensitivity	32
NR2B mechanosensitivity regulated by intracellular C-terminal tail	34
PKC regulation of NMDAR mechanosensitivity	37
Implications of selective NR2B mechanosensitivity.....	39
<i>Chapter 3: Stochastic model of NMDA receptor subtype activation during physiologic glutamatergic neurotransmission</i>	41
ABSTRACT.....	41
INTRODUCTION.....	42
METHODS	45
Geometry and receptor content.....	45
Glutamate release.....	46
Glutamate receptor state modeling	47
Model parameters	48
Analysis	48
Calcium entry	49

RESULTS	54
Sensitivity to glutamate diffusion rate	55
Dynamic range of activation for synaptic glutamate receptors.....	57
Fidelity of the synaptic response is receptor dependent.....	61
NMDAR subtypes show distinct temporal activation receptor ‘flickering’ behavior	62
A shift in the pattern of NMDAR subtype activation occurs with stimulation frequency	65
Developmental changes in synaptic NMDAR content alters synaptic calcium influx	69
DISCUSSION	76
Subunit-specific dynamic range of NMDAR activation.....	78
The role of NMDAR subtypes in synaptic plasticity are influenced by synaptic content.....	83
<i>Chapter 4: Immediate and persistent changes in NMDA receptor subtype activation and signaling following traumatic mechanical injury: an in silico investigation</i>	<i>87</i>
ABSTRACT.....	87
INTRODUCTION.....	88
METHODS	92
Primary cell culture and in vitro stretch injury.....	92
Geometry and content of modeled dendritic spine	94
Glutamate release and glutamate receptor activation parameters	94
Calcium entry	95
Calmodulin activation model	97
Simulations and analysis	98
RESULTS	100
Mechanical injury to cultured cortical neurons shows a strong association with NMDAR activation and requires presynaptic glutamate release	100
Presynaptic glutamate release caused by mechanical injury causes a significant shift in the profile of NMDAR activation.....	103
Stretch-induced loss of Mg ²⁺ block significantly enhances calcium influx...108	
Injury mediated calcium influx controls the activation of calmodulin.....111	
Prolonged loss of Mg ²⁺ block alters NMDAR signaling in the post acute period after injury.....	114
DISCUSSION	118
Injury induced activation patterns of NMDAR subtypes	121
Selective NR2B mechanosensitivity functions as a pathological sensor switch.....	122
Stretch-induced changes in NMDARs alter physiological synaptic signaling and enhance synaptic ‘noise’	124
<i>Chapter 5: Summary and Conclusions</i>	<i>127</i>
SUMMARY OF FINDINGS	128
Selective mechanosensitivity of NR2B containing NMDARs.....	128

Differential effectiveness of NMDAR antagonists in mitigating NR2B mechanosensitivity	130
Influence of C-terminal NR2B in its mechanosensitivity	131
PKC activity and ser-1323 on NR2B regulates NR2B mechanosensitivity ..	132
Development of computational model of stochastic glutamatergic signaling at a single dendritic spine.....	133
Differential dynamic ranges of activation among NMDAR subtype	134
Frequency of presynaptic stimulation alters patterns of NMDAR subtype activation	135
Synaptic subtype content influences extent and fidelity of signaling.....	136
Simulated injury mediated glutamate release enhances contribution of NR2B containing NMDARs	137
Combined effects of injury mediated glutamate release and selective mechanosensitivity	137
Persistent loss of Mg²⁺ block can alter fidelity of network signaling	138
LIMITATIONS AND FUTURE DIRECTIONS	140
CONCLUSIONS	145
Bibliography	147
Appendix A: Smoldyn Code: Activation of AMPARs and NMDAR subtypes	163
Appendix B: Matlab Code: Calculations of the sites and times of calcium entry following simulations of NMDAR activation.....	180
Appendix C: Smoldyn Code: Modeling of Calmodulin – Calcium binding within the dendritic spine.....	190

List of Tables

Chapter 3

Table 1. Model parameters 48

Table 2. Reaction rates used for AMPAR and NMDAR subtype activation..... 53

Chapter 4

Table 1. Reaction rates and other model parameters for simulations of intracellular
CaM activation 99

List of Figures

Chapter 1

Figure 1. TBI has two unique consequences impacting NMDAR activity.....	7
---	---

Chapter 2

Figure 1. <i>In vitro</i> stretch injury device.....	18
--	----

Figure 2. NR1/NR2B-NMDARs are more sensitive to stretch than NR1/NR2A.....	21
--	----

Figure 3. Intermediate mechanosensitivity in triheteromeric NR1/NR2A/NR2B receptors.....	23
--	----

Figure 4. NR1/NR2B stretch response is dependent on glutamate activity.....	25
---	----

Figure 5. NR2B C-terminal tail confers mechanosensitivity.....	27
--	----

Figure 6. PKC inhibition in recombinant NMDARs and primary neurons reduces receptor mechanosensitivity.....	29
---	----

Figure 7. NR2B mechanosensitivity is critically regulated by a single PKC phosphorylation site.....	31
---	----

Chapter 3

Figure 1. Dendritic spine model geometry and receptor activation schemes.....	52
---	----

Figure 2. Differential sensitivity to diffusion rate among glutamate receptors.....	56
---	----

Figure 3. NMDAR subtype specific dynamic range.....	58
---	----

Figure 4. Subtype activation scalability to physiological synapse.....	60
--	----

Figure 5. Fidelity of subtype activation.....	61
---	----

Figure 6. Slower kinetics and increased receptor flickering prolong NR2B activation.....	64
--	----

Figure 7. Frequency mediated shifts in NMDAR subtype activation patterns.....	66
---	----

Figure 8. NR2A-NMDARs desensitize and recover faster than other subtypes.....	68
---	----

Figure 9. Increasing synaptic NR2A content during development enhances response and improves fidelity	71
Figure 10. Changing subtype content during development improves calcium potentiation during paired stimulations	73
Figure 11. Presence of NR1/NR2A-NMDAR in the ‘mature’ subtype preferentially enhances calcium influx at low frequency stimulation.....	75
<u>Chapter 4</u>	
Figure 1. TBI has two distinct consequences influencing NMDAR activity	89
Figure 2. Injury induced calcium influx dependent on NMDAR activation and glutamate vesicle release.....	102
Figure 3. Injury mediated glutamate release alters both the extent and patterns of NMDAR subtype activation	106
Figure 4. Injury induced glutamate release enhances calcium entry through NMDAR subtypes.....	108
Figure 5. Selective mechanosensitivity and loss of Mg ²⁺ block in NR2B containing NMDARs greatly enhances injury induced calcium influx.....	110
Figure 6. CaM activation is potentiated by injury release with a concurrent loss of Mg ²⁺ block in NR2B.....	113
Figure 7. Persistent loss of Mg ²⁺ block in the post acute period results in two distinct phenotypes of calcium response to univesicular release in injured spines	115
Figure 8. Persistent loss of Mg ²⁺ block increases calcium entry and CaM activation in the subset of physiologic postsynaptic responses that result in NR1/NR2B activation	117

Chapter 1: Background and Significance

INTRODUCTION

Traumatic brain injury (TBI) is a major source of death and disability, estimated to inflict 1.7 million Americans annually (www.cdc.gov). This, however, is likely to underestimate the actual prevalence of TBI as many injuries are considered to be mild TBI, many of which are not reported or treated. There has been increased awareness that even mild TBI, such as concussion, can lead to long term neurological, motor, and cognitive deficits (Anderson et al 2006, Hoge et al 2008). Recent attention to TBI in sports and in the military has led to increased funding and research into the mechanisms and potential treatments of TBI. However, to date there remain very few clinical treatment options that exist following injury. The NMDA receptor (NMDAR), an integral glutamate receptor found throughout the central nervous system, has long been implicated in neuronal dysfunction following injury (Faden et al 1989, McIntosh et al 1990, Smith et al 1993, Arundine and Tymianski 2004). In spite of their observed pathologic role in injury, the importance of NMDARs in physiologic neurological function has limited their ability to be targeted in potential treatments for TBI and other neurological disorders (Morris et al 1999, Ikonomidou and Turski 2002). Our work uses several new models to further investigate how injury impacts the activity of NMDARs, with specific emphasis on the role of specific NMDAR subtypes that exist within the brain. This knowledge can aid in the understanding of the molecular consequences of TBI and can be exploited in the search for more directed therapeutic strategies.

TRAUMATIC BRAIN INJURY

Traumatic brain injury has numerous causes including falls, motor vehicle accidents, and assault. These injuries lead to a variety of short term and long term consequences which can severely impact psychological, motor, and cognitive function. The pathology seen after TBI is often broken into the primary injury, including the damage done at the moment of initial insult, and secondary injury, which includes the subsequent damage to the brain seen in the hours to days after initial injury (Werner and Engelhard, 2007). Primary injury, particularly injuries involving impact, can result in lesions, bleeding within the brain, and subdural hematoma outside the brain. These injuries can typically be detected through CT scan but unless treated can all result in an increase in pressure within the skull that can cause further neuronal damage (Ghajar 2000). Additionally, deformation of brain tissue through rapid acceleration and deceleration can also cause diffuse regions of injury that may not be detected through current means. While the primary injury may be impossible to treat, the delayed secondary injuries caused by the numerous changes in neurological signaling at the cellular and molecular levels remain to be areas of intense research.

Among the first observations of the consequences of injury on the sub-tissue level was an increase in the extracellular concentration of excitatory amino acids, specifically glutamate (Faden et al 1989, Nilsson et al 1994). Glutamate is the most common neurotransmitter, responsible for a majority of the physiologic excitatory synaptic communication throughout the brain. However, excessive glutamate results in the over-excitation of neurons, leading to activation of harmful enzymes and eventual cell death

(Olney 1969, Choi et al 1987, Lipton and Rosenberg 1994). This injury induced damage seen after TBI has largely been attributed to the over activation of the NMDAR (Faden et al 1989, McIntosh et al 1990, Smith et al 1993, Rao et al 2001, Geddes-Klein et al 2006, Deridder et al 2006), a calcium permeable glutamate receptor with physiologic roles in development, learning, and memory (Morris et al 1986, Sakimura et al 1995, Shi et al 1999, Huerta et al 2000). However, NMDARs also mediate pathologic signaling, where excessive activation leads to neuronal death (Choi et al 1987, Arundine and Tymianski 2004). Additionally, a unique aspect of TBI is the mechanical perturbation of the neuronal network, which has direct impact on NMDAR activity. NMDARs are mechanosensitive, where stretch results in a unique mechano-regulation of the receptor that allows for the stretch injured NMDAR to more easily conduct calcium, potentially exacerbating the injury response (Zhang et al 1996). Antagonism of NMDARs, during and after injury, results in decreased cell death and improved cognitive function following models of injury in rodents (Faden et al 1989, McIntosh et al 1990, Hicks et al 1994). These studies led to clinical trials with the hopes of finding an effective treatment options for mitigating secondary injury following TBI. However, clinical trials using NMDAR antagonists have failed due to the presence of prohibitive psychological side effects (Morris et al 1999). NMDARs have a vital role in the physiological function of neurons, and thus the complete blockade of NMDAR mediated signaling has proven to be an unacceptable strategy for treating TBI in the clinical population (Ikonomidou and Turski 2002). Thus, despite being the primary mediator of dysfunction after TBI, much of the research has shifted to investigate alternative strategies. However, there are

several types of NMDAR subtypes, and it has become increasingly apparent that these subtypes can have differing roles in both physiologic and pathologic NMDAR function (Cull-Candy et al 2001, Waxman and Lynch 2005, Liu et al 2007). This has led to further studies from our lab and others demonstrating that NMDAR subtypes have differential roles in mediating the neuronal response to TBI (DeRidder et al 2006). We build on these studies to investigate how two different mechanisms of injury, NMDAR mechanosensitivity and excessive glutamate release, can differentially affect NMDAR subtypes.

THE NMDA RECEPTOR

Glutamatergic signaling occurs between neurons at synapses where glutamate is released from the presynaptic cell and activates glutamate receptors at specialized compartments called dendritic spines. AMPA receptors (AMPA receptors) and NMDARs are the most prevalent and the most studied of the glutamate receptors. These receptors are ionotropic in which they allow for ionic flux through a pore when activated. Whereas AMPARs typically conduct only sodium, NMDARs conduct sodium as well as calcium. NMDARs are activated through simultaneous binding of glutamate and glycine, allowing for the influx of sodium and calcium as well as the efflux of potassium. NMDARs also contain a voltage dependent magnesium block, and thus depolarization is also required for ionic flux through the receptor (Dingledine et al 1999). NMDAR activation mediates several important neuronal processes including synaptic plasticity, the underlying mechanism behind memory formation (Liu et al 2004, Massey et al 2004, Barria and

Malinow 2005, Bartlett et al 2007). However, an overactivation of NMDARs causes sustained levels of intracellular calcium, leading to excitotoxicity and cell death (Choi et al 1987, Arundine and Tymianski 2004). NMDAR activation must, therefore, be under precise control to promote neuronal growth and survival without inducing excitotoxicity (Hardingham and Bading 2003). It has become increasingly apparent that the complexity of NMDAR function stems from the multiple subpopulations of receptors that exist. Distinguishing between the specific functions of each subpopulation is necessary to fully understand the role of NMDARs in injury or disease.

The NMDAR is a tetramer composed of two NR1 subunits, and two subunits from the NR2 family. There are four members of the NR2 family (NR2A, NR2B, NR2C, and NR2D). The NR2 subunits in a functional receptor are of one or a combination of two members of the family (Dingledine et al 1999, Cull-Candy and Leszkiewicz 2004). The identity of the NR2 subunit governs functional properties of the receptor including conductance and deactivation kinetics (Cull-Candy et al 2001). Furthermore, NR2 subunits are localized differently throughout the brain with NR2A and NR2B subunits predominating in most regions including the cortex and hippocampus, the brain regions where we apply most of our focus (Monyer et al 1994). Thus, in these regions NMDARs can be diheteromeric, containing either 2 NR2A (NR1/NR2A-NMDARs) or 2 NR2B (NR1/NR2B-NMDARs), or they can be triheteromeric, containing one of each NR2 subunit (NR1/NR2A/NR2B-NMDAR). NR2 subunits are also developmentally regulated, with NR2B subunits predominant during development. As the brain matures, the number of NR2A subunits steadily increases and replaces NR2B subunits at most

synaptic sites, while NR2B remains prevalent at extrasynaptic sites (Williams et al 1993, Monyer et al 1994, Liu et al 2004). NR1 splice variants and NR2 subunits create distinct NMDAR subpopulations, whose functional properties allow them to mediate different cellular functions. Given emerging evidence for specific NMDAR subtypes to have different and opposing roles in the determination of cell fate during disease (Hardingham and Bading 2003, Waxman and Lynch 2005, Liu et al 2007), it is vital to recognize the specific patterns of NMDAR subtype activation during injury.

The development of NMDAR subtype specific antagonists has allowed the study of subtype specific functions in both physiological and pathological conditions. Ifenprodil and the related compound, Ro 25-6981, specifically block NR2B-NMDARs (Williams 1993, Gallagher et al 1996), whereas NVP-AAM077 is more specific for NR2A-NMDARs (Auberson et al 2002). These pharmacological manipulations have led to the observation that NR2B containing receptors are responsible for cell death following stretch injury, while NR2A containing receptors mediate pro-survival signaling after injury (DeRidder et al 2006). While these specific antagonists have aided in the study of NMDAR subtype specific functions, their use has become recently scrutinized, as the specificity of NVP-AAM077 has now been called into question (Neyton and Paoletti 2006). Thus, alternative models are necessary to better study NMDAR subtypes.

RESEARCH GOALS

Despite the recent advances made in investigating the role of NMDARs in mediating the neuronal response to TBI, questions remain as to how these receptors, and

more specifically how subtypes of these receptors, mediate the initial response to an injury event. NMDAR sourced calcium influx during injury can be affected by two distinct mechanisms: (1) NMDAR mechanosensitivity and (2) excessive extracellular glutamate concentration. Here, we aimed to use new models to study the role of NMDAR subunit composition in each of these mechanisms independently and to examine how these mechanisms work in concert to result in excessive calcium influx (Figure 1).

NMDARs have been shown to be mechanosensitive (Zhang et al 1996), but the subtype dependence and regulation of this unique characteristic has yet to be determined. We sought to investigate its regulation by using a recombinant system which allows for complete control over the identity of expressed receptor subtypes. Further, this model system allows for the expression of mutant receptors, which allows for the examination of the roles of particular domains or residues in receptor mechanosensitivity. In order to better understand how injury induced increases in glutamate can alter NMDAR activity, we aimed to develop a computational model that could be used to quantitatively examine differences in NMDAR subtype activation at time and length scales not possible with current experimental methods. We first sought to explore how patterns of activation differ among NMDAR subtypes in the physiological regimes of glutamate stimuli. Next, we aimed to further use this model to examine how injury induced glutamate alone, and then in concert with NMDAR mechanosensitivity, affects the extent and source of calcium entry during injury conditions. Thus, these unique models were used to enable

us to further explore how injury may differentially affect the activities of specific receptor subtypes.

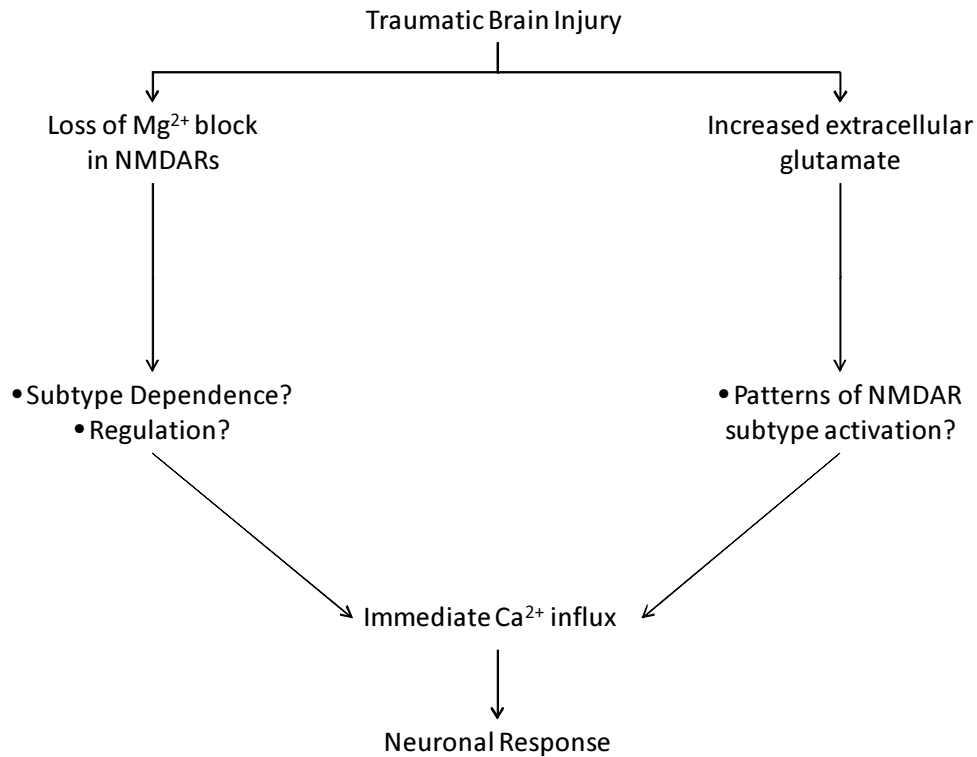


Figure 1: TBI has two unique consequences impacting NMDAR activity.

SUMMARY OF CHAPTERS

These studies were conducted to build upon work from our lab and others on the role of NMDAR subtypes in the injury induced calcium influx. We utilized an *in vitro* stretch injury model and an *in silico* computational model of glutamatergic signaling to specifically demonstrate that NMDAR subtypes have a differential role in mediating the injury response and that the NR2B subunit remains an intriguing target for manipulation in the development of prophylactic or treatment options.

In chapter 2, we utilized a recombinant system of human embryonic kidney 293 cells (HEK-293s) that were transfected with known combinations of NMDAR subunits. This model gives us complete control over the identity of NMDAR subtypes expressed and also eliminates the synaptic geometry of neurons which can complicate the ability to observe a direct mechano-response. NMDARs have previously been shown to be mechanosensitive (Zhang et al 1996), with stretched cultures losing their native Mg^{2+} block. However, the role of subunit composition in this mechanosensitivity has yet to be elucidated. Using this system we show that NR2B-NMDARs are more sensitive to stretch than NR2A-NMDARs. Additionally, with the use of truncation and point mutations, we isolated the Ser-1323 residue of NR2B as an integral mediator of NR2B mechanosensitivity. With the knowledge that this residue is a known phosphorylation site for PKC, we showed that inhibition of PKC eliminated the stretch induced calcium influx in both neurons and NR1/NR2B transfected HEKs. These findings demonstrate that NR2B is a critical mediator of injury induced calcium influx and suggests that specific antagonism of NR2B containing NMDARs, while leaving NR2A-NMDARs unblocked, may represent a potential strategy to mitigate excitotoxic calcium influx during injury.

In chapter 3, we describe the development of a new stochastic computational model of glutamatergic signaling using Smoldyn, a stochastic simulator of biochemical reactions. While several computational models have been used to examine NMDAR activation, until recently the ability to discriminate between NMDAR subtypes in these models was not possible. The development of subtype specific activation schemes by

Erreger et al (2005) has allowed us to further investigate subtype specific activation with the temporal and spatial resolution not afforded to us by conventional experimental models. Using this model, we show that NMDAR subtypes have different dynamic ranges, with NR2A-NMDARs displaying scalability in its activation at lower levels of released glutamate while NR2B-NMDARs and NR2A/NR2B-NMDARs scale in activation at much higher glutamate levels. We also demonstrate that a physiological representation of mixed NMDAR subtypes along the dendritic spine allow for unique patterns of subtype activation in response to glutamate release of varied frequencies, with implications in how different subtypes are involved in mediating modes of synaptic plasticity. Finally, we show that changes in the relative subtype content of the dendritic spine significantly alter the extent and reliability of observed NMDAR activation. These findings demonstrate the utility of computational models while enhancing our understanding of how NMDAR subtypes can differentially transmit a variety of physiological glutamate signals into functional outcomes.

In chapter 4, we continue our use of our *in silico* model of glutamatergic signaling to investigate the changing patterns of NMDAR subtype activation in injury induced excessive glutamate release. With a physiological representation of the numbers and locations of receptor subtypes, we demonstrated that an injury induced simultaneous release of numerous glutamate vesicles significantly altered both the extent of total NMDAR activation and the relative contribution of different subtypes. We show that NR2B containing receptors, including extrasynaptic NR2B-NMDARs, contribute significantly more under injury conditions than they do after physiological univesicular

glutamate release. Finally, we demonstrate that a loss of Mg^{2+} block in NR2B-NMDARs drastically increases the extent of observed calcium influx in response to both injury mediated glutamate release and also physiological spontaneous single vesicle release. As it has been shown that the loss of Mg^{2+} block can last several hours, and we have now shown that this may be restricted to the NR2B subunit, our findings suggest that injury results in enhanced calcium influx through these receptors which can alter the normal balance of signaling. NR2B-NMDARs and extrasynaptically located NMDARs have both been shown to mediate pro-death signaling and thus injury can cause a sustained shift toward the activation of these pathways which can influence the extent of secondary injury.

Finally, in chapter 5, we summarize our data and highlight the significance of this work in furthering our understanding of the differential roles of NMDAR subtypes in TBI. We will provide our overall conclusions while suggesting how our new findings can lead to some exciting future research with the eventual hopes of developing more effective treatment options for TBI.

Chapter 2: NMDA receptor mechanosensitivity is governed by the C-terminus of the NR2B subunit

ABSTRACT

N-methyl-D-aspartate receptors (NMDARs), critical mediators of both physiologic and pathologic neurological signaling, have previously been shown to be sensitive to mechanical stretch through the loss of its native Mg^{2+} block. However, the regulation of this mechanosensitivity has yet to be further explored. Furthermore, as it has become apparent that NMDAR mediated signaling is dependent on specific NMDAR subtypes, as governed by the identity of the NR2 subunit, a crucial unanswered question is the role of subunit composition in observed NMDAR mechanosensitivity. Here, we used a recombinant system to assess the mechanosensitivity of specific subtypes and demonstrate that the mechanosensitive property is uniquely governed by the NR2B subunit. NR1/NR2B-NMDARs displayed significant stretch sensitivity, while NR1/NR2A-NMDARs did not respond to stretch. Furthermore, NR2B mechanosensitivity was regulated by PKC activity, as PKC inhibition reduced stretch responses in transfected HEK 293 cells and primary cortical neurons. Finally, using NR2B point mutations, we identified a PKC phosphorylation site, Ser-1323 on NR2B, as a unique critical regulator of stretch sensitivity. This data suggests that the selective mechanosensitivity of NR2B can significantly impact neuronal response to traumatic brain injury, and illustrates that the mechanical tone of the neuron can be dynamically regulated by PKC activity.

INTRODUCTION

N-methyl-D-aspartate receptors (NMDARs) are glutamate receptors whose activation is important for the proper health and maintenance of neurons and neuronal networks (Ikonomidou et al 1999, Hardingham 2006, Hetman and Kharebava 2006). Functional NMDARs are usually comprised of 2 NR1 subunits and 2 subunits from the NR2 family (NR2A, NR2B, NR2C, and NR2D) (Dingledine et al 1999, Cull-Candy and Leszkiewicz 2004). The relative composition of expressed NMDARs varies throughout brain regions (Monyer et al 1994), changes over neural development (Williams et al 1993, Monyer et al 1994, Liu et al 2004), and directs the activation of selective signaling networks through the unique coupling of proteins to the C terminus of each NR2 subunit (Kohr et al 2003, Kim et al 2005, Li et al 2006, Jin and Feig 2010). Proper regulation of receptor activity is vital, as excessive activation of NMDARs is the primary mediator of excitotoxic cell death in numerous disease states (Lynch and Guttman 2002, Arundine and Tymianski 2004, Waxman and Lynch 2005, Hardingham and Bading 2010), while the tonic synaptic activation of the receptor can stimulate key neuronal survival programs (Ikonomidou et al 1999, Ikonomidou et al 2000). Although the competing roles of the NMDAR lead to a more complex view of how NMDAR stimulation directs physiological processes including synaptic plasticity (Liu et al 2004, Massey et al 2004), dendritic growth (Espinosa et al 2008, Ewald et al 2008), and recovery from injury (Hardingham et al 2002, DeRidder et al 2006), this more complete view provides new opportunities for developing directed NMDAR-targeted therapies. Several recent papers show that it is

possible to use the molecular diversity of the NMDAR, including the selective action or blockade of specific receptor subpopulations, to promote necessary maintenance of neural circuits (Kinney et al 2006), minimize the over-activation of pathological pathways (Waxman and Lynch 2005, Zhou and Baudry 2006), and effectively treat neurological disease (Okiyama et al 1997, Gogas 2006, von Engelhardt et al 2007, Chen et al 2008).

The NMDAR is considered by many as one of the common mediators for the acute and progressive events that occur following traumatic brain injury (TBI) (Faden et al 1989, McIntosh et al 1990, Shapira et al 1990, Smith et al 1993, Deridder et al 2006, Geddes-Klein et al 2006). Based partly on studies showing an increased glutamate concentration in the extracellular space (Faden et al 1989, Palmer et al 1993, Nilsson et al 1994, Bullock et al 1995), many consider TBI an extension of glutamate excitotoxicity. However, TBI has an important and unique mechanical etiology that can contribute to the heterogeneity of the disease in the clinical population. Moreover, the mechanical causality of TBI appears at the molecular level of the NMDAR. The NMDAR is mechanosensitive, and expresses a unique switch in behavior following mechanical stimulation. Specifically, rapid neuronal stretch induces a persisting loss in the voltage dependent Mg^{2+} block of NMDARs (Zhang et al 1996). Similar to a phosphorylation event or proteolysis, the mechanical event can function as a distinct regulator of NMDAR function. However, no data exists that describes how this mechanically initiated switch in NMDAR behavior is regulated among its receptor subunits. The diversity in the dynamic mechanosensing properties of NMDAR subtypes may prove important in

understanding the post-acute regulation of neuronal homeostasis after traumatic mechanical injury, similar to how the diversity in NMDAR composition has led to a more complete understanding of signaling occurring after excitotoxicity (Lynch and Guttman 2002, Liu et al 2007, von Engelhardt et al 2007). Finally, identifying the potential domains of regulation across NMDAR subunits or, alternatively, within individual subunits will inform how normal physiological signaling acting upon the receptor can potentially augment the mechanical tone of NMDARs.

In this report, we systematically characterize the direct effects of mechanical stretch on calcium influx through the NMDAR. To distinguish between changes in calcium influx occurring from increased extracellular glutamate versus stretch induced mechanosensitivity of the NMDAR, we expressed recombinant receptors in HEK 293 cells using a minimal representation of the postsynaptic structure that included the subunits and an anchoring protein (PSD-95). A secondary advantage of this approach was eliminating the need for subtype specific antagonists needed for testing in dissociated neuronal cultures, as the specificity of some antagonists is currently under debate (Neyton and Paoletti 2006). We examine key regulatory mechanisms of mechanosensitivity and test if there are crucial domains on subunits that control this sensitivity to stretch. Together, our data reveals that dynamic mechanosensitivity of NMDARs is controlled by the intracellular domain of the NR2B subunit, in which a PKC mediated phosphorylation site, Ser-1323, is critical for NR2B stretch sensitivity. Given the prominent role of NR1/NR2B NMDARs controlling neuronal fate in models of neurological disease, this points to a likely pathway whereby mechanical force is

transferred into subunit-specific signaling cascades after mechanical trauma and influences cell fate after injury.

METHODS

Cell culture: HEK 293T cells (ATCC) were cultured and maintained with Dulbecco's Modified Eagle Medium (DMEM) with L-glutamine, supplemented with 5% fetal bovine serum in a humidified incubator at 37°C and 5% CO₂. For experimentation, HEK 293 cells were plated onto a transparent, silicone substrate (Sylgard 184 + 186 mix). These membranes were attached to stainless steel wells, leaving an exposed area (area – size of a single well from a 24well plate) of membrane for plating. Following sterilization, membranes were coated with poly-D-lysine (0.01mg/mL) for 1hr, rinsed with sterile water, and coated with laminin (10µg/mL) for 1hr. After membranes were rinsed again, HEK 293 cells were plated at 1:20 dilution from a fully confluent flask.

For primary cortical cultures, cortical neurons were isolated from E18 embryonic rats and plated on poly-D-lysine coated silicone membranes at a density of 0.3 million/mL.

Cultures were plated in Minimum Essential Medium (MEM) with glutamax + 10% horse serum which was removed at 24hrs and replaced with Neurobasal (Gibco) + B-27 supplement (Invitrogen). At 24 hours post plating, cells were treated with AraC (1µM) to prevent the growth of astrocytes. AraC was removed at 3 DIV and cells were cultured in a humidified incubator at 37°C and 5% CO₂. Primary cortical cultures were used at 12-15 DIV, an age which contains a diverse content of NMDAR subtypes.

Plasmids: NR1a, NR2A, and NR2B cDNA plasmids have been obtained and subcloned from rat brain library as previously described (Boeckman and Aizenman 1994, Boeckman and Aizenman 1996, Gallagher et al 1996). The NR2B-1036X and NR2B-1433X truncation mutants were generated by replacing fragments of wildtype NR2B and introducing a stop codon at amino acid 1037 (Wu et al 2007) and 1434 respectively by PCR. Using wildtype NR2B in the PRK7 vector as a template, the NR2B point mutants S1303A and S1323A were made using the PCR-based site directed mutagenesis kit by Stratagene (Agilent Technologies). The mutations were verified by DNA sequencing through the Nucleic Acid/Protein Research Core at Children's Hospital of Philadelphia. The plasmid encoding GFP-PSD95 was a generous gift supplied by Dr. David Brecht.

Transfection: HEK 293 cells were transfected 24 hours after plating with Lipofectamine 2000 according to product instructions. All cultures were transfected with GFP tagged PSD95 to provide a visual marker of successful transfection. The total amount of DNA transfected per well was held constant over all conditions (0.8µg/well). Due to the tonic vesicular release of glutamate in HEK 293 cells, cells were transfected in the presence of the NMDA antagonist APV (Sigma-Aldrich, 100µM) throughout the transfection period and until the time of plating. For cultures transfected with NR1 and NR2 subunits, the ratio of transfected DNA was 2:1:1 (GFP-PSD95:NR1:NR2). This ratio did not vary for any of the mutant NR2 subunits.

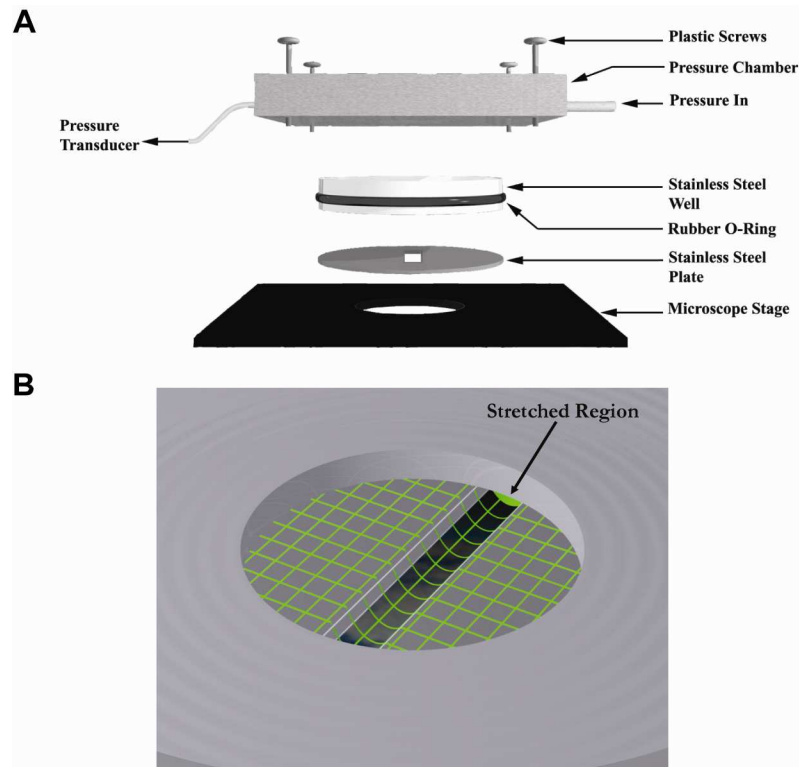


Figure 1: In vitro stretch injury device. (A) Schematic of the in vitro injury device in which cells plated on stainless steel wells are placed upon a microscope stage and sealed into the pressure chamber. A defined air pulse is applied to the chamber deflecting the membrane. (B) The 6mm slit in the stainless steel plate allows a uniform membrane stretch in the defined stretched region.

In vitro stretch injury: Transfected HEK 293 cells were used 16-20 hours after transfection. Cultures were incubated with the fluorescent calcium indicator, Fura 2-AM (5 μ M, Invitrogen), in controlled saline solution (126mM NaCl, 5.4mM KCl, 2mM MgCl₂, 1.8mM CaCl₂, 10mM HEPES, 25mM glucose) supplemented with 100 μ M APV for 40 minutes at 25°C. Cultures were placed in an apparatus that would apply a brief pressure to the exposed culture, producing a uniaxial stretch which deforms the membrane in proportion to the applied pressure (Lusardi et al 2004) (Fig 1). We used the amount of membrane deformation (40%) as a measure of the mechanical input delivered to the HEK 293 cells. In a separate group of cultures, we used a 100 μ M NMDA

application to evaluate the response of transfected cells to agonist. All cultures were imaged continuously before and after the mechanical or chemical insult, collecting images at the emission fluorescence of 510nm that appeared when cultures were alternately excited at 340nm and 380nm every 3 seconds. A pair of emission images from each wavelength was used to generate a Fura ratio (340nm/380nm) image at each time point. Cultures were imaged for 30 seconds before stimulation and up to 3 minutes following stimulation. Following Fura imaging, cells were excited at 488nm to detect the presence of GFP within the cells. The GFP signal was not detected during the 340nm or 380nm excitation during Fura imaging.

For testing stretch sensitivity of primary cortical neurons, the test protocol remains the same, with one primary difference. Cortical neurons were incubated with Fura 2-AM prior to stimulation for 40 minutes at 37C in saline solution (51.3mM NaCl, 5.4mM KCl, 2mM MgCl₂, 1.8mM CaCl₂, 26mM NaHCO₃, 0.9M NaH₂PO₄, 10mM HEPES, 25mM glucose) without the addition of APV.

Data Analysis: Stimulation of HEK 293 cells was analyzed using MetaMorph to quantify the extent of calcium influx following injury or NMDA stimulation. Traces of Fura ratio (F340/F380) over time were collected for all GFP-positive cells. Cells with a baseline Fura ratio of greater than 0.95, indicating an elevated initial calcium level, were excluded from analysis. The response was quantified for each individual cell by calculating the peak fractional change in Fura ratio post stimulation over the average

baseline ratio pre stimulation ($\frac{F_{peak} - F_{baseline}}{F_{baseline}}$). To normalize data, the peak response for each cell was normalized by the peak response for the NR1/NR2B group for the given stimulation, either stretch or NMDA. Significance between groups was determined with a one-way ANOVA and post hoc Tukey's test.

RESULTS

Subunit composition of the NMDAR influences mechanosensitivity

Following dynamic 40% stretch of NMDAR transfected HEK 293 cells, we observed two different calcium responses: 1.) a significant and gradual rise in cytosolic calcium, indicated by a relative increase in the Fura-2 fluorescence ratio, which occurred and plateaued within the first two minutes post stretch, and 2.) no significant increase in the relative Fura-2 ratio. We did not observe any stretch induced calcium increase in nontransfected cells, indicating the stretch level was not sufficient to cause the formation of nonspecific, transient pores in the plasma membrane (data not shown). Moreover, cells transfected with only GFP-PSD95 showed little to no change in intracellular calcium, indicating that a functional NMDAR was necessary to elicit a response following mechanical stimulation.

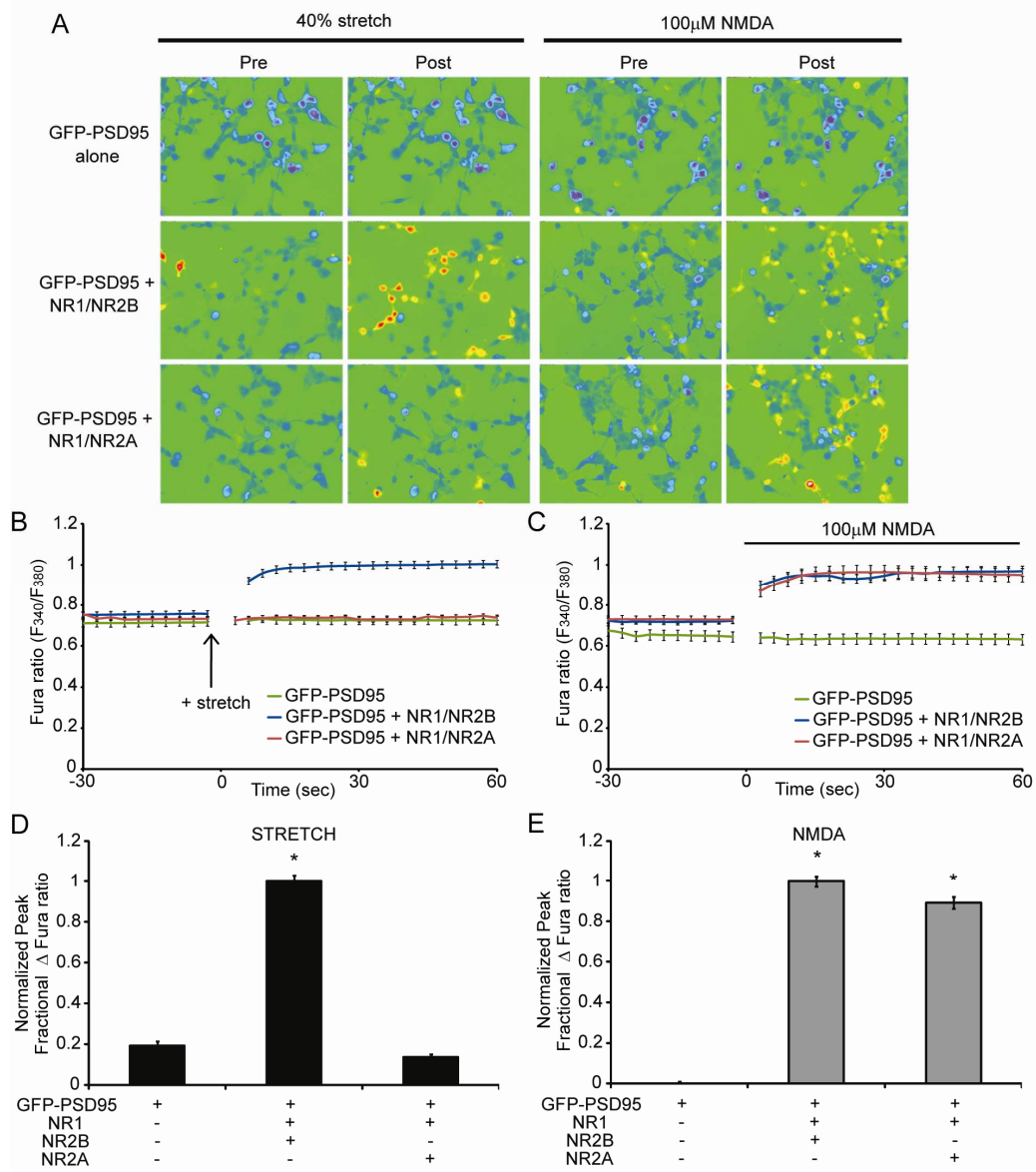


Figure 2: NR1/NR2B-NMDARs are more sensitive to stretch than NR1/NR2A. HEK 293 cells, plated on flexible membranes, were transfected with GFP-PSD95 alone, or along with NR1 and either NR2A or NR2B. (A) Representative images of transfected cells, pre and post stimulation, that were stimulated by either 40% stretch (left) or 100uM NMDA (right). Average fura ratio, representing intracellular calcium, following (B) stretch or (C) NMDA stimulation, demonstrates that while NR1/NR2B and NR1/NR2A expressing cells have a similar response to NMDA, stretch induced calcium influx is greater in NR1/NR2B expressing cells. (D) The average peak fractional change in fura ratio, normalized to the NR1/NR2B response, following stretch demonstrates significant stretch sensitivity in NR1/NR2B transfected cells (* $p < 0.05$ compared to GFP-PSD95), while NR1/NR2A stretch responses are not different from control GFP-PSD95 responses. (E) Normalized response to NMDA stimulation was similar among NR1/NR2A and NR1/NR2B transfected cells (* $p < 0.05$ compared to GFP-PSD95).

Cells were transfected with GFP-PSD95 alone or along with NR1 and NR2A (NR1/NR2A) or with NR1 and NR2B (NR1/NR2B). NR1/NR2B NMDARs expressing cells respond to the stretch stimulus with an immediate rise in intracellular calcium while cells expressing NR1/NR2A do not show a stretch induced calcium rise (Fig 2). Quantified, the normalized peak percent change in the calcium signal was significantly greater in NR1/NR2B transfected cells compared to GFP-PSD95 control ($p < 0.05$), while transfection of NR1/NR2A was not different from control (Fig 2D) (mean \pm standard error; NR1/NR2B, 1.0 ± 0.03 ; NR1/NR2A, 0.14 ± 0.01 ; GFP-PSD95, 0.19 ± 0.02). Although NR1/NR2A and NR1/NR2B transfected cells display differential response to stretch, cells transfected with the different subunits respond similarly to the application of $100\mu\text{M}$ NMDA (Fig 2E) (NR1/NR2B, 1.0 ± 0.03 ; NR1/NR2A, 0.90 ± 0.03 ; GFP-PSD95, 0.01 ± 0.01). This data suggests that, among the common diheteromeric forms of the NMDAR expressed in the cortex and hippocampus, the NR1/NR2B NMDARs are significantly more sensitive to mechanical stretch than NR1/NR2A NMDARs.

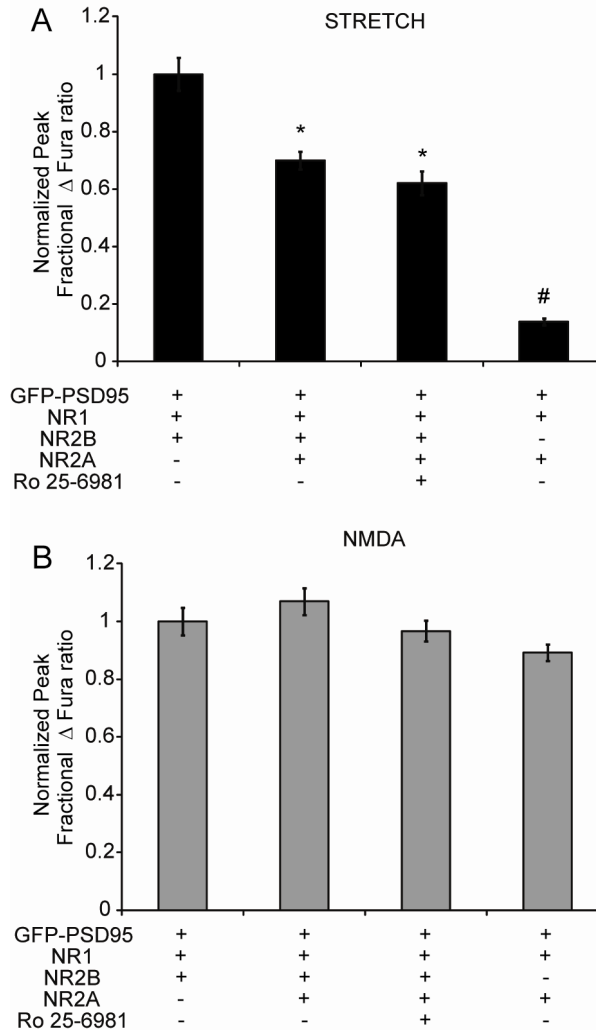


Figure 3: Intermediate mechanosensitivity in triheteromeric NR1/NR2A/NR2B receptors. Cells were transfected with GFP-PSD95 and with either, NR1 and NR2B, or with NR1, NR2A and NR2B. Cells transfected with all subunits were either left untreated, or treated with NR1/NR2B specific antagonist, Ro 25-6981. (A) Normalized response to stretch was significantly decreased, but not eliminated, in cells expressing NR1, NR2A, and NR2B, demonstrating that these cells exhibit intermediate mechanosensitivity (* $p < 0.05$ compared to NR1/NR2B). (B) Response to 100uM NMDA application was not different. Treatment with Ro 25-6981 did not alter the response of NR1/NR2A/NR2B transfected cells, suggesting that expressed NMDARs in these cells are primarily triheteromeric.

To assess the mechanosensitivity of triheteromeric NR1/NR2A/NR2B NMDARs, HEK 293 cells were transfected with plasmids for GFP-PSD95, NR1, NR2A, and NR2B. Interestingly, the stretch response of cells expressing the combination of both the NR2A

and NR2B subunits was significantly decreased from those expressing NR1/NR2B (NR1/NR2A/NR2B, 0.70 ± 0.03 ; NR1/NR2B, 1.0 ± 0.06 ; $p < 0.05$), but was not diminished to levels seen for NR1/NR2A (Fig 3A). The response to mechanical stretch was distinct from the chemical agonist response, as $100\mu\text{M}$ NMDA stimulation produced a calcium response in triheteromeric NMDARs that was not different from the NR1/NR2B receptor combination (Fig 3B). One possibility that could lead to an uncertain interpretation of triheteromeric receptor experiments was that functional receptors in these transfected cultures could be composed of mixture of diheteromeric and triheteromeric receptor combinations. To address this uncertainty, we treated NR1/NR2A/NR2B transfected cultures with Ro25-6981 ($20\mu\text{M}$), an antagonist which blocks NR1/NR2B receptors but has minimal effect on triheteromeric receptors (Hatton and Paoletti, 2005). In both mechanical and chemical stimulation experiments, pretreatment with Ro25-6981 produced no significant differences in comparison to untreated triheteromeric cultures. Thus, we can conclude that NR1/NR2A/NR2B NMDARs display an intermediate form of mechanosensitivity, between that of NR1/NR2A and NR1/NR2B receptors.

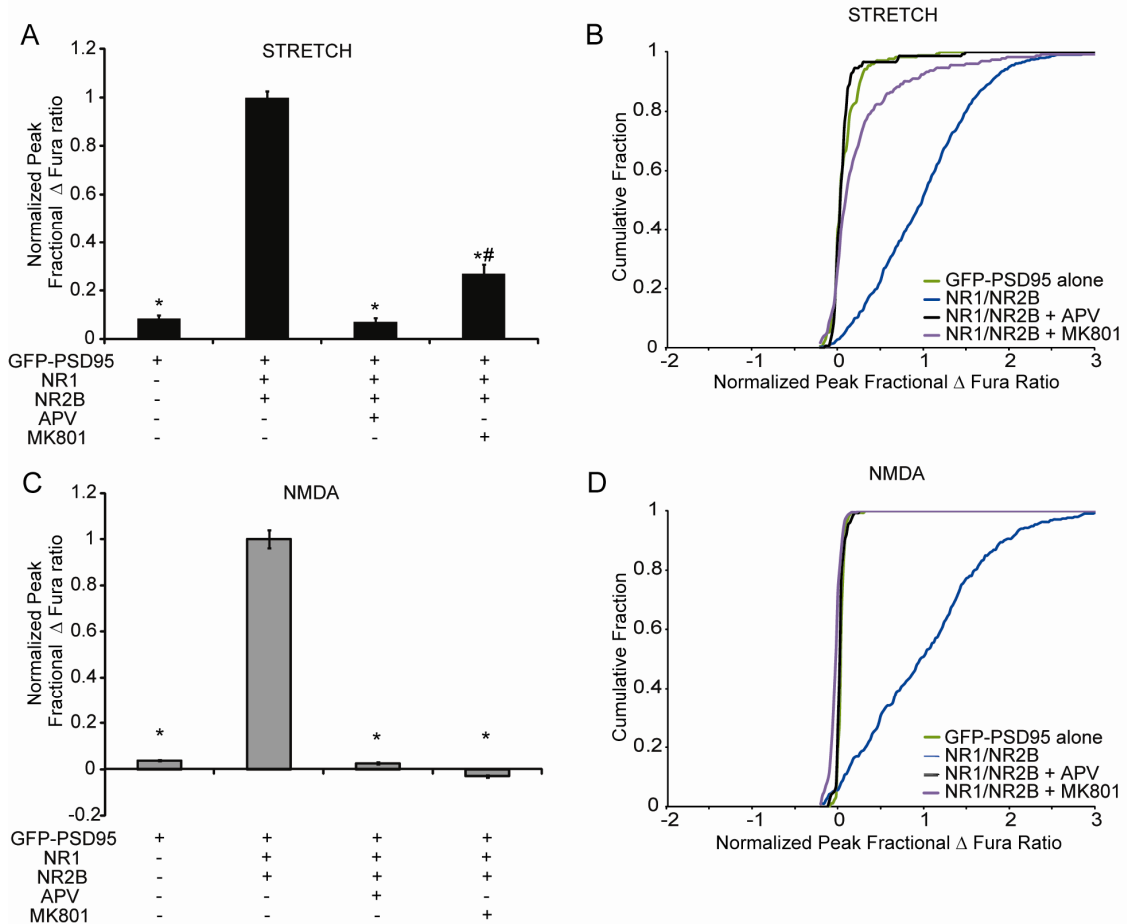


Figure 4: NR1/NR2B stretch response is dependent on glutamate activity. Cells transfected with GFP-PSD95, NR1, and NR2B were left untreated or pretreated with NMDAR competitive antagonist, APV, or NMDAR pore blocker, MK801. (A) Normalized peak change in fura ratio after stretch that treatment with either antagonist significantly reduced stretch response (* $p < 0.05$ compared to NR1/NR2B).

We next tested if the stretch sensitivity of NR1/NR2B-NMDARs can be modulated by alternatively blocking two modes of receptor activity: glutamate binding or ionic flux through the channel pore. NR1/NR2B transfected cultures were stimulated with or without the pretreatment of NMDAR antagonists, APV (200 μ M) and MK801(50 μ M). Pretreatment of cultures with APV, a competitive NMDAR antagonist that inhibits glutamate binding on the NR2 subunit, led to no significant stretch response. In comparison, pretreatment of cultures with MK801, which binds to and blocks the

channel pore, resulted in a significant decrease in calcium response compared to untreated NR1/NR2B transfected cells (Fig 4A). Further, significant differences among the cumulative distributions of individual responses demonstrated that antagonism increases the amount of “non-responding” cells after stretch (Fig 4B). In comparison, APV pretreatment decreased the stretch response significantly more than MK801 (NR1/NR2B + APV, 0.07 +/- 0.02; NR1/NR2B + MK801, 0.27 +/- 0.04; $p < 0.05$) and further reduced the number of responding cells, as measured by the differential response distributions among antagonists. Both APV and MK801 completely eliminated the NMDA response to levels not different from responses from cells transfected with only GFP-PSD95 (Fig 4C,D).

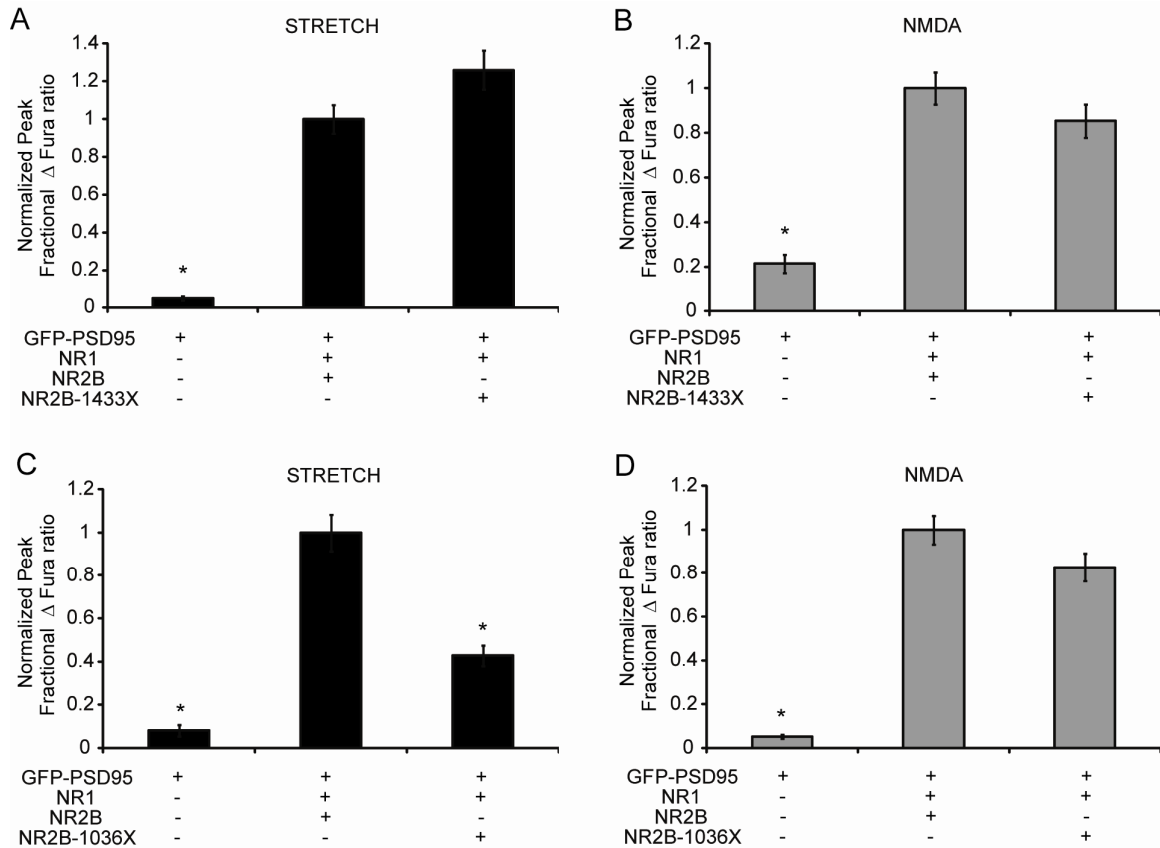


Figure 5 NR2B C-terminal tail confers mechanosensitivity. Cells were transfected with NR2B or with truncation mutants of NR2B, NR2B-1036X or NR1433X, which truncate the c-terminal tail distal to amino acid 1036 and 1433 respectively. (A) Normalized stretch response was significantly decreased in cells expressing NR2B-1036X, while (B) response to 100uM was not different. (C) Response to stretch was slightly increased in cells expressing NR2B-1433X, while (D) response to NMDA stimulation was not different among NR2B and NR2B-1433X. This suggests that NR2B mechanosensitivity is conferred by the intracellular domain within amino acids 1036-1433. (* $p < 0.05$ compared to NR1/NR2B response)

NR2B C-terminal tail confers mechanosensitivity

The NR2A and NR2B subunits share approximately 70% homology (Monyer et al 1992), but contain important differences in the sequence and structure of their C-terminal tails. These differences are important in dictating subunit specific functions of receptors, leading to differential cytoskeletal anchoring, protein binding, and association in signaling complexes (Wyszynski et al 1997, Wechsler and Teichberg 1998, Kohr et al

2003, Krapivinsky et al 2003, Kim et al 2005, Li et al 2006, Foster et al 2010). We examined if the C-terminal tail of the NR1/NR2B receptor confers the observed mechanosensitivity of the receptor by studying the response of recombinant receptors composed of NR2B truncation mutants. One key regulatory domain is the distal region of the C-terminal tail, which contains the binding domain for PSD95. However, cells expressing NR2B-1433X, an NR2B truncation mutant which eliminates only the distal portion of the C-terminal tail, did not display any difference in mechanosensitivity compared to wildtype NR2B (Fig 5A). Cells that express NR2B-1036X, which eliminates the majority of the C-terminus including numerous cytoskeletal binding sites and phosphorylation sites, displayed a significantly reduced level of mechanosensitivity (NR1/NR2B, 1 ± 0.08 ; NR1/NR2B-1036X, 0.43 ± 0.05 , $p < 0.05$) (Fig 5C). Neither mutant displayed a difference in the chemical agonist response ($100\mu\text{M}$ NMDA) when compared with the NR1/NR2B wildtype. (Fig 5B,D). This data suggests that the intermediate region of the NR2B C-terminus between amino acids 1036-1433 confers NR2B mechanosensitivity, but does not affect the normal agonist response of the receptor.

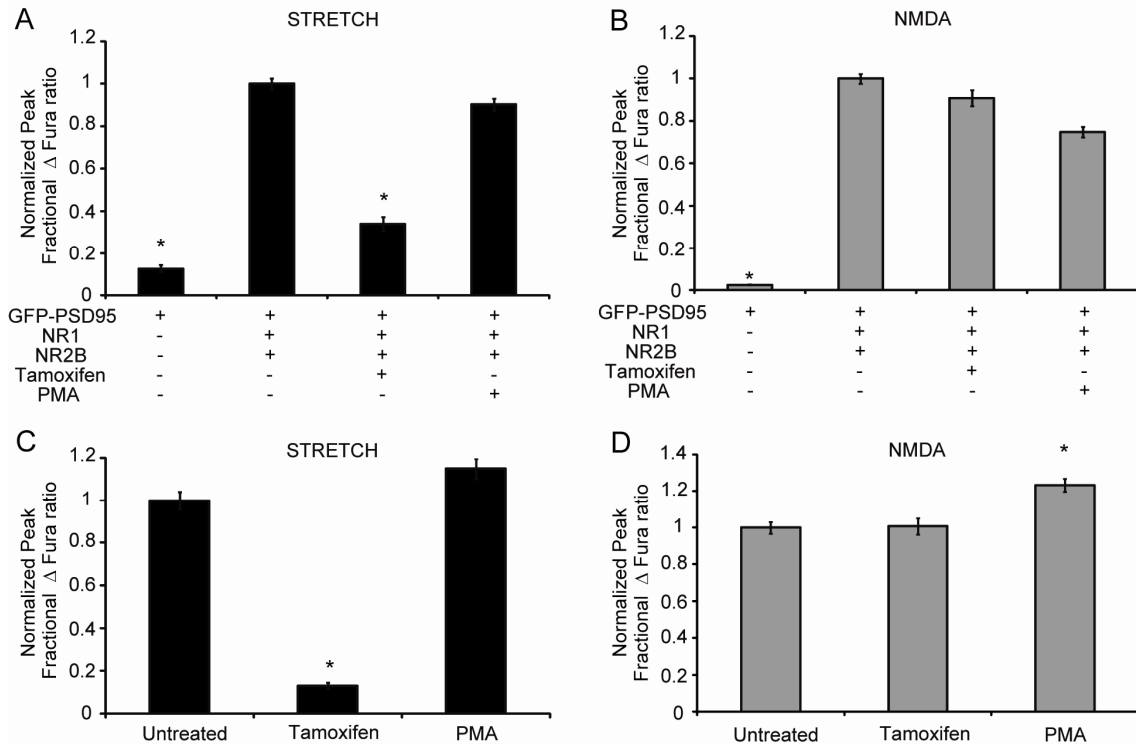


Figure 6: PKC inhibition in recombinant NMDARs and primary neurons reduces receptor mechanosensitivity. HEK 293 cells were transfected with GFP-PSD95, NR1, and NR2B were left untreated or treated with PKC inhibitor, tamoxifen, or PKC activator, PMA. (A) Tamoxifen treatment significantly decreased stretch response, while PMA had no effect (* $p < 0.05$ compared to NR1/NR2B). (B) Neither treatment produced significant change following NMDA stimulation in transfected HEKs. Primary cortical cultures (DIV 15) were treated left untreated, or treated with tamoxifen or PMA. (C) Stretch response, normalized to response of untreated cultures, was significantly reduced in tamoxifen treated cultures, while PMA had no effect (* $p < 0.05$ compared to untreated). (D) Response to 100uM NMDA stimulation was unchanged in tamoxifen treated cells, but increased in PMA treated cells (* $p < 0.05$ compared to untreated).

Regulation of NR2B mechanosensitivity by PKC phosphorylation site on NR2B

The identified mechanoregulatory domain of the NMDAR (a.a.1036-a.a.1433) contains numerous phosphorylation sites that can influence receptor function (Waxman and Lynch 2005, Chen and Roche 2007). Among these phosphorylation sites are Ser-1303 and Ser-1323, which are phosphorylated by protein kinase C (PKC). PKC has been shown in previous studies of NMDAR mechanoactivation to partially restore the injury-

induced loss of Mg^{2+} block observed after injury (Zhang et al 1996). Thus, we examined the role of PKC activity in both primary cortical cultures and NR1/NR2B transfected HEKs. In primary cortical neurons pretreated with 20 μ M tamoxifen citrate, an inhibitor for PKC binding to its substrates, the response to mechanical stretch was nearly eliminated (Fig 6A), while the response of the neurons to 100 μ M NMDA was not significantly changed. Pretreatment with a PKC activator, PMA (500nM), did not change the injury mediated response in primary neurons. In response to 100 μ M NMDA, PMA treatment slightly enhanced the calcium response, in agreement with previous reports, while PKC inhibition had no effect (Fig 6B). Similar results were seen when PKC activity was modulated in NR1/NR2B transfected HEKs. Tamoxifen citrate pretreatment significantly decreased the stretch response when compared to untreated cells (tamoxifen, 0.13 +/- 0.01; untreated, 1 +/- 0.04, $p < 0.05$), while pretreatment with PMA had no effect (Fig 6C). In response to 100 μ M NMDA in transfected HEKs, PMA treated cells displayed a slightly reduced response, while tamoxifen produced no change (Fig 6D). It is important to note that neither PKC activation nor inhibition significantly altered baseline calcium levels in transfected HEKs or cultured neurons. Thus, in agreement with previous reports of NMDAR mechanoactivation, PKC activity is observed to be crucial for the mechanical stimulation of NR1/NR2B NMDARs.

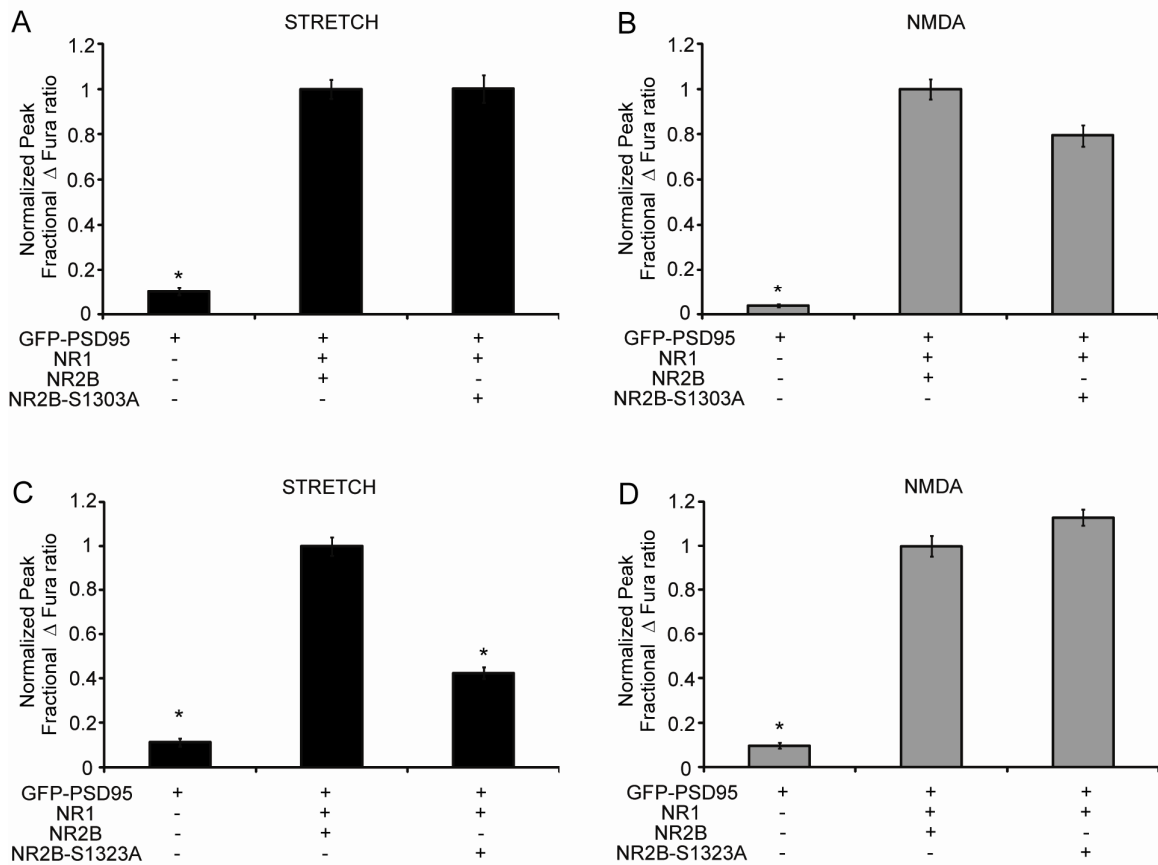


Figure 7: NR2B mechanosensitivity is critically regulated by a single PKC phosphorylation site. Cells were transfected with NR2B or with NR2B point mutations, NR2B-S1303A or NR2B-S1323A, which contain serine to alanine point mutations at PKC phosphorylation sites Ser-1303 or Ser-1323, respectively. (A) Normalized stretch response and (B) NMDA response was unchanged with the expression of NR2B-S1303A. (C) Response to stretch was significantly decreased in cells expressing NR2B-S1323A, while (D) response to NMDA stimulation was not different among NR2B and NR2B-S1323A. This suggests that NR2B mechanosensitivity is regulated by the PKC phosphorylation site, Ser-1323, on the NR2B c-terminal tail. (* $p < 0.05$ compared to NR1/NR2B response)

To examine if the observed PKC dependence of NR2B mechanoactivation was mediated through the PKC phosphorylation sites, two plasmids encoding NR2B point mutations were generated where each contains a serine to alanine point mutation at these residues. Expression of NR2B-S1303A in HEK cells produced no change in observed calcium influx, compared to cells expressing wildtype NR2B, after stimulation with

stretch or 100 μ M NMDA (Fig 7A,B). However, expression of NR2B-S1323A significantly decreases the stretch response compared to wildtype NR2B (Fig 7C) (NR1/NR2B, 1 +/- 0.04; NR1/NR2B-S1323A, 0.42 +/- 0.03, $p < 0.05$). Response to 100 μ M NMDA, however, was not different with the NR2B-S1323A recombinant receptor (Fig 7D). These results establish that Ser-1323 on NR2B is a necessary determinant for NR2B mechanosensitivity, providing an intriguing mechanism for potentially augmenting the mechanical tone of NMDARs.

DISCUSSION

In this report, we examine the mechanisms regulating the dynamic mechanosensitivity of the NMDAR. Using a recombinant system, we showed that the mechanosensitivity of the NMDAR is prominently regulated by the NR2B subunit. Furthermore, we identified that the NR2B C-terminal tail and a known PKC phosphorylation site significantly controls mechanosensitivity. This suggests that PKC mediated phosphorylation of NR2B can influence mechanical tone of the NMDAR, similar to how post-translation modifications can alter receptor activity.

Models used to evaluate NMDAR mechanosensitivity

These data build on previous studies of the mechanical responsiveness of the NMDAR conducted by Paoletti, Casado, and Ascher (Paoletti and Ascher 1994, Casado and Ascher 1998), and are linked to studies conducted by Zhang et al (1996) in the same time period. Using a series of isolated membrane patch samples from mouse cortical

neurons or recombinant receptors expressed in HEK 293 cells, Ascher and colleagues showed that the membrane tension is a primary factor that influences NMDAR mechanosensitivity. Partly because the mechanical input in these past experiments was transferred through the plasma membrane by applying positive or negative pressures to the isolated patch, these past studies showed little role for the intracellular domains of either the NR2A or NR2B subunits in modulating the measured mechanosensitivity (Casado and Ascher 1998). Moreover, any effect of slowly applied membrane tension was reversible when the mechanical perturbation was removed. Rather than using slowly applied membrane expansion or contraction of membrane patch samples, our studies more closely resemble the work by Zhang et al. who exposed cells adhered to a flexible membrane to a single dynamic stretch. In the Zhang studies, the mechanical perturbation was temporary and the cells were returned to their pre-stretch state within 100 milliseconds. We estimate that our model, along with that used by Zhang and colleagues, is different from the Ascher model as mechanical forces are exerted on NMDARs through both the plasma membrane and indirectly through the intracellular domains coupled to the cytoskeleton. Unlike the Ascher studies, this dynamic perturbation causes an irreversible change in the physiological properties of the NMDAR, leading to a persisting calcium increase and, in primary neurons, an altered response to NMDA (Zhang et al 1996).

Our studies extend this past work by evaluating subunit specificity and regulation of NMDAR mechanosensitivity. We eliminated the potential complicating factors caused by studying mechanical stretch in cortical neurons by investigating

mechanosensitivity on recombinant receptors in a well characterized expression system (Kendrick et al 1996, Grant et al 1998, Guttman et al 2001, Lynch and Guttman 2001, Wu et al 2007). Potential confounding factors in cortical neurons include the enhanced or rapid release of glutamate vesicles in the presynaptic bouton after stretch, the transient impairment of glutamate uptake by astrocytes, or the physical widening of the synaptic cleft caused by mechanical stretch – all of which can mask the observation of the direct stretch effect on the NMDAR. Our recombinant receptor approach also avoids the complications from blocking different receptor populations in primary neurons with antagonists, some of which are known to have only modestly higher affinity for different subunits (Neyton and Paoletti, 2006). We minimized or eliminated these confounding factors in our system, and used the recombinant receptor approach to study how the receptor subunit composition and domains of individual receptors control this dynamic mechanosensitivity and identified, for the first time, a specific site on the NR2B subunit which provides significant control of NMDAR mechanosensitivity.

NR2B mechanosensitivity regulated by intracellular C-terminal tail

These data show that the NR2B intracellular domain is a critical regulator of mechanosensitivity. One mechanism that can regulate this differential effect is the physical coupling of the NMDAR subunits to the structural elements of the neuronal cytoskeleton. Past work demonstrates that cytoskeletal destabilization in cultured neurons significantly reduces the stretch response (Geddes-Klein et al 2006). Although both NR2A and NR2B have identified cytoskeletal binding sites, NR2B is thought to be

more strongly tethered through its binding of alpha-actinin (Wyszynski et al 1997) and spectrin (Wechsler and Teichberg 1998). Indeed, much of this tethering of NR2B occurs within the intracellular domain (aa 1036-1433) of NR2B that we have identified as a critical region in defining NR2B mechanosensitivity. However, the loss of stretch sensitivity in truncated NR2B expressing receptors was not complete and suggests that residual stretch sensitivity may be due to force transfer through the remaining C-terminal tail or through the plasma membrane. This coupling to the cytoskeleton may be modulated by the distal C-terminus as well, where we found evidence suggesting that the mechanosensitivity is slightly enhanced when this region is deleted. One possibility is that proteins binding to this domain, including PSD-95, may serve as a mechanical clutch by instituting a mechanical compliance to the stretch sensitivity of the receptor. Furthermore, as the postsynaptic density of a dendritic spine contains numerous and diverse set of proteins, the entire macromolecule structure may serve to potentially mitigate force transfer from the cytoskeleton to the receptor. One intriguing possibility, for further study, is the potential regulation of mechanosensitivity by alternatively spliced cassettes in NR1. We utilized NR1a in our studies, which contains all alternatively spliced regions, but there is evidence that alternatively spliced cytoplasmic regions of NR1 are responsible for tethering to neurofilament (Ehlers et al 1998) and microtubule filaments (Matsuda and Hirai 1999), providing a mechanism for different NR1 splice variants to exhibit differential stretch sensitivity. Unfortunately, our attempts to further examine the cytoskeletal role in mechanosensitivity were hampered by the inability to

sufficiently destabilize the cytoskeleton network in HEK 293s without adversely affecting cell health.

Although the C-terminus of the NR2B subunit is crucial for stretch sensitivity of the NMDAR, the mechanism that regulates the change in NMDAR physiology after stretch appears linked to the pore region of the NR2 subunit. Past work showed that dynamic stretch directly changes the efficiency of the magnesium block at normal resting membrane potential (Zhang et al 1996). We observed that MK801 pretreatment reduced, but did not eliminate, the proportion of cells responding to stretch, unlike its complete inhibitory effect in NMDA stimulated cultures. MK801 and Mg^{2+} both block conductance through binding of a well defined region of the NMDAR pore (Kashiwagi et al 2002), and thus stretch may induce a change in the pore region that could alter both the inherent Mg^{2+} block as well as MK801 effectiveness. This change in the pore region appears to persist, as others note the stretch-induced relief of the magnesium block can persist for at least 6 hours after the initial, single stretch. It is important to note, that glutamate binding is still necessary for the mechanosensitivity of NMDARs, as treatment with the competitive antagonist APV completely eliminated the stretch response. We have no data measuring any potential change in affinity for either glutamate or NMDA to activate these recombinant receptors after stretch, which may be key information to collect in the future to understand if stretch will also selectively alter this physiological feature of the receptor. In many ways, these studies point to the possibility that mechanical force can selectively modulate the physiology of the NMDAR by enhancing currents, differentially controlling activation of different subtypes, and altering the

affinities of agonists and modulatory agents. Thus, stretch induced receptor modulation can potentially act as a post-translational modification, similar to phosphorylation events which are known to significantly alter receptor activity (Chen and Roche 2007).

PKC regulation of NMDAR mechanosensitivity

Pinpointing a single residue on NR2B that controls a majority of the NMDAR mechanosensitivity is potentially important in the regulation of neuronal injury. Both serine/threonine and tyrosine phosphorylation sites on NR2 subunits are well known regulatory mechanisms that can augment NMDAR current (Lynch and Guttman 2001, Salter and Kalia 2004, Jones and Leonard 2005, Chen and Roche 2007). PKC has phosphorylation sites on both NR2A and NR2B and its activity is known to both directly and indirectly potentiate NMDAR current (Liao et al 2001, Lynch and Guttman 2001, Salter and Kalia 2004, Jones and Leonard 2005). The specific site that we found to regulate mechanosensitivity of NR2B, Ser-1323, is one of two PKC phosphorylation sites known to be directly linked to PKC and insulin mediated enhancement of NMDAR currents (Liao et al 2001). Although it is unknown how this site functionally relates to changes in NR1/NR2B-NMDAR activity, PKC potentiation of NMDAR current mediates a reduction in the normal magnesium block of the receptor (Chen and Huang 1992). The role of PKC in NMDAR mechanosensitivity is less clear. In their observation of stretch induced loss in Mg^{2+} block, Zhang et al (1996) showed that PKC inhibition partially restored the block. However, results from our own lab have showed that PKC activity, acting upon the NR1 subunit, can reduce NMDAR cytoskeletal anchoring and decrease

stretch induced calcium influx (Geddes-Klein et al 2006). Here, we demonstrate that mutation of Ser-1323 and PKC inhibition through tamoxifen treatment significantly reduced stretch sensitivity of NR2B. As PKC stimulation was not required for mechanosensitivity, it suggests that some basal level of PKC activity is sufficient to induce stretch sensitivity. There is only a slight overlap, though, among the PKC regulation sites influencing NMDAR current regulation and the sites regulating the mechanosensitivity of the receptor. The Ser-1303 site on the NR2B subunit, also known to potentiate NMDAR current, does not have an effect on NR2B mechanosensitivity. Furthermore, the NR2A subunit has two analogous PKC phosphorylation sites at Ser-1291 and Ser-1312, and we found that the NR2A subunit does not confer mechanosensitive properties to the receptor. It thus remains an interesting question as to why one, but not all, of these similar sites has a role in NMDAR mechanosensitivity. Our data adds to the debate over how PKC and its targets play a role in traumatic brain injury, where PKC inhibition can reduce mechanosensitivity (Zhang et al 1996) but PKC activation has recently been reported to improve learning and memory after mild TBI (Zohar et al 2011). Certainly, much of these disparate findings stem from the promiscuous actions of PKC, which have multiple direct and indirect roles in cellular signaling (Nelson et al 2008). Systematically introduced mutations in NR2B now identify a specific region of the NR2B subunit which regulates mechanosensitivity and now provide a template for future studies to test how the control of this mechanosensitivity can affect the post-traumatic consequences of mechanical injury to primary neurons in networks.

Implications of selective NR2B mechanosensitivity

Robust NR2B-based mechanosensitivity, coupled with the absence of sensitivity for NR1/NR2A diheteromeric receptors, is in direct contrast with traditional chemical agonist activation of the NMDAR, where NR1/NR2A-NMDARs are more readily activated than NR1/NR2B-NMDARs (Erreger et al 2005, Santucci and Raghavachari 2008). Interpreted strictly, this would suggest that stretch will preferentially activate NR1/NR2B NMDARs. Importantly, extrasynaptically located NMDARs, which are primarily of the NR1/NR2B subtype are linked to pro-death signaling in models of excitotoxicity through its actions on nitric oxide production (Sattler et al 1999), mitochondrial dysfunction (Hardingham et al 2002), and inhibition of pro-survival transcription (Hardingham et al 2002, Hardingham and Bading 2010). Certainly, NMDARs are well established as mediators of the pathology seen after TBI (Rao et al 2001, Arundine and Tymianksi 2004, Spaethling et al 2007). The rapid blockade of NR1/NR2B NMDARs appears an especially attractive option for treating the consequences of TBI, as it would aid in mitigating calcium influx and resultant signaling from NR2B-NMDARs altered by injury, and this approach is supported by past studies (Okiyama et al 1997, Dempsey et al 2000, DeRidder et al 2006). Additionally, glutamate spillover and glutamate release from glia may provide a means to enhance the activation of nonsynaptic (NR1/NR2B) NMDARs on mechanically injured neurons, pointing to glia as a second potential therapeutic target for controlling the effects of mechanical injury on neurons *in vivo*. However, triheteromeric NMDARs also display mechanosensitive

behavior. There remains some debate within the literature on the timing and relative distribution of triheteromeric NMDARs, with some suggesting that these receptors comprise a significant fraction of only synaptic NMDARs, while others suggest that these receptors also extend into extrasynaptic locations (Tovar and Westbrook 1999, Al-Hallaq et al 2007, Rauner and Kohr 2010). Our past work shows that synaptic NMDARs represent a majority of the immediate stretch induced calcium flux in primary cortical neurons, (Geddes-Klein et al 2006). These past data, when combined with our current results, suggest that synaptic triheteromeric NMDARs could represent a significant fraction of the calcium influx in primary neurons after stretch. Synaptic signaling through NMDARs is receiving attention for its ability to stimulate prosurvival programs, suggesting that mechanoactivation of NR1/NR2B and triheteromeric NMDARs may provide competing signals for neuronal survival. Determining how these two primary signaling pathways contribute across the mechanical injury spectrum, and how these signaling sources are influenced by nonmechanical factors that include enhanced presynaptic glutamate release, alterations in glutamate uptake and recycling, and glial-based glutamate release, are key factors in understanding how mechanical injury may be distinct from excitotoxic neuronal injury. Given our results, it is likely that mechanical activation of the receptor will lead to biochemical signaling profiles that are distinct from chemical NMDA activation profiles. Future work in this area can help elucidate distinct injury consequences that may prove to be better therapeutic targets and therefore warrant new treatment strategies.

Chapter 3: Stochastic model of NMDA receptor subtype activation during physiologic glutamatergic neurotransmission

ABSTRACT

NMDA receptors (NMDARs) are the major mediator of the postsynaptic response during synaptic neurotransmission. The diversity of roles for NMDARs in influencing synaptic plasticity and neuronal survival is often linked to selective activation of multiple NMDAR subtypes (NR1/NR2A-NMDARs, NR1/NR2B-NMDARs, and triheteromeric NR1/NR2A/NR2B-NMDARs). However, the lack of available pharmacological tools to block specific NMDAR populations leads to debates on the potential role for each NMDAR subtype in physiological signaling, including different models of synaptic plasticity. Here, we developed a computational model of glutamatergic signaling at a prototypical dendritic spine to examine the patterns of NMDAR subtype activation at temporal and spatial resolutions that are difficult to obtain experimentally. We demonstrate that NMDAR subtypes have different dynamic ranges of activation, with NR1/NR2A-NMDAR activation sensitive at univesicular glutamate release conditions, and NR2B containing NMDARs contributing at conditions of multivesicular release. We further show that NR1/NR2A-NMDAR signaling dominates in conditions simulating long-term depression (LTD), while the contribution of NR2B containing NMDAR significantly increases for stimulation frequencies that approximate long-term potentiation (LTP). Finally, we show that NR1/NR2A-NMDAR content significantly enhances response magnitude and fidelity at single synapses during chemical LTP and spike timed dependent plasticity induction, pointing out an important developmental

¹Parts of chapter 3 are reprinted from Singh et al, 2011. PLoS Comp Biol. 7(6)

switch in synaptic maturation. Together, our model suggests that NMDAR subtypes are differentially activated during different types of physiological glutamatergic signaling, enhancing the ability for individual spines to produce unique responses to these different inputs.

INTRODUCTION

Synaptic neurotransmission in excitatory neural circuits is governed primarily by the activation of AMPA receptors (AMPA receptors) and NMDA receptors (NMDARs), two types of ionotropic glutamate receptors located on dendritic spines. Although AMPARs are critical in mediating action potential firing through neuronal networks, NMDARs are often more critical in adaptation of the network during neuronal development (Shi et al. 1999, Adesnik et al. 2008), learning, and memory (Morris et al. 1986, Sakimura et al. 1995, Tsien et al. 1996, Huerta et al. 2000). Moreover, recent evidence shows activation of synaptic NMDA receptors is essential for proper health and maintenance of the neuronal network (Ikonomidou et al. 1999, Hardingham 2006, Hetman and Kharebava 2006). In contrast, persisting high levels of NMDAR activation leads to the induction of numerous signaling pathways that contribute to neuronal death and loss of network function (Dugan et al. 1995, Hardingham et al. 2002, Lynch and Guttman 2002, Arundine et al. 2003). Therefore, activation of NMDARs is a precise balancing act that can control the function and integrity of *in vivo* and *in vitro* neural circuits.

Recent evidence points to the molecular composition of the NMDAR as a possible critical point for regulating the influence of NMDAR activation in networks.

Functional NMDARs are expressed on the neuronal surface as a tetramer, comprised of 2 NR1 subunits and 2 subunits from the NR2 family (NR2A, NR2B, NR2C, and NR2D) (Dingledine et al. 1999, Cull-Candy and Leszkiewicz 2004). The NR2A and NR2B subunit expression dominates in the cortex and hippocampus, with past work showing functional NMDARs are expressed either in a diheteromeric (NR1/NR2A, NR1/NR2B) or triheteromeric form (NR1/NR2A/NR2B) (Monyer et al. 1994, Cull-Candy and Leszkiewicz 2004). Moreover, the NMDAR composition changes through development, with one diheteromeric form (NR1/NR2B) dominating in immature neurons, eventually augmented by NR2A-containing NMDARs at synaptic sites (Williams et al. 1993, Monyer et al. 1994, Liu et al. 2004a). The molecular composition of the receptor, as well as its location, can regulate synaptic plasticity (Liu et al. 2004b, Massey et al. 2004, Foster et al. 2010), receptor trafficking (Kim et al. 2005), and the activation of specific synaptic signaling networks (Waxman and Lynch 2005a, Jin and Feig 2010). More recent reports show that regulation of synaptic changes can be confined to one or a few individual spines, suggesting a need to understand the broad diversity in glutamate receptor signaling that occurs in individual spines (Fedulov et al. 2007, Lee et al. 2009). However, developing a more precise relationship between presynaptic glutamate release and the activation of specific NMDAR subtypes on individual synapses is difficult and technically demanding. Ongoing discussions in the literature and the considerable limitations and caveats of current pharmacological manipulations of individual subtypes (Neyton and Paoletti 2006) have created the need for alternative methods to better examine the activity of specific NMDAR subtypes.

Computational modeling offers an alternative approach for examining the relative balance of NMDAR activation in single spines, with past simulations of glutamatergic signaling used to investigate synaptic communication at temporal and spatial resolutions that are difficult or impossible to study experimentally. The stochastic nature of glutamate receptor activation (Franks et al. 2002, Franks et al. 2003) and their contribution to the quantal properties of synaptic transmission (Franks et al. 2003, Raghavachari and Lisman 2004) reveal the conditions necessary for receptor saturation and explain variation in postsynaptic response. Further investigation into the role of glutamate uptake (Holmes 1995, Rusakov and Kullmann 1998) and spillover (Rusakov and Kullmann 1998, Pankratov and Krishtal 2003, Mitchell et al. 2007) identify their critical roles in modulating the activation profiles at neighboring synapses. The development of NMDAR subtype specific reaction schemes (Erreger et al. 2005) extend the utility of computational models to investigate the differences in activation of different NMDAR subtypes, with a recent study demonstrating the greater probability of activation of NR1/NR2A-NMDARs compared to NR1/NR2B-NMDARs and the role of different subtypes in mediating downstream signaling (Santucci and Raghavachari 2008). Less well described, though, is how synaptic signaling through NMDARs may provide a mechanism to scale synaptic inputs over the physiological range, and how the relative composition of NMDARs on the postsynaptic surface may shape the scaling of the NMDAR response over conditions that span long-term depression (LTD) and long-term potentiation (LTP). Moreover, little is known about how neuronal development

influences NMDAR signaling, and if these changes in neuronal development will shift the NMDAR-based signaling from one receptor subpopulation to another.

In this report, we use computational simulations to examine how NMDAR subtype and overall NMDAR content of the dendritic spine can impact the extent and reliability of synaptic transmission. Further, we determine how the unique properties of activation among NMDAR subtypes create distinct activation patterns among synapses with differing compositions. We show that NR2A-containing NMDARs provide the most dynamic range across univesicular and, to a lesser extent, multivesicular release conditions. Alternatively, the NR2B-containing NMDARs play a larger role in simulated multivesicular release conditions, and contribute more significantly to the NMDAR input during high frequency stimulation. These data are supported by past studies in the literature, and illustrate how the existence of multiple NMDAR subpopulations at individual spines enables the efficient transduction of a wide variety of glutamate signals into unique postsynaptic responses.

METHODS

Geometry and receptor content: We modeled spine geometry as a typical thin spine with an octagonal-shaped spine head (500nm diameter) and long spine neck. We represented the postsynaptic face as a 300nm x 300nm square, separated by 20nm from an identically shaped presynaptic face (Harris et al. 1992). A membrane surrounded the entire presynaptic bouton and postsynaptic spine head, also separated by a 20nm distance from the apposing surfaces. Glutamate receptors randomly decorated the postsynaptic surface

using previous estimates of NMDA and AMPA receptor density along the postsynaptic surface for CA1 neurons (80 AMPARs, 20 NMDARs) (Racca et al. 2000, Sheng and Hoogenraad 2007). To examine differences in activation parameters among NMDAR subtypes, simulations used a uniform composition of receptors along the postsynaptic face, represented with either 20 NR1/NR2A-NMDARs, 20 NR1/NR2B-NMDARs, or 20 NR1/NR2A/NR2B-NMDARs. Based on the relative amounts of NR2A and NR2B shown to be localized within the postsynaptic density (PSD) (Cheng et al. 2006), we developed another distribution for some simulations, where the 20 synaptic NMDARs were divided into 8 NR1/NR2A-NMDARs, 8 NR1/NR2A/NR2B-NMDARs and 4 NR1/NR2B-NMDARs. As previous reports show that approximately 30% of all NMDARs are located extrasynaptically (Harris and Pettit 2007), we placed 10 extrasynaptic NR1/NR2B-NMDARs randomly along the sides of the spine head.

Glutamate release: Glutamate was released in the synaptic cleft as a point source near the center of the face of the presynaptic bouton. Both univesicular and multivesicular release profiles were simulated. Single vesicles of glutamate ranged from 500-1,500 molecules, as defined by previous reports (Burger et al. 1989, Schikorski and Stevens 1997). We modeled multivesicular release using the simultaneous release of a larger number of glutamate molecules (2,500-10,000) in the cleft, assuming an available releasable pool of 5-20 vesicles in the hippocampal synapse (Schikorski and Stevens 2001). A limited set of simulations showed that the release of a large number of

glutamate molecules from the center of the cleft did not produce results significantly different from simulations using multiple release of individual vesicles (data not shown).

In simulations of varied frequency stimulus trains, presynaptic stimulation (5-100Hz for 1 second) was modeled to generate random glutamate vesicle release profiles, defined by the calculation of frequency dependent release probabilities (Pr) (Kandaswamy et al. 2010). Briefly, this model utilizes stimulus trains to calculate presynaptic facilitation and augmentation, two calcium dependent components which influence the probability of vesicle release. Additionally, the state and recovery of two glutamate vesicle pools, the readily releasable pool and recycling pool, are observed to account for vesicle rundown during the stimulus. Frequency dependent parameters (personal communication, V. Klyachko) were thus used to generate Pr at each individual spike which, along with the state of the readily releasable pool, was used to determine if each spike resulted in a released vesicle. Distinct vesicle release profiles were generated for 100 simulations per frequency, each of which was applied to our dendritic spine model with a physiologic representation of NMDAR subtypes.

Glutamate receptor state modeling: Glutamate binding and activation of AMPARs and NMDAR subtypes was modeled by implementing previously published reaction schemes (Fig 1). The AMPAR activation model of Jonas et al. includes the binding of two glutamate molecules and three receptor desensitized states (Jonas et al. 1993). NMDAR activation was modeled using the reaction scheme of Erreger et al. (2005), which contains specific reaction rates for both NR2A-NMDARs and NR2B-NMDARs (Table

1). This scheme includes the binding of two glutamate molecules as well as a dual stage activation and two desensitized states which occur after glutamate binding. The reaction scheme for triheteromeric NMDARs was developed by modeling glutamate binding to both a NR2A and a NR2B subunit and using reaction rates that were averages of the rates for NR2A and NR2B (personal communication – K. Erreger, Santucci and Raghavachari 2008).

D_{glut}	0.2$\mu\text{m}^2\text{ms}^{-1}$ (unless otherwise noted) (Saftenku 2005)
Number of AMPARs	80 (Keller et al.2008)
Total number of synaptic NMDARs	20 (Racca et al. 2000, Sheng and Hoogenraad 2007)
Number of extrasynaptic NMDARs	10 (Harris and Pettit 2007)
Synaptic cleft width	20nm (Harris et al.1992)
Glutamate molecules per vesicle	1,500 (unless otherwise noted) (Burger et al.1989, Schikorski and Stevens 1997)

Table 1: Model parameters

Model parameters: The parameters used in the model are summarized in Table 1. Unless otherwise noted, our models used a glutamate diffusion constant of $0.2\mu\text{m}^2/\text{ms}^{-1}$ (Saftenku 2005), which is on the lower end of the range of estimated glutamate diffusion constants that have been reported in the literature. All surface boundaries of the spine, presynaptic membrane, and surrounding neuropil membrane reflected glutamate molecules. Table 2 summarizes the rate constants used to describe receptor kinetics for AMPARs and NMDAR subtypes.

Analysis: Simulations were carried out using Smoldyn 1.84, a spatial stochastic simulator for biochemical reaction networks (Andrews and Bray 2004, Andrews 2009).

Smoldyn models biomolecular reactions by using reaction rates to compute binding radii and diffusion rates to determine spatial position of potential reactants. All simulations had time steps of 0.01ms, based on a numerical convergence study showing that the simulations results did not differ between time steps of either 0.01ms or 0.001ms. Unless otherwise noted, simulations were terminated when the solution reached 1 second. The state of all available receptors (glutamate bound, open, glutamate unbound, etc), the number of receptors in each state, the location of all receptors, and the position of released glutamate molecules was tracked for all simulations. Post-processing of model results was performed with user-generated scripts developed in MATLAB (Mathworks, Natick, MA). Statistical significance among multiple group comparisons was found using ANOVA and posthoc Tukey's analysis. Analyzing receptor opening distribution profiles was accomplished using two-sample Kolmogorov-Smirnov tests to determine significance between cumulative frequency distributions.

Calcium entry: Calcium entry into the spine was computed by using an iterative process to calculate change in membrane voltage potential (V_m) and the probability for open NMDARs to be blocked by magnesium (Mg^{2+}). We used the relationship established by Jahr and Stevens (1990) to calculate the probability of each receptor to be blocked by magnesium at each time step, defined as

$$P_{unblocked}(V_m) = \frac{1}{1 + e^{-(0.062V_m)} \cdot [Mg^{2+}] / 3.57}$$

We assumed a magnesium concentration of 0.8mM, and calculated V_m at each time step by finding the incremental change in V_m dictated by total ionic flux through AMPARs and NMDARs by

$$\Delta V_m = \frac{(I_{AMPA} + I_{NMDA} - I_{leak})}{C_m} \Delta t ,$$

where I_{AMPA} , I_{NMDA} , and I_{leak} are calculated using

$$I_{AMPA} = g_{AMPA} (V_m - E_{AMPA}) N_{AMPA}$$

$$I_{NMDA} = g_{NMDA} (V_m - E_{NMDA}) N_{NMDA}$$

$$I_{leak} = g_{leak} (V_m - E_{leak})$$

N_{AMPA} and N_{NMDA} are the number of open receptors of each receptor type. It was assumed that g_{AMPA} and g_{NMDA} , the single channel conductance for each receptor, was 12pS and 45pS respectively. The reversal potentials, E_{AMPA} and E_{NMDA} , for both AMPARs and NMDARs were assumed to be 0mV. In computing a generalized leak current, a leak conductance, g_{leak} , was assumed to be 10nS, with a reversal potential of -60mV. Finally, the membrane capacitance (C_m) of the spine was found using a reported capacitance density of $1\mu\text{F}/\text{cm}^2$ (Dolowy 1984). The probability for a receptor to be unblocked by magnesium ($P_{unblocked}$) was then used to determine if each individual activated NMDAR, as defined by Smoldyn simulations, was able to conduct calcium in that time step. The number of calcium ions entered per open NMDAR per time step was calculated using a probability distribution of ions entered given by

$$p(n) = \frac{(N_{Ca})^n}{n!} e^{-N_{Ca}}$$

Here, N_{Ca} is the average number of calcium ions entered and is computed by

$$N_{Ca} = \frac{\gamma_{NMDA,Ca} \cdot V_m}{Z_{Ca} \cdot e_c} \Delta t ,$$

where the single channel calcium conductance for NMDARs, $\gamma_{NMDA,Ca}$, is assumed to be 4.5pS, Z_{Ca} is the valence for Ca^{2+} ($z = 2$), and e_c is the elementary charge ($1.6 \times 10^{-19}C$).

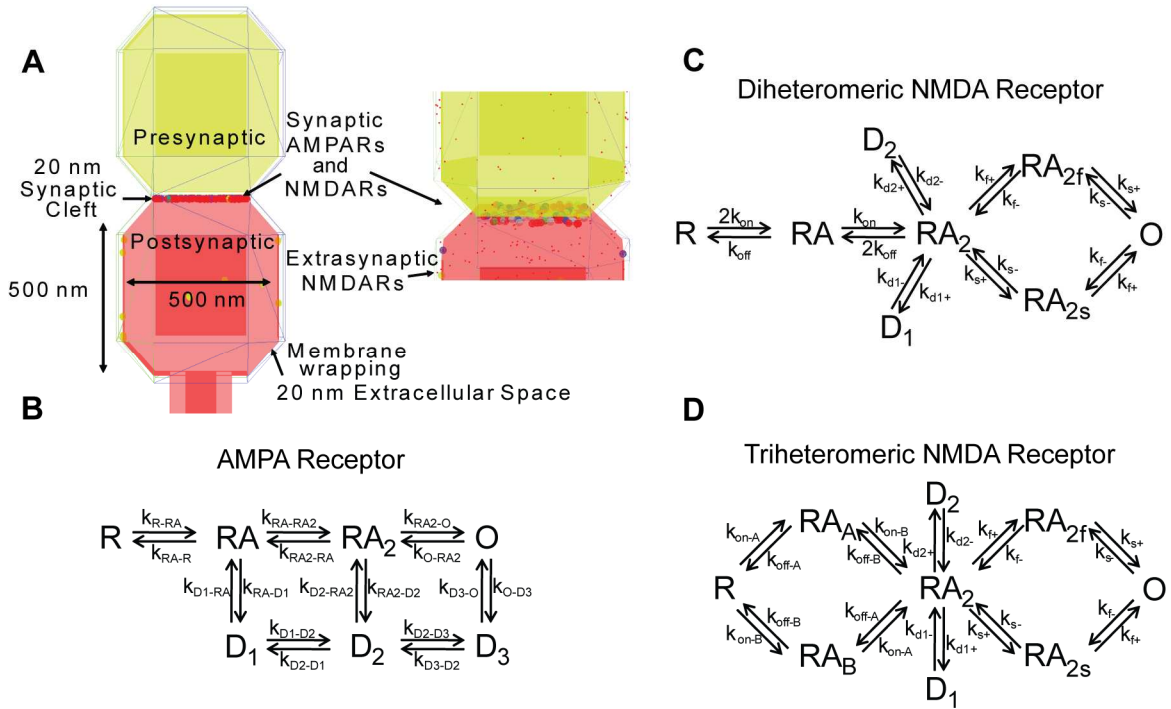


Figure 1: Dendritic spine model geometry and receptor activation schemes. (A) Representation of the computational model of the dendritic spine, which includes a 20nm synaptic cleft. The postsynaptic compartment contains synaptic AMPARs and NMDARs and extrasynaptic NMDARs. Activation of glutamate receptors were determined using previously established reaction schemes for (B) AMPARs, (C) NR2A-NMDARs and NR2B-NMDARs, and (D) triheteromeric NR2A/NR2B-NMDARs. Constants used in the reaction schemes are provided in Table 2. Simulations tracked all receptor states, and reported the fraction of open receptors.

		NR2A- NMDAR (Erreger et al 2005)	NR2B- NMDAR (Erreger et al 2005)	NR2A/NR2B- NMDAR (Santucci and Raghavachari 2008)	AMPA (Jonas et al 1993)
k_{on}	($\text{nm}^3 \text{ms}^{-1}$)	52,456	4,698		
k_{on-A}	($\text{nm}^3 \text{ms}^{-1}$)			52,456	
k_{on-B}	($\text{nm}^3 \text{ms}^{-1}$)			4,698	
k_{off}	(ms^{-1})	1.010	0.0381		
k_{off-A}	(ms^{-1})			1.010	
k_{off-B}	(ms^{-1})			0.0381	
k_{s+}	(ms^{-1})	0.230	0.048	0.139	
k_{s-}	(ms^{-1})	0.178	0.230	0.204	
k_{f+}	(ms^{-1})	3.140	2.836	2.988	
k_{f-}	(ms^{-1})	0.174	0.175	0.1745	
k_{d1+}	(ms^{-1})	0.0851	0.550	0.318	
k_{d1-}	(ms^{-1})	0.0297	0.0814	0.0556	
k_{d2+}	(ms^{-1})	0.230	0.112	0.171	
k_{d2-}	(ms^{-1})	0.00101	0.00091	0.00096	
k_{R-RA}	($\text{nm}^3 \text{ms}^{-1}$)				7619.4
k_{RA-R}	(ms^{-1})				4.260
k_{RA-RA2}	($\text{nm}^3 \text{ms}^{-1}$)				47,144
k_{RA2-RA}	(ms^{-1})				3.260
k_{RA2-O}	(ms^{-1})				4.240
k_{O-RA2}	(ms^{-1})				0.900
k_{RA-D1}	(ms^{-1})				2.890
k_{D1-RA}	(ms^{-1})				0.0392
k_{RA2-D2}	(ms^{-1})				0.172
k_{D2-RA2}	(ms^{-1})				0.000727
k_{O-D3}	(ms^{-1})				0.0177
k_{D3-O}	(ms^{-1})				0.004
k_{D1-D2}	($\text{nm}^3 \text{ms}^{-1}$)				2,108.2
k_{D2-D1}	(ms^{-1})				0.0457
k_{D2-D3}	(ms^{-1})				0.0168
k_{D3-D2}	(ms^{-1})				0.1904

Table 2: Reaction rates used for AMPAR and NMDAR subtype activation.

RESULTS

We created a stochastic model of glutamatergic signaling at the dendritic spine to study the differences in NMDAR subtype activation among several physiological conditions. We used Smoldyn (Version 1.84) (Andrews and Bray 2004, Andrews 2009), a spatial stochastic simulator for biochemical reaction networks, and developed a model using the typical dimensions of a mature, thin spine (Harris et al. 1992) (Fig 1A). With the understanding that activity across multiple types of synapses throughout the brain can vary significantly, in these studies we intended to examine receptor activation at a prototypical synapse to broaden the applicability of our results. We utilized previously published reaction schemes (Fig 1B,C,D) for the activation of specific NMDAR subtypes (Erreger et al. 2005) and AMPARs (Jonas et al. 1993) (see methods for more details). We restricted nearly all of our analysis to the open state for each receptor, defined when glutamate is bound to receptor subunits and has transitioned into an activated state. We studied three primary aspects of synaptic signaling with this model: the scaling and relative activation of different synaptic glutamate receptors across conditions of univesicular and multivesicular release, the transition in signaling that occurs for physiological conditions that span LTP and LTD, and the relative change in NMDAR-based synaptic signaling that occurs during synaptic maturation, when synapses shift from containing nearly all NR1/NR2B-NMDARs to a mix of either NR1/NR2A or NR2A/NR2B-NMDARs.

Sensitivity to glutamate diffusion rate

We first sought to examine the sensitivity of receptor activation to the glutamate diffusion rate (D_{glu}). Published estimates on the effective glutamate diffusion rate have varied from 0.2 to $0.76 \mu\text{m}^2\text{ms}^{-1}$ (Mitchell et al. 2007) and it is likely that this variation can affect the extent of activation among AMPARs and NMDAR subtypes. Similar to previous models (Franks et al. 2002, Keller et al. 2008) we populated the postsynaptic face of the spine with 80 AMPARs and 20 NMDARs of a single type - NR1/NR2A-NMDARs, NR1/NR2B-NMDARs, or triheteromeric NR1/NR2A/NR2B-NMDARs. Activation was observed after a point release of 3000 glutamate molecules with varied D_{glu} , $0.2 - 0.4 \mu\text{m}^2\text{ms}^{-1}$, a range of commonly used rates in recent models (Rusakov 2001, Franks et al. 2002, Saftenku 2005, Mitchell et al. 2007). Predictably, the general trend for all receptors was increased numbers of activated receptors for the slower diffusion rates (Fig 2A). Quantified, the peak percent of activated receptors after glutamate release was significantly greater at $D_{\text{glu}} = 0.2 \mu\text{m}^2\text{ms}^{-1}$, for AMPARs and all NMDAR subtypes ($p < 0.05$ compared to $0.4 \mu\text{m}^2\text{ms}^{-1}$) (Fig 2B). Interestingly, AMPAR activation was the most sensitive to D_{glu} , producing the largest percent change among receptors, while all NMDAR subtypes had similar sensitivities. This suggests that while D_{glu} may effectively scale NMDAR activation, the relative patterns of activation among subtypes is unaffected. Thus, with the understanding that D_{glu} can impact receptor activation, all subsequent simulations were conducted with a rate of $0.2 \mu\text{m}^2\text{ms}^{-1}$, a rate which is reported to account for molecular obstacles and overcrowding (Saftenku 2005). To provide a direct comparison between the subsequent simulations and earlier studies of

AMPA and NMDAR activation (Jonas et al. 1993, Franks et al. 2002, Erreger et al. 2005, Santucci and Raghavachari 2008), we used the same kinetic parameters for the receptor activation scheme as used in these previous studies.

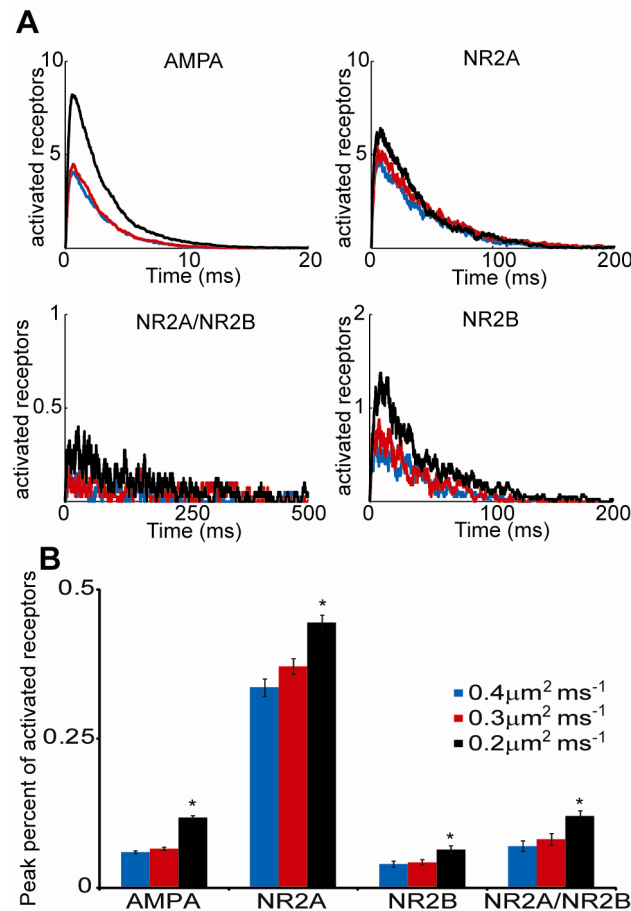


Figure 2: Differential sensitivity to diffusion rate among glutamate receptors. (A) Activation of synaptically localized 80 AMPARs and 20 NMDARs of single subtype was observed in response to a release of 3000 glutamate molecules with differing glutamate diffusion rates ($0.2 \mu\text{m}^2 \text{ms}^{-1}$, black; $0.3 \mu\text{m}^2 \text{ms}^{-1}$, red; $0.4 \mu\text{m}^2 \text{ms}^{-1}$, blue). (B) The peak percent of open receptors was predictably decreased for all receptors at higher glutamate diffusion rates. AMPARs displayed the most sensitivity of diffusion rate between 0.2 and $0.4 \mu\text{m}^2 \text{ms}^{-1}$, while NMDAR subtypes all behaved similarly. (* $p < 0.05$ compared to $0.4 \mu\text{m}^2 \text{ms}^{-1}$)

Dynamic range of activation for synaptic glutamate receptors

Our next objective was to define how either a single or near simultaneous release of multiple glutamate vesicles from the presynaptic bouton would activate AMPARs and NMDARs on the postsynaptic surface. Again, the postsynaptic face of the spine with 80 AMPARs and 20 NMDARs of a single type - NR1/NR2A-NMDARs, NR1/NR2B-NMDARs, or triheteromeric NR1/NR2A/NR2B-NMDARs. Physiologically, the size and glutamate concentration of synaptic glutamate vesicles can vary, with approximate glutamate content of 500 – 1,500 molecules (Burger et al. 1989, Schikorski and Stevens 1997). Across this entire range of glutamate release conditions, the concentration of glutamate in the synaptic cleft decayed rapidly to less than 10% of its peak value within 3-5 milliseconds. AMPAR peak activation significantly increased throughout the entire range of released glutamate (Fig 3D), ranging from 0.8% +/- 0.1% (mean +/- standard error) at 500 molecules to 42.1% +/- 0.4% at 10,000 molecules. The AMPA response showed no noticeable saturation across the range of glutamate release conditions tested, indicating this receptor population will show a dynamic scaling across the entire range of simulated conditions.

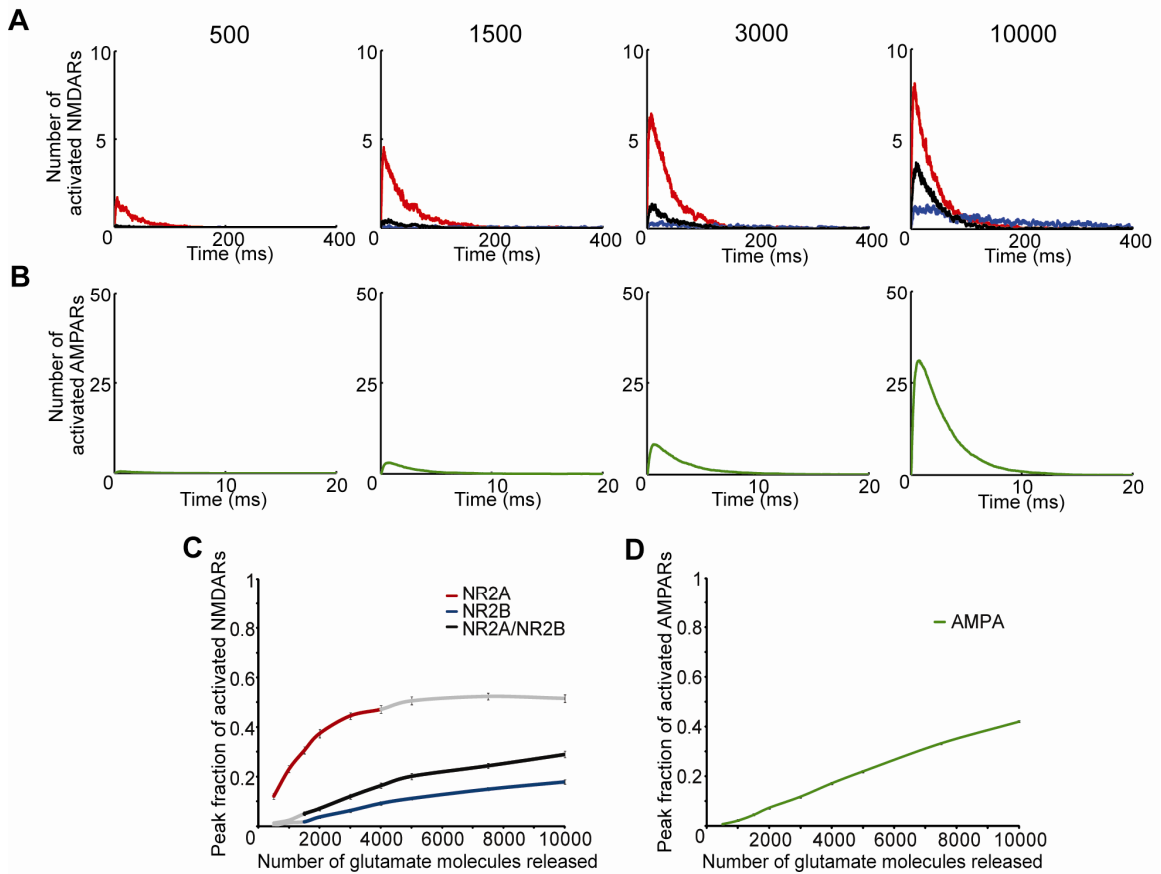


Figure 3: NMDAR subtype specific dynamic range. Activation or opening of each receptor subtype was observed in response to varied levels of glutamate release (500 – 10,000 molecules, number denoted above graphs in A). Number of activated (A) NMDA receptors over time is shown for NR2A (red), NR2B (blue), and NR2A/NR2B (black) and (B) AMPA receptors in response to 500, 1,500, 3,000, and 10,000 molecules. (C) NR2A-NMDARs show a significantly higher fraction activation compared to the other subtypes. NR2A-NMDAR activation increases ($p < 0.05$) over the physiological range of univesicular glutamate release (500-1,500 molecules), but saturates at larger glutamate levels (shaded in gray), while activation of NR2B-containing NMDARs significantly increases only in the range of multivesicular glutamate release (2,000-10,000) ($p < 0.05$). Colored segments represent regimes of increased activation compared to preceding release amount ($p < 0.05$) (D) Peak percent of AMPARs significantly increases over the entire range of modeled glutamate release ($p < 0.05$). ($n = 40$ simulations per condition)

In contrast to AMPAR response, the activation of different NMDAR subtypes was influenced strongly by the amount of initial glutamate release. The peak percent of activated receptors increased most rapidly with NR1/NR2A-NMDARs, in agreement with results from Santucci and Raghavachari (2008). Across conditions modeling

univesicular release, a scaled NMDAR response occurred only with NR1/NR2A-NMDARs. After a release of 500 molecules, mean peak percent of activated receptors was 12.1% \pm 1.1% for NR1/NR2A-NMDARs, 1.3% \pm 0.4% for triheteromeric NMDARs, and 0.4% \pm 0.2% for NR1/NR2B-NMDARs, compared to 30.6% \pm 1.4%, 5.1% \pm 0.8%, and 1.8% \pm 0.5%, respectively, after release of 1,500 molecules (Fig 3C). In conditions approximating multi-vesicular release, NR1/NR2A-NMDAR activation saturates, with no additional significant increase after 4,000 molecules. In comparison, activation significantly increases for both NR1/NR2B-NMDARs and triheteromeric NMDARs; from 1,500 to 10,000 molecules, the activation of NR1/NR2B-NMDARs steadily increases from 1.9% \pm 0.5% to 17.9% \pm 0.9%, while the NR1/NR2A/NR2B-NMDARs increase from 5.1% \pm 0.8% to 29% \pm 1.3%. Together, these simulation results show three behavior regimes for NMDARs – an initial phase dominated by NR1/NR2A-NMDAR activation, followed by a second phase that includes contribution of all NMDAR subtypes, and a third phase where scaling of the synaptic NMDAR response is prominently driven by the NR1/NR2B-NMDARs.

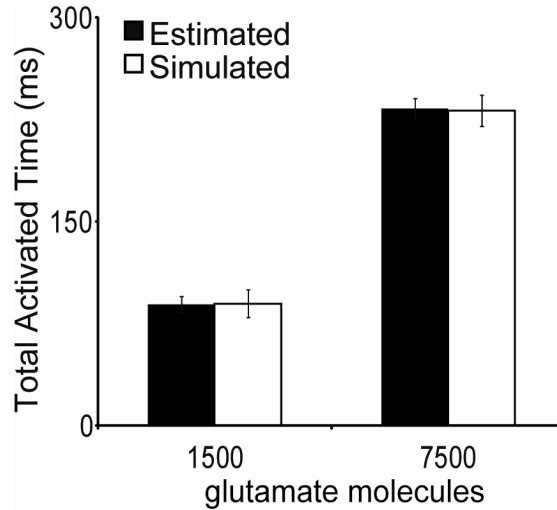


Figure 4: Subtype activation scalability to physiological synapse. Average response of an individual receptor for each subtype can be used to estimate the total synaptic response of a mixed population of receptor subtypes (8 NR2A, 8 NR2A/NR2B, and 4 NR2B) that is not different from responses observed when the activation of this mixed population is indeed simulated. (n = 40 simulations per condition)

Although these results illustrate the behavior of subtypes in isolation, they do not provide a realistic picture of the synaptic composition that appears over time in cultured neurons, or in different brain regions. Rather than using a large number of simulations to examine all possible combinations of NR2A, NR2A/NR2B, and NR2B NMDARs at a physiological synapse, we tested if predictions from a proportional scaling of the response from individual receptor subtypes would match simulations of synapse populated with a mixture of different NMDAR subtypes. We computed the average activation time for an individual receptor for each subtype, scaled this proportionally for the number of these receptors appearing at a ‘mixed’ synapse, and produced estimates of the total synaptic activation time from a single, glutamate release event. Our ‘mixed’ synapse included 8 NR1/NR2A-NMDARs, 8 NR1/NR2A/NR2B-NMDARs, 4 and NR1/NR2B-NMDARs. Proportional scaling estimates of the total activation time for a

release of 1500 and 7500 glutamate molecules were not statistically different from stochastic simulation of the same ‘mixed’ synaptic formulation (Fig 4). These results indicate that it is possible to use the response of individual subtypes to correctly predict the synaptic response to a diverse set of receptors.

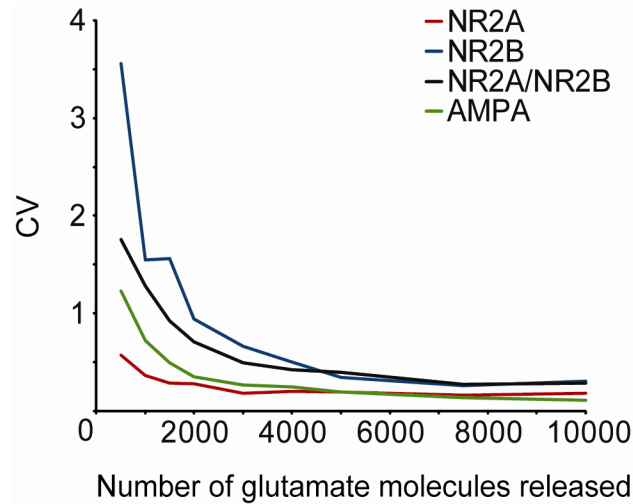


Figure 5: Fidelity of subtype activation. The stochastic variation in response, reflected in the coefficient of variance calculated for receptor opening, is greatest for NR2B-containing NMDARs at low levels of glutamate release, but variation is decreased for each glutamate receptor subtype at large numbers of released glutamate.

Fidelity of the synaptic response is receptor dependent

These simulations also provide information on the consistency or fidelity of the synaptic response. We define the fidelity of the response as the variance in the numbers of receptors activated for a specified number of glutamate molecules released from the presynaptic bouton. As expected, an increase in the amount of glutamate released leads to a decrease in the calculated coefficient of variance (CV) for the postsynaptic AMPAR response. In general, the CV for all receptors asymptotically decreased at larger levels of released glutamate (Fig 5), and the range of the predicted stabilized CV is within the

range of similar measures reported for dissociated hippocampal neurons and slice cultures (0.2-0.6) (Lisman et al. 2007). Each receptor type showed a different transition point for achieving a stable synaptic signal response. For simulations releasing more than 5,000 glutamate molecules, there was no significant reduction in the CV for the AMPAR response. Similarly, the CV of the NR1/NR2A-NMDAR did not change significantly when more than 3,000 molecules were released. The NR1/NR2B-NMDARs produced the most variable response, with a relatively large CV calculated for the univesicular release conditions and stable CV achieved for simulations releasing more than 5,000 glutamate molecules. Together, these simulations show that NR1/NR2A-NMDARs provide the largest dynamic range and highest signaling fidelity under conditions of univesicular release, and AMPARs provide a somewhat smaller dynamic range and more variability across the same conditions. At higher levels of glutamate release, the AMPARs retain their dynamic range and improve their fidelity of signaling. Conversely, the NR1/NR2B-containing NMDARs show a more usable dynamic range and improvement in signaling fidelity under multivesicular release conditions.

NMDAR subtypes show distinct temporal activation receptor ‘flickering’ behavior

Both the magnitude and timing of glutamate receptor activation are key parameters that contribute to the type and extent of resultant signaling. The time to the peak activation of AMPARs following the initial release of glutamate was shortest among the studied glutamate receptors, indicating these receptors are well suited as rapid event detectors for glutamate release. Interestingly, the rise time was not significantly different

between NR1/NR2A-NMDARs and NR1/NR2A/NR2B-NMDARs (mean \pm SE; 7.37 \pm 0.30 ms (NR1/NR2A) vs. 12.07 \pm 1.66 ms (NR1/NR2A/NR2B)). Based partly on the affinity of glutamate for the NR2B subunit, the time to peak activation of the NR1/NR2B-NMDARs is significantly slower than all other glutamate receptor types (49.9 \pm 7.2 ms; $p < 0.01$; Fig 6A). Once opened, the NR1/NR2A-NMDARs remained open longer than either the NR1/NR2A/NR2B or NR1/NR2B-NMDARs before transitioning to a bound, closed state (Fig 6B,C) (Kolmogorov–Smirnov test, $p < 0.01$). All NMDARs showed a significantly longer initial activation period than AMPARs ($p < 0.01$).

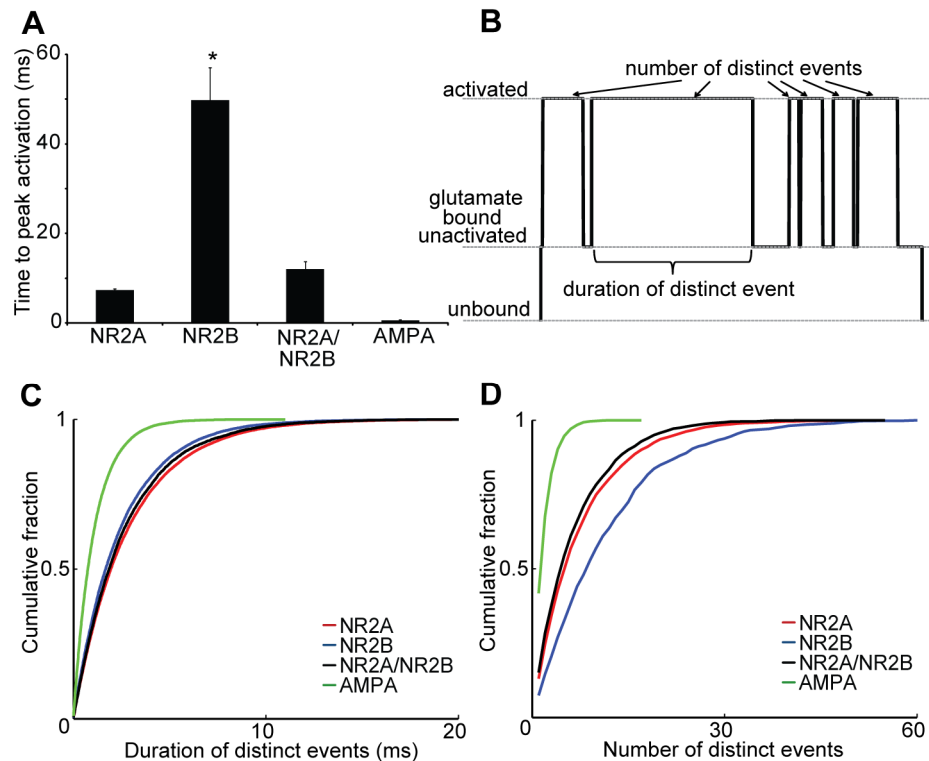


Figure 6: Slower kinetics and increased receptor flickering prolong NR2B activation. The activation events for all NMDARs were analyzed to discern differences in the temporal activation patterns among subtypes. (A) NR2B-NMDARs reach peak activation significantly slower than NR2A-NMDARs and NR2A/NR2B-NMDARs (* $p < 0.05$ NR2B vs NR2A and NR2B vs NR2A/NR2B). (B) Receptor “flickering”, defined by the ability for a receptor to have multiple activation events without glutamate unbinding was analyzed using cumulative distributions to (C) demonstrate that NR2A-NMDARs (red) have significantly longer durations of individual events compared to NR2B-NMDARs (blue), triheteromeric NMDARs (black) and AMPARs (green) (KS test - $p < 0.01$). (D) However, NR2B-NMDARs have significantly more distinct events per binding compared to other subtypes (KS test - $p < 0.01$).

Following the initial activation and opening of each glutamate receptor subtype, all studied receptors showed a stochastic switching between the bound/open and bound/closed state or ‘flickering’ of the receptor (Fig 6D) before dissociation of glutamate from the receptor subunit. Simulations show that NR1/NR2B-NMDARs have more flickering events per glutamate binding than NR1/NR2A-NMDARs and NR1/NR2A/NR2B-NMDARs (Fig 6E,F). For the NR1/NR2B-NMDARs, these results explain why, despite the shorter receptor activated time, NR1/NR2B mediated calcium

currents typically have a slower decay than NR1/NR2A mediated currents (Monyer et al. 1994, Vicini et al. 1998). Again, the diverse responses of these subtypes better allow for unique postsynaptic currents at synapses populated with a diverse set of receptors.

A shift in the pattern of NMDAR subtype activation occurs with stimulation frequency

Activation of NMDARs is a major mediator in several models of synaptic plasticity, including LTP and LTD. Recently, conflicting evidence has emerged on the specific role of distinct NMDAR subtypes for certain types of plasticity (Liu et al. 2004b, Massey et al. 2004, Barria and Malinow 2005, Bartlett et al. 2007). We used our simulations to evaluate glutamatergic signaling and observed the activation patterns of NMDAR subtypes in response to various frequencies of presynaptic stimulation. For these simulations, the spine model was populated with physiologically relevant numbers and localizations of NMDAR subtypes: 8 synaptic NR1/NR2A-NMDARs, 8 synaptic triheteromeric NMDARs, 4 synaptic NR1/NR2B-NMDARs, and 10 extrasynaptic NR1/NR2B-NMDARs. Using common stimulation protocols in the literature (Bear and Malenka 1994) presynaptic stimulation was varied from 5Hz-100Hz and lasted for 1 second. Presynaptic glutamate release was stochastically determined using a recent model of presynaptic vesicular release dynamics (Kandaswamy et al. 2010). All simulations were performed with a uniform synaptic vesicle content (1,500 glutamate

molecules).

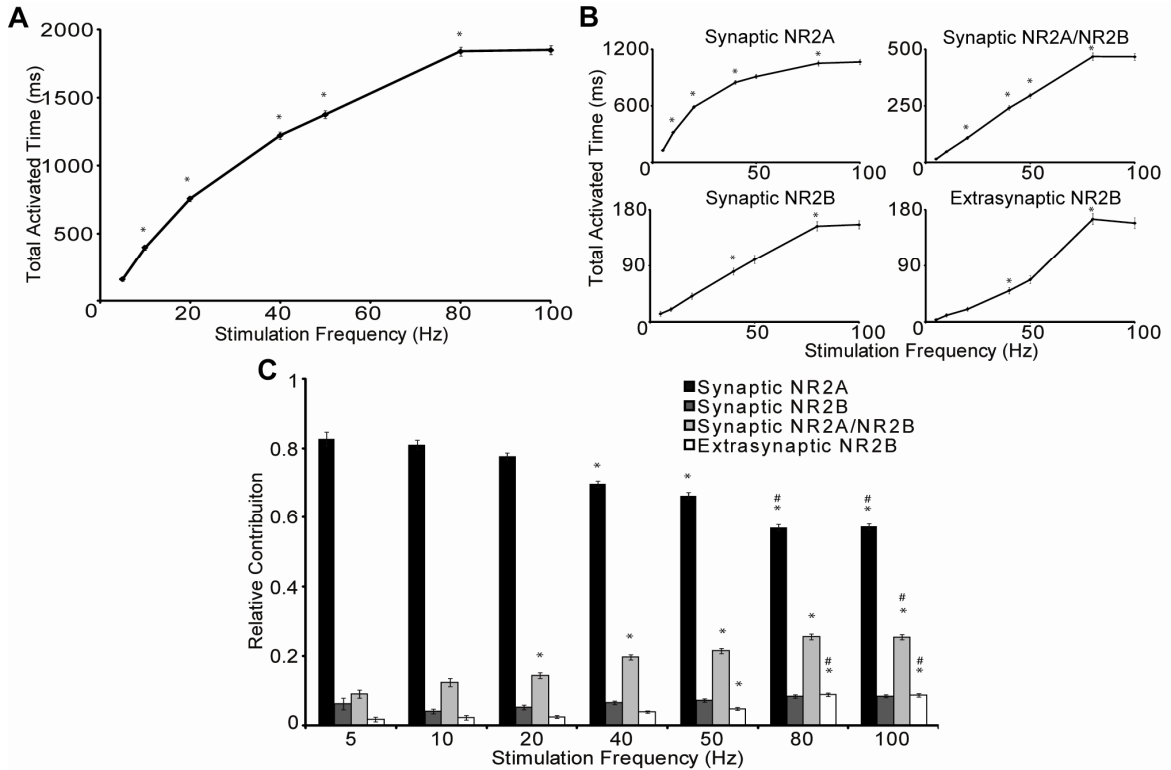


Figure 7: Frequency mediated shifts in NMDAR subtype activation patterns. The dendritic spine model (80 AMPARs, 8 NR1/NR2A NMDARs, 4 NR1/NR2B NMDARs, 4 NR1/NR2A/NR2B, and 10 extrasynaptic NR1/NR2B NMDARs) was subjected to presynaptic stimulation of various frequencies (5Hz – 100Hz), and the stochastic release of glutamate vesicles was simulated using an approach developed for hippocampal synapses [Kandaswamy et al, 2010]. Total activated time increases for (A) all NMDARs and (B) for each NMDAR subtype individually as the stimulation frequency is increased (* $p < 0.05$ significant increase from previous frequency). (C) Relative contribution for each subtype to the total receptor open time shows the changing patterns of NMDAR subtype activation during frequency stimulation, with NR2A-NMDAR contributing less and NR2B containing NMDARs contributing more at high frequency stimulations. (* $p < 0.05$ compared to contribution at 5Hz, # $p < 0.05$ compared to 50Hz) (n = 100 simulations per condition).

The period of NMDAR activation increased significantly across most of the stimulation frequency range, showing saturation above 80 Hz. Activation of the NR1/NR2A-NMDARs at the synapse increased most rapidly at low stimulation frequencies (< 25Hz), tapering slightly beyond 5Hz. In comparison, synaptic

NR1/NR2B-NMDARs, synaptic NR1/NR2A/NR2B-NMDARs, and extrasynaptic NR1/NR2B-NMDARs showed a linear increase in activation over nearly the entire stimulation range. Although the total activation time is dominated by NR1/NR2A-NMDARs at all frequencies, its contribution significantly decreased while the contribution of other subtypes, including NR1/NR2A/NR2B-NMDARs and extrasynaptic NR1/NR2B-NMDARs, significantly increased at higher stimulation frequencies (Fig 7C). This finding demonstrates that the activation patterns of NMDARs differ across stimulation frequencies, suggesting potential NMDAR subtype dependent mechanisms for different modes of synaptic plasticity. As NMDAR subtypes are known to activate different signaling pathways, increasing contribution of NR2B containing NMDARs at higher frequency stimulation may alter the balance of subtype specific signaling, inducing long term synaptic changes.

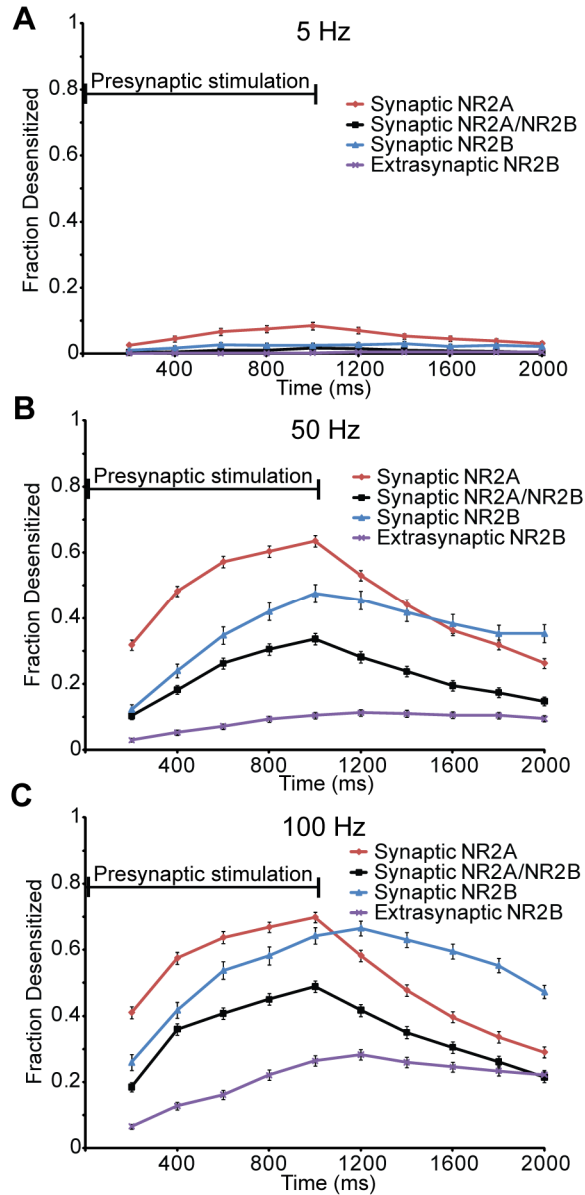


Figure 8: NR2A-NMDARs desensitize and recover faster than other subtypes. The fraction of receptors that are desensitized over a one second stimulation, and one second post stimulation, were recorded for each NMDAR subtype. (A) At 5Hz, only a small portion of NMDARs is desensitized, these are primarily NR2A-NMDARs. At (B) 50Hz and (C) 100Hz, NR2A-NMDARs have a significantly greater fraction of desensitized receptors compared to all other subtypes, while synaptic NR2B-NMDARs show a significantly greater fraction of desensitized receptors compared to triheteromeric NMDARs ($p < 0.05$).

To investigate why NR1/NR2A-NMDAR contribution decreases at higher frequencies, we examined the extent of receptor desensitization for each receptor subtype

both during and after the presynaptic stimulation. Following a 5Hz presynaptic stimulation, only a small fraction of receptors desensitized, and most of these desensitized receptors are NR1/NR2A-NMDARs (Fig 8A). After a 50Hz and 100Hz stimulation (Fig 8B,C), a significantly larger fraction of NR1/NR2A-NMDARs become desensitized compared to other subtypes, primarily due to their higher probability of glutamate binding. Moreover, synaptic NR1/NR2B-NMDARs exhibit a significantly larger fraction of desensitized receptors compared to triheteromeric NR1/NR2A/NR2B-NMDARs and extrasynaptic NR1/NR2B-NMDARs at higher stimulation frequencies, indicating the triheteromeric and extrasynaptic NMDARs may play an important role in sensing a sustained, bursting behavior in networks. In contrast, the NR1/NR2A-NMDARs and NR1/NR2A/NR2B-NMDARs recover faster from receptor desensitization compared to other subtypes (recovery at 1 sec post 100Hz stimulation- NR1/NR2A-NMDARs: 58.5%, NR1/NR2A/NR2B-NMDARs: 56.0%, synaptic NR1/NR2B-NMDARs: 26.5%, extrasynaptic NMDARs: 15.9%), suggesting these receptor subpopulations may provide a mechanism to detect repeated interval bursts in a network.

Developmental changes in synaptic NMDAR content alters synaptic calcium influx

Given the diversity of the postsynaptic response over both stimulation frequency and receptor composition, we sought to explore the potential differences in NMDAR synaptic signaling that can occur over development, as well as in disease states. The content of NMDARs at synaptic sites is highly dependent on neuronal age, with a developmental switch from predominantly NR2B expression early to increased NR2A

expression later in development (Williams et al. 1993, Monyer et al. 1994, Liu et al. 2004a). Moreover, brain injury may cause a change in the balance of NMDAR composition (Giza et al. 2006), yet the effect of this change on synaptic signaling is largely unknown. To this end, we used the flexibility of these computational simulations to explore the potential diversity in synaptic signaling that can occur during synaptic maturation.

Several experimental models of LTP appear in the literature. In the previous section (Fig 7), we simulated the most well established protocol for LTP induction (100Hz, 1 sec duration) (Sarvey et al. 1989). In comparison, other common models include chemically-induced LTP and spike timing dependent plasticity (STDP). To extend our findings and develop testable predictions for *in vitro* studies, we used our computational model to examine the role of subtype content in simulated chemically-induced LTP.

To examine how the identity of synaptic NMDAR subtypes can influence overall receptor activation, we simulated several possible configurations of synaptic NMDAR content. We compared activation across spines populated with different mixtures of NMDAR subtypes - from synaptic NMDARs consisting of only NR1/NR2B-NMDARs, to simulate a spine in early development before NR2A expression, up to and including synaptic NMDAR content of only NR1/NR2A-NMDARs as a representation of the canonical 'mature spine'. In all cases, the number of synaptic NMDARs was kept at 20, and the number and identity of AMPARs and extrasynaptic NR1/NR2B-NMDARs were constant. Finally, we computed the net calcium influx that occurred during each

simulation, using techniques to account for the magnesium block of the receptor and AMPAR-induced depolarization of the spine (see Methods for more details).

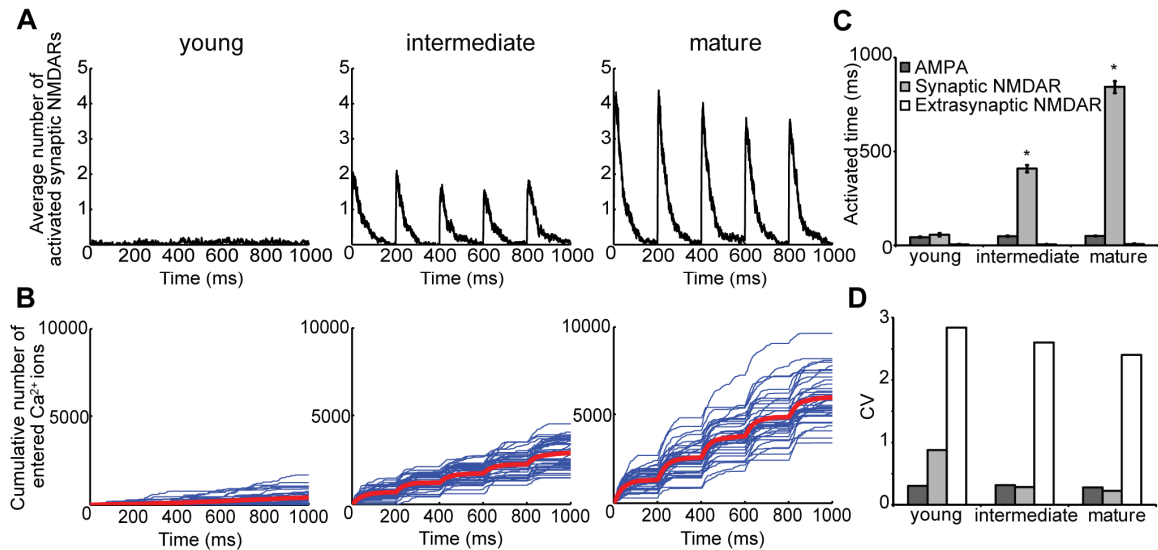


Figure 9: Increasing synaptic NR2A content during development enhances response and improves fidelity. Induction of chemically induced late phase LTP was simulated with a 5Hz frequency of glutamate release on three different representations of synaptic NMDAR content; ‘young’ (20 NR2B-NMDARs), ‘intermediate’ (8 NR2A-NMDARs, 8-NR2A/NR2B-NMDARs, 4 NR2B-NMDARs), and ‘mature’ (20 NR2A-NMDARs). (A) Traces of the average number of activated synaptic NMDARs over all simulations and (B) cumulative calcium entry (blue: individual simulations, red: averaged over all simulations) demonstrate that younger cultures, dominated by NR2B, result in less predicted calcium influx. (C) Quantification of total activated time and (D) its coefficient of variance show that changes in relative synaptic NMDAR subtype content occurring through development result in significantly greater activation and less variance, suggesting that NR2A content is a major driving force in the reliability and magnitude of downstream signaling (* $p < 0.05$ compared to other distributions, $n = 40$ simulations per condition).

Chemically induced LTP relies on a sustained period of action potential bursts that propagate through the network, where the duration of each burst can last for 1-3 seconds and the frequency of measured synaptic responses within each burst is approximately 5Hz (Arnold et al. 2005, Wiegert et al. 2009). Our simulation results show that 5Hz glutamate release results in significant differences that occur in the NMDAR-mediated signaling in the spine across these different NMDAR subtype

configurations. As expected, observed synaptic NMDAR activation was significantly reduced in a model representation of the immature spine (i.e., 100% NR1/NR2B-NMDARs) when compared to spines with a physiological mix of NMDAR subtypes and with more mature representations (Fig 9A,C). Increasing the fraction of NR1/NR2A and NR1/NR2A/NR2B NMDARs increased significantly the ability to elicit a defined synaptic NMDAR activation during simulated chemical LTP induction. Furthermore, predicted calcium influx through the NMDAR was significantly different in all three configurations suggesting that synaptic content can significantly impact the resultant signaling from this stimulation (Fig 9B). Additionally, we found the reliability of synaptic NMDAR activation is increased through maturation, as measured by the observed decrease in coefficient of variance of synaptic NMDAR activation (Fig 9D). Our data suggests that the NR2A content of the synapse is the major driving force in both the reliability and extent of the NMDAR response and provides a potential mechanism to age dependent functional outcomes.

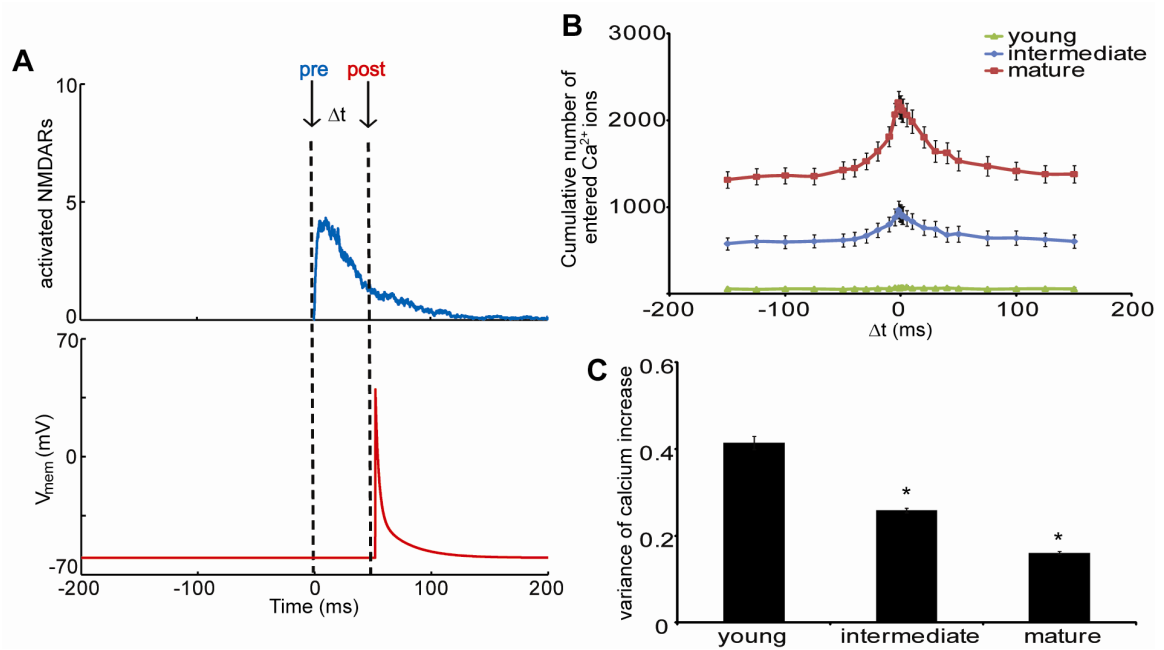


Figure 10: Changing subtype content during development improves calcium potentiation during paired stimulations. (A) Spike time dependent plasticity (STDP) was simulated by pairing presynaptic glutamate release with postsynaptic depolarization at different time intervals. (B) Calcium influx was greatest in the mature subtype content and was increased by paired stimulation when pre and post spikes were given simultaneously ($\Delta t = 0$). (C) The variance in the fold increase of calcium influx generated by paired depolarization was greatest for young cultures, again demonstrating that NR2A content significantly improves the extent and reliability of signaling during this model of plasticity (* $p < 0.05$ compared to other distributions).

STDP relies on the precise timing of presynaptic and postsynaptic stimulation, with the time interval between stimulation defining the potential for long term synaptic changes (Buchanan and Mellor 2010, Shouval et al. 2010). Thus, we computed calcium influx at the different developmental NMDAR subtype content configurations at distinct time intervals (Δt) between presynaptic glutamate release and postsynaptic depolarization. Depolarization, modeled as an immediate increase in membrane potential with a slow hyperpolarizing tail (Shouval et al. 2002), induces a transient relief of the Mg^{2+} block which, dependent on receptor activity during depolarization, can potentiate calcium influx caused by the presynaptic spike (Fig 10A). We demonstrate that

postsynaptic spikes significantly potentiates influx in our model of the intermediate and mature spine, with greatest increase at $\Delta t = 0$, whereas influx was not significantly potentiated at young configurations. As demonstrated previously, activation of synaptic receptors is significantly decreased at NR2B dominated young configurations, and thus calcium influx increases as NR2A content increases (Fig 10B). Interestingly, the maximal fold increase of calcium entry, compared to conditions without a postsynaptic spike, was similar for both intermediate and mature spine configurations at approximately 1.7, suggesting that the ability for spike timing to potentiate initial calcium influx holds for varying subtype content. However, the variance in the fold increase is significantly smaller in mature conditions (Fig 10C), again demonstrating that NR2A content improves the fidelity of NMDAR signaling.

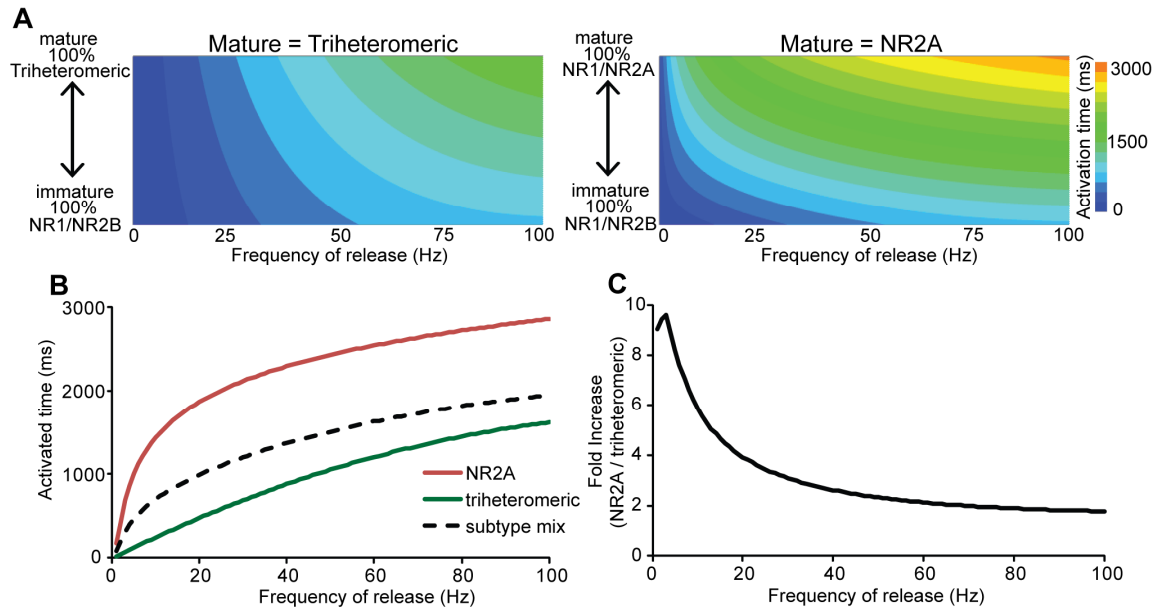


Figure 11: Presence of NR1/NR2A-NMDAR in the ‘mature’ subtype preferentially enhances calcium influx at low frequency stimulation. Synaptic responses were calculated from changing configurations of synaptic content simulating spine maturation, where the ratio of NMDARs was alternatively adjusted from (immature) all NR2B to (mature) either all NR2A or NR2A/NR2B. (A) Distribution of responses demonstrates that transitioning to a triheteromeric ‘mature’ state provides more stability in synaptic response through maturation process, particularly at lower stimulation frequencies. (B) Activation of the mature states compared to synaptic mix of subtypes, as defined by reported PSD content [100] demonstrate how subtype content influence overall activation. The enhancement in activation time was especially evident at low stimulation frequencies (C), where the relative increase in NR2A-NMDAR synapses was almost ten times the response of synapses containing only triheteromeric NMDARs.

Finally, we estimated the synaptic NMDAR response to glutamate release at different frequencies for two alternative views of NMDAR content at a mature spine. Some have suggested that in the mature brain, NMDARs are dominated by the triheteromeric NR1/NR2A/NR2B-NMDAR subtype (Tovar and Westbrook 1999, Rauner and Khor 2010). Others suggest a mixture of NR1/NR2A and triheteromeric NMDARs (Al-Hallaq et al. 2007). To study the possible range of responses, we used average frequency dependent responses per receptor to calculate the total synaptic NMDAR activated time at spines in which the ratio of synaptic NMDARs was alternatively adjusted between NR1/NR2B-NMDARs and NR1/NR2A-NMDARs or, alternatively,

between NR1/NR2B-NMDARs and triheteromeric NMDARs. We found that the developmental transition to a triheteromeric mature state provides more stability in the postsynaptic responses through the spine maturation process (Fig 11A). Moreover, the most dramatic difference between the two views of the mature spine appears at low frequency stimulation, where the activation at the NR2A mature spine was approximately 10 times greater compared to the triheteromeric mature spine (Fig 11C). This suggests that calcium-sensitive processes are likely particularly sensitive to the identity of the ‘mature’ subtype in low frequency conditions, and NR1/NR2A-NMDAR content at a mature synapse enhances the ability to distinguish between different types of low frequency glutamate signals. Interestingly, the relative difference between the two views of the mature spine is less significant at higher stimulation frequencies (Fig 11B) where the proportional change in activation between higher frequency stimulation is not different between the two synaptic representations.

DISCUSSION

In this report, we utilize a computational model of glutamatergic signaling at a single excitatory synapse to study activation patterns of specific NMDAR subtypes during spontaneous and coordinated neurotransmission. The importance of NMDAR subtype in neuronal signaling is widely recognized, with differences in kinetics, localization, and developmental regulation among NMDAR subtypes shaping the influence and timing of signals to promote survival, programmed cell death, and even the local activation of signaling networks within individual spines (Cull-Candy et al. 2001,

Waxman and Lynch 2005b, Hardingham and Bading 2010). Our current work builds upon previous computational models of glutamatergic signaling by investigating the role that NMDAR subunit composition plays in synaptic transmission across a broad physiological range including univesicular, multivesicular, and repeated glutamate release events that occur when a burst of action potentials arrive at the presynaptic bouton. Three new aspects emerge from our current work. First, each NMDAR subtype shows a distinct dynamic range before saturation, highlighting how the varied composition of the individual NMDAR subtypes at single spines can significantly shape the postsynaptic response. Second, the relative contribution of each NMDAR subtype changes across different input stimulation frequencies, with an increased diversity of receptor activation occurring at higher stimulation frequencies. Finally, the developmental expression of NMDARs impacts signaling through NMDARs across all physiological conditions, with immature synapses showing relatively modest activation compared to more mature synapses. Coupled with the knowledge that NMDAR composition can vary over development, these simulations suggest that a single physiological process, such as either LTD or LTP, may have distinct regulating mechanisms that change throughout development and partly explain the existing confusion surrounding the role of NMDAR subtypes on single neuron, as well as neuronal network, function.

Subunit-specific dynamic range of NMDAR activation

Our data illustrates that NR1/NR2A-NMDARs are robustly activated when single vesicles within the physiological range of glutamate content (500-1,500 molecules) (Burger et al. 1989, Schikorski and Stevens 1997) are released. For the geometry we studied, the NR1/NR2A-NMDARs represent the only significant and reliable component of the NMDAR population activated across this physiological range of glutamate vesicles. Past reports suggest that variability among individual vesicles can represent an important source of variation in postsynaptic responses of AMPARs (Hanse and Gustafsson 2001, Franks et al. 2003, Ventriglia and DiMaio 2003). Our work shows that NR1/NR2A-NMDARs share a similar ability to vary the postsynaptic response, also in direct proportion to the number of glutamate molecules in the vesicle. Moreover, this variation in response occurs with relatively high fidelity; the coefficient of variance for NR1/NR2A-NMDAR activation across the univesicular range is approximately 4-6 times less than either the NR1/NR2A/NR2B or NR1/NR2B receptors. Therefore, among the NMDARs at the synapse, the NR1/NR2A-NMDARs appear ideally suited to detect a vesicular release event, and to scale this detector response in proportion to the amount of glutamate released from the vesicle. The consistency of NR1/NR2A-NMDAR activation under spontaneous release conditions – i.e., its ability to detect discrete, synaptic release events - may facilitate the pro-survival role of synaptic NMDARs, the preferential location for NR1/NR2A-NMDARs (Hardingham 2009, Hardingham and Bading 2010). Indeed, a smaller number of studies highlight the specific and important role of NR1/NR2A-NMDARs in mediating pro-survival signaling (DeRidder et al. 2006, Liu et

al. 2007), in pathological conditions. Therefore, maintaining the activation of synaptic NMDARs across a broad range of conditions appears to be an ideal advantage of NR2A-containing NMDARs. The unique advantage of NR1/NR2A-NMDARs to ‘detect’ and ‘scale’ their response during univesicular release (UVR) is less clear. Graded responses in NMDAR activation will naturally produce proportional graded responses in secondary messengers including calcium, calcium bound calmodulin, and enzymes such as calpain, a protease directly activated by calcium binding. However, many intracellular signaling networks, including MAP kinase activation (Huang and Ferrell 1996) and CaMKII phosphorylation (Okamoto and Ichikawa 2000, Bradshaw et al. 2003), function to convert graded signals into strong switch like signals. Thus, the graded response of NMDAR activation can produce similarly graded outcomes in some signaling pathways while also being used by other pathways to simply approach a critical threshold.

A notable shift in the dynamic range of NMDAR populations occurs with multivesicular release (MVR) conditions; the relative activation of NR1/NR2A-NMDARs saturates and the proportional activation property shifts to NR1/NR2B-NMDARs and NR1/NR2A/NR2B-NMDARs receptors. Similar to NR1/NR2A-NMDARs functioning as detectors during UVR conditions, this shift in the NMDAR activation pattern suggests NR2B-containing NMDARs are the primary detectors of MVR. It is important to note that MVR occurs at some, but not all types of synapses, with notable absence of MVR at mossy fiber – granule cell (Gulyas et al. 1993) and CA3 – interneuron connections (Silver et al. 1996, Lawrence et al. 2004). Furthermore, there has been great controversy on the presence of MVR at Schaffer collateral – CA1

synapses (Hanse and Gustafsson 2001a, Hanse and Gustafsson 2001b, Christie and Jahr 2006). This variability indicates that, in the absence of other compensatory mechanisms, the role of NR2B in physiological signaling may be somewhat limited in MVR lacking synapses. Interestingly, our observed shift in the scaling of the NMDAR populations also occurs simultaneously with an improvement in the consistency or fidelity of signaling mediated through NR2B-containing NMDARs, as indicated by the lowered coefficient of variance (CV) predicted from the MVR simulations. This improvement in signaling fidelity may seem inconsistent with published reports, as multivesicular release is often reported with high values of CV calculated from miniature excitatory postsynaptic currents (mEPSCs) (Umekiya et al. 1999, Conti and Lisman 2003, Ricci-Tersenghi et al. 2006). Our simulations indicate that in response to large, nonvariable numbers of glutamate molecules, the stochastic nature of NMDAR activation contributes little to the variability observed at high CV synapses. The high CV observed experimentally during MVR is instead likely mediated by presynaptic mechanisms, including vesicular glutamate content (Wilson et al. 2005, Wu et al. 2007) and number of vesicles released (Conti and Lisman 2003, Raghavachari and Lisman 2004, Ricci-Tersenghi et al. 2006).

Perhaps most interesting is the transition or shift in the activation of different NMDAR populations at the synapse for MVR (also reported in Santucci and Ragavachari, 2008) that can significantly impact the type and extent of downstream signaling. More emphasis is placed in recent studies to discriminate among NMDARs, as specific NMDAR subtypes are tied to different and often opposing pathways (Cull-Candy and Leszkiewicz 2004, Kim et al. 2005, Waxman and Lynch 2005a). For a synapse

dominated by NR1/NR2B-NMDARs, our simulations suggest that MVR, or other compensatory mechanisms, is necessary to improve the consistency of the signaling mediated through the synaptic NMDARs. It is interesting to note that several studies cite the increased frequency of MVR in immature neuronal cultures, where the expression of NR1/NR2B-NMDARs dominates (Iwasaki and Takahashi 2001, Ricci-Tersenghi et al. 2006). Alternatively, if a synapse contains a majority of triheteromeric NMDARs, the synapse would have a broadened ability to respond more consistently to both UVR and MVR, although this synapse would still have limited ability to reliably detect NMDAR signaling for small, single vesicles containing less than approximately 1,000 molecules. In this synaptic configuration, commonly described for mature synapses, the synapse would show the broadest operating range for NMDAR signaling. Moreover, the insertion of NR1/NR2A-NMDARs into a synapse clearly provides ability to detect even more subtle single vesicle release events, and offers a dramatic improvement in the fidelity of signaling compared to either the NR1/NR2B or NR1/NR2A/NR2B-NMDARs (approximately 4:1) over the range of single vesicles containing 500-1,500 glutamate molecules. To this end, past work shows that NMDAR trafficking will show a preference for inserting NR2A-containing NMDARs when the NMDAR activity is suppressed for a significant period of time, or when the selective activity of synaptic NMDARs is suppressed (Aoki et al. 2003, von Engelhardt et al. 2009).

An equally important consideration for NMDAR-mediated signaling is the gradual activation of extrasynaptic NR1/NR2B-NMDARs, an event that is unlikely for the release of single vesicles or low frequency stimulation, but is more probable for MVR

and high frequency stimulation. A number of studies now show the relative balance between synaptic and extrasynaptic NMDARs is important for determining the net resultant role for NMDARs, e.g., the sustained activation of NR2B-containing NMDARs are linked to activation of p38 MAPK (Poddar et al. 2010), inhibition of pro-survival transcription, and swelling of neuronal mitochondria (Hardingham et al. 2002), all of which contribute to neuronal death. Among the receptor populations analyzed, the extrasynaptic NR1/NR2B-NMDAR exhibits the lowest probability of activation, and their relatively sparse number indicates they will not significantly contribute to the predicted overall NMDAR current. This does not exclude the possibility that these receptors can contribute meaningfully to the response across the physiological range, as only the brief activation of extrasynaptic NMDARs has been reported to alter PKC activation and AMPAR subunit composition (Sun and June Liu 2007) as well as having a role in LTD induction (Massey et al. 2004). However, the kinetics and localization of extrasynaptic NMDARs make it well suited for the transduction of excitotoxic signals in pathological conditions. Together, these simulations suggest a tight regulation of synaptic transmission is necessary to ensure the proper health of the neuronal network. In addition, the multiple subtypes of NMDARs and their differential dynamic ranges allows for a single mature synapse to be able to receive and transmit various types of physiological glutamate signals into appropriate intracellular signaling pathways.

The role of NMDAR subtypes in synaptic plasticity are influenced by synaptic content

Experimentally, Liu et al. and others (Liu et al. 2004b, Massey et al. 2004, Yang et al. 2005) show that low frequency stimulation (5Hz) mediates a long-term synaptic depression dependent on NR2B-containing NMDARs, and not on the activation of NR1/NR2A-NMDARs. However, others report that NR2B is not essential for LTD (Morishita et al. 2007). Our simulations show that neither synaptic nor extrasynaptic NR1/NR2B-NMDARs contribute significantly to the total NMDAR activation observed under low frequency stimulation, seemingly in agreement with NR2B playing no role in LTD. However, as the low frequency stimulation for LTD is applied over several minutes (typical duration 10-15 minutes) (Bear and Malenka 1994), one clear possibility is that the modest and sustained activation of the NR1/NR2B-NMDAR over several minutes will integrate to activate the signaling necessary to trigger LTD. An alternative possibility is if elements of the LTD signaling pathway were localized to the macromolecule signaling domains of the NR1/NR2B-NMDAR, where even low levels of NMDAR activation would produce sufficient calcium influx to activate molecules within a highly localized signaling complex near individual NMDARs. In this condition, the local activation of the NR1/NR2B-NMDAR would be relatively insensitive to the more robust activation of the NR1/NR2A-NMDAR. Nanodomain-mediated signaling for NMDARs is receiving more attention lately, as this local activation is capable of changing synaptic AMPAR number (Kim et al. 2005), composition, and the relative activation of MAPK signaling modules in the spine (Kim et al. 2005, Li et al. 2006). One

intriguing possibility is the direct physical interaction of NR2B with Ras-GRF1 and SynGAP, required for the successful activation of p38 MAPK (Li et al. 2006) and inhibition of ERK (Kim et al. 2005), respectively. Both pathways result in reduced AMPAR surface expression and LTD induction - therefore raising the possibility that LTD may be partly influenced by nanodomain-signaling mediated by NR1/NR2B-NMDAR activation.

The role of the NMDAR subtype on the induction of LTP is widely debated, with several reports suggesting that it is dependent on NR2A (Liu et al. 2004b, Massey et al. 2004), on NR2B (Barria and Malinow 2005, Foster et al. 2010), or that both subunits are involved (Zhou et al. 2005, Bartlett et al. 2007, Jin and Feig 2010). Our simulations show that there is a distinct shift in the patterns of NMDAR subtype activation for higher frequency stimulations; the contribution of NR1/NR2A-NMDARs is significantly decreased, while the contribution of synaptic NR1/NR2A/NR2B-NMDARs and extrasynaptic NR1/NR2B-NMDARs is significantly increased. Certainly, one straightforward explanation for the NMDAR-dependent threshold of LTP is that higher frequency stimulation simply activates more NDMARs, and this more significant activation of the NMDARs will lead to a shift in the intracellular signaling that favors LTP. This argument suggests that the induction of LTP is dependent on overall global increase in calcium, a commonly cited mechanism for regulating LTP (Yang et al. 1999, Berberich et al. 2007). An alternative explanation, though, is that the LTP is triggered by a transition in the activation of more NR2B-containing NMDARs for higher frequency stimulations (Barria and Malinow 2005, Zhou et al. 2007), a prediction borne out in our

simulations. There is support for both possibilities in the literature. Several reports demonstrate that LTP induction is mediated by an overall calcium load (Berberich et al. 2005, Bartlett et al. 2007, Muller et al. 2009), while others have identified specific NMDAR subtype specific signaling complexes that can control LTP (Kohr et al. 2003, Li et al. 2006). Furthermore, a recent report shows that both NR2A and NR2B containing NMDARs can induce LTP, but use distinct signaling pathways (Jin and Feig 2010). Our simulations suggest that the composition of the NMDARs at the synapse is a key factor that can influence the relative likelihood for each proposed mechanism. For example, a synapse dominated by NR1/NR2B-NMDARs will produce relatively modest calcium influx and therefore increase the importance of physically localized signaling complexes. Alternatively, mechanisms relying more on global increases in calcium would apply more prominently in a maturing synapse containing a higher fraction of NR2A-containing NMDARs. A key experimental tool needed to test these possibilities is specific inhibition of each NMDAR pool, a tool that remains elusive (Neyton and Paoletti 2006). Once such a tool is available, our simulation studies of different stimulation protocols and receptor content will provide guidance in investigating exactly how NMDAR subtypes and overall calcium load influence activation of intracellular signaling pathways and initiation of long term synaptic changes associated with synaptic plasticity.

Together, our data demonstrates the unique properties of NMDAR subtype specific activation, and shows how subtypes may be suited for specific roles in NMDAR signaling. Further, we illustrate the patterns of NMDAR activation can change under different glutamate release conditions, during different developmental states, and that

receptor content is an important factor in the reliability of NMDAR signaling. The unique properties of these subtypes provides flexibility to synaptic transmission allowing efficient transfer of different types of glutamate signals into distinct patterns of NMDAR subtype activation. Future simulations in concert with experimental investigations will be vital in the understanding of regulatory mechanisms at the synapse and how they impact observed diversity in NMDAR function.

Chapter 4: Immediate and persistent changes in NMDA receptor subtype activation and signaling following traumatic mechanical injury: an *in silico* investigation

ABSTRACT

Traumatic brain injury has two distinct components which can influence the activity of NMDA receptors (NMDARs) during the neuronal response to injury: (1) excessive extracellular glutamate and (2) NMDAR mechanosensitivity. These two components combine to produce a unique paradigm that distinguishes TBI from other neurological disorders. In this report we use a computational model of glutamatergic signaling to examine how injury induced glutamate release and NMDAR stretch sensitivity influence the activation patterns of NMDAR subtypes as well as resultant calcium entry and calmodulin activation. We demonstrate that injury induced glutamate release significantly shifts the patterns of NMDAR subtype activation, with enhanced contribution from synaptic and extrasynaptic NR2B containing receptors. Further, mechanosensitivity, modeled as a loss of the inherent Mg^{2+} block in NR2B containing NMDARs, significantly increases calcium entry and calmodulin activation at the time of injury. We demonstrate that the extrasynaptic contribution to the total NMDAR response in our injury simulations is consistent with measurements of the extrasynaptic contribution following *in vitro* stretch injury. Finally, we use our computational model to predict that mechanical sensitivity of the NR2B subunit can result in prolonged dysfunction in synaptic signaling, a potential factor in secondary cell death and disrupted network communication. Collectively this data points to an increased role of NR2B

during the acute and post-acute periods after injury, highlighting the potential for NMDAR subtype specific influences on the functional outcome of TBI.

INTRODUCTION

Traumatic brain injury (TBI) produces a unique environment among neurological diseases, as it includes both biochemical and mechanical components that can contribute to progressive cell death and dysfunction after the initial injury (Fig 1). Several past studies show the central role of the NMDA receptor (NMDAR) in mediating molecular consequences of TBI, beginning with the initial calcium influx (Geddes-Klein et al 2006) at the moment of injury and including the reshaping of synaptic signaling days to weeks following injury (Weber et al 1999, Giza et al 2006, Goforth et al 2011). Although antagonism of NMDARs provides neuroprotection in experimental models of TBI (Faden et al 1989, McIntosh et al 1990b, Shapira et al 1990, Smith et al 1993), this protection has a short therapeutic window. Moreover, evidence now shows a delayed therapeutic window where NMDA stimulation can improve outcome after TBI (Biegon et al 2004). This dual role for the NMDAR in the traumatically injured brain is likely due to the unique roles of NMDAR subtypes in activating neuronal survival programs or, alternatively, controlling neuronal fate through apoptosis or autophagy (Waxman and Lynch 2005, Liu et al 2007, Bigford et al 2009, Hardingham and Bading 2010). Given the diverse roles of NMDAR subtypes in neuronal signaling, understanding both the acute and post-acute changes in NMDAR-mediated signaling will provide a more

informed approach for alternative and potentially more effective strategies to improve outcome after TBI.

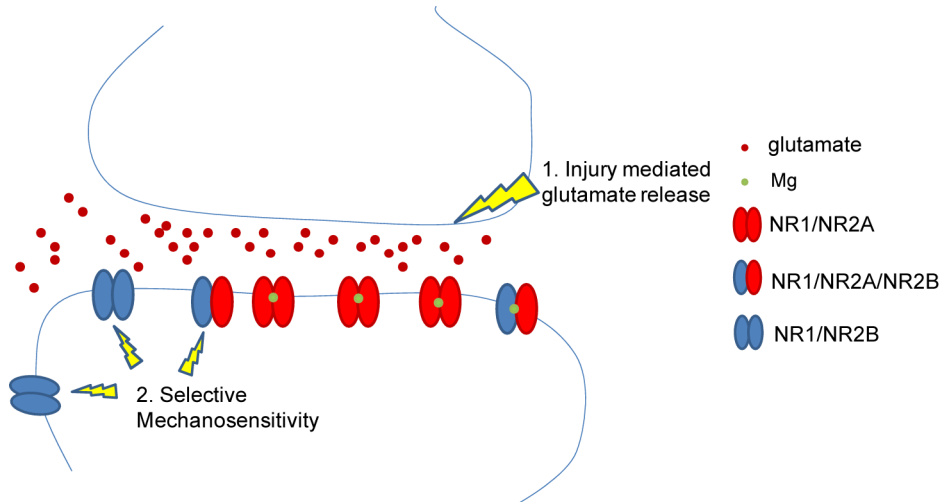


Figure 1: TBI has two distinct consequences influencing NMDAR activity. TBI distinguishes itself from other neurological disease states as it has two unique components that combine to influence neuronal dysfunction. Both of these components, (1) increased glutamate release and (2) mechanosensitivity, converge on the activity of NMDARs, enabling these receptors to be the primary initiator of the neuronal response to injury.

An early biochemical component of TBI is the immediate increase in levels of extracellular glutamate within the brain. Although glutamate is the primary excitatory neurotransmitter necessary for physiological neurotransmission, excessive glutamate can lead to over excitation of the neural network, initiation of pro-death signaling, and eventual neuronal loss (Choi 1988, Arundine and Tymianski 2004). Intracerebral microdialysis after TBI shows a large increase in the extracellular glutamate that dissipates within hours after injury (Faden et al 1989, Nilsson et al 1994). Several sources can account for this elevation in extracellular glutamate, including excessive presynaptic glutamate release, astrocytic glutamate release, cytoplasmic glutamate release through shearing of plasma membranes, and disruption of the blood brain barrier (Yi and

Hazell 2006). Cultured cortical neurons exposed to traumatic mechanical injury *in vitro* show an immediate increase in cytosolic calcium dependent on glutamate binding to NMDARs, suggesting that the glutamate-based biochemical component of TBI will begin immediately after injury (Geddes-Klein et al 2006). This early, immediate event at the synapse could represent an important first step in defining the response and fate of a mechanically injured neuron, as a shift in the activation of NMDAR subtypes can thus alter the balance of intracellular signaling and influence the determination of cell fate. Despite this importance, there is little evidence documenting the mechanisms that regulate the immediate calcium influx following mechanical injury, and how this initial injury response differs from the normal patterns of NMDAR mediated signaling that occurs during physiologic neurotransmission.

A unique mechanical component of TBI also acts upon the NMDAR, as mechanical stretch induces the loss of the NMDAR voltage dependent Mg^{2+} block (Zhang et al 1996). The Mg^{2+} block of the NMDAR is an important regulatory mechanism that provides tight control over NMDAR induced calcium influx (Dingledine et al 1999, Cull-Candy et al 2001). A partial loss in the Mg^{2+} block in mechanically injured neurons leads to a significant increase in calcium influx after a brief application of agonist (Zhang et al 1996), and will substantially enhance NMDAR signaling in both physiological and pathophysiological releases of glutamate. Interestingly, our past work has demonstrated subunit dependence in this mechanosensitive property, where stretch sensitivity is critically linked to the NR2B subunit (Chapter 2). However, it is still unknown how this selective loss in Mg^{2+} block can affect the calcium entry patterns from

NMDAR subtypes both during and following the primary injury insult. With a shift towards enhancing the calcium flux through NR2B-containing NMDARs, it is possible that even normal neurotransmission may adversely affect neuronal survival by promoting NR2B mediated pro-death signaling.

Determination of cell fate, as well as changes in synaptic strength and network communication, is critically linked to intracellular signaling pathways, many of which originate within the synaptic environment. One of the most common early signaling proteins which link calcium from NMDARs to numerous pathways is calmodulin (CaM), an abundant regulatory protein found throughout the CNS. CaM progressively binds calcium ions, which enhances its affinity to numerous CaM regulated enzymes, including cyclic AMP, CaMKII, calcineurin, and nitric oxide synthase (Xia and Storm 2005). Through the modulation of these proteins, CaM plays a major role in the induction of both long term depression (Mulkey et al 1993) and long term potentiation (Malenka et al 1989, Storm et al 1998). Further, recent reports have alternatively shown the necessary role of CaM in directing both neuronal death (Cohen et al 1997, Shirasaki et al 2006) and survival (Cheng et al 2003, Papadia et al 2005). Thus, given the abundance and importance of CaM mediated pathways, assessing the activation of CaM is the first key step in understanding how TBI influences intracellular signaling and functional outcomes during the initial insult and in the critical post-acute period following injury.

Here, we examined how injury mediated glutamate release and NMDAR mechanosensitivity influence the patterns of NMDAR subtype activation and resultant calcium entry after injury, linking these events to the activation of calmodulin. We study

both acute and persisting changes in signaling that can occur through the NMDAR after injury. Given the difficulty in obtaining both the spatial and temporal resolutions necessary to discriminate between NMDAR subtypes with conventional experimental methods, we utilize a computational model of glutamatergic signaling at the dendritic spine (Chapter 3) to define the difference in activation and calcium influx for specific NMDAR subtypes during and following primary injury. Our experiments show that the initial calcium influx following mechanical injury requires glutamate release from the presynaptic bouton, and our simulations show that this acute event will shift the initial activation profile of NMDARs to include more NR1/NR2B-NMDARs. Moreover, the computational model predicts the loss of the magnesium block from NR2B-containing NMDARs creates an infrequent, yet significant, calcium influx through NR2B-NMDARs that can significantly shift the balance of glutamatergic signaling during physiologic signaling. We find these predictions from the computational model match measurements from mechanically injured cortical neurons. Together, this work shows that selective mechanosensitivity of NR2B containing receptors significantly alters the source specificity of calcium influx both during and after injury, providing a potential pathological switch in the postsynaptic response of the injured synapse.

METHODS

Primary cell culture and in vitro stretch injury: Primary cortical cultures were isolated from E18 embryonic rats as described previously (Geddes-Klein et al 2006). Dissociated cells were plated on silicone substrates that were pretreated with PDL (0.01mg/mL) and

laminin (1 μ g/mL). Cells were plated in Minimum Essential Media (MEM) with glutamax + 10% horse serum, and replaced 24 hours after plating with Neurobasal + B27 Supplement. Further, cultures were incubated with 1 μ M AraC from DIV2-4 to prevent astrocytic growth. Cultures were incubated at 37°C and 5% CO² until used for experimentation at DIV 15-18, an age in which cultures contain a diverse set of NMDAR subtypes.

Prior to mechanical stimulation, cultures were loaded with calcium indicator, Fura 2-AM or Fluo4, as indicated. During loading, cultures were pretreated with TTX (1 μ M) to prevent network oscillations, known to influence stretch induced calcium influx (Geddes-Klein et al 2006). Cultures were alternatively left untreated or treated with APV (25 μ M) to block all NMDARs, Ro-256981 (1 μ M) or with Bafilomycin A1 (500nM) to block glutamate loading into vesicles. To block only synaptic NMDARs, cultures were treated with bicuculline and MK801 as previously described (Hardingham et al 2002, Geddes-Klein et al 2006).

Cultures were injured using our custom built *in vitro* stretch injury device, which utilizes a defined air pulse to provide a controlled stretch of specific rate and magnitude to plated neurons (Smith et al 1999, Wolf et al 2001, Lusardi et al 2004). Intracellular calcium was monitored for 30 seconds prior to stretch to provide a baseline, and up to 3 minutes post stretch. For Fura-2AM loaded cultures, cells were alternatively excited at 340nm and 380nm every 3 seconds, while Fluo4 loaded cells were continuously excited at 488nm. All emission data for cells in the field of view were post processed to calculate the change for each cell, normalized to its baseline. Responses across

conditions were then normalized to the average response for untreated cells, to obtain the relative stretch response for drug treated cells. Reporting of relative responses minimizes the impact of the buffering capability of calcium indicators, assuming that buffering capabilities of the calcium indicator across drug treated and untreated conditions are similar.

Geometry and content of modeled dendritic spine: We used a previously developed model of the spine geometry: an octagonal-shaped spine head (500nm diameter) and long spine neck as described previously (Chapter 3). A mix of AMPA and NMDA receptors were randomly placed along the postsynaptic surface (80:20 AMPA:NMDAR ratio; 100 total receptors) and an additional 10 NR2B-NMDARs were placed randomly along the extrasynaptic surface (Racca et al. 2000, Sheng and Hoogenraad 2007). The synaptic NMDARs were divided among the three subtypes as defined by the relative amount of NR2 protein found within the PSD (Cheng et al 2006): 8 NR1/NR2A-NMDARs, 8 NR1/NR2A/NR2B-NMDARs, and 4 NR1/NR2B-NMDARs. A membrane representing an ensheathing adjacent cell was separated by 20nm distance from the apposing extrasynaptic surfaces.

Glutamate release and glutamate receptor activation parameters: Vesicular content was assumed to be 1500 glutamate molecules per vesicle, within the range associated with vesicles in a CA1 hippocampal presynaptic terminal (Burger et al 1989, Schikorski and Stevens 1997). Based on *in vitro* stretch data which demonstrates a role for synaptically

released glutamate in stretch induced calcium increases (Fig 2), injury was simulated as the immediate release of multiple synaptic glutamate vesicles. Simulations assumed two different types of presynaptic release profiles at the moment of injury: (1) the release of 5 vesicles from the readily releasable pool, and (2) the release of the entire pool of vesicles docked and available for release, assumed to be 15 vesicles. These injury simulations were compared to physiologic release profiles that consist of a release of a single vesicle (univesicular release). Diffusion rate for glutamate was held at $0.2\mu\text{m}^2\text{ms}^{-1}$, a commonly used diffusion rate that accounts for molecular obstacles and molecular overcrowding (Saftenku 2005). As described previously, activation of AMPARs and NMDARs was modeled with previously reported reaction schemes and reaction rates (Jonas et al 2003, Erreger et al 2005).

Calcium entry: Calcium entry was computed after simulations of glutamate receptor activation by utilizing model results to iteratively calculate change in membrane voltage potential (V_m) and the probability for open NMDARs to be blocked by magnesium (Mg^{2+}). Using a relationship established by Jahr and Stevens (1990), we calculated the probability of each receptor to be blocked by magnesium at each time step, defined as

$$P_{\text{unblocked}}(V_m) = \frac{1}{1 + e^{-(0.062V_m)} \cdot \left[\frac{\text{Mg}^{2+}}{3.57} \right]}$$

As mechanical stretch is known to reduce the Mg^{2+} block in injured cultures, we modeled mechanosensitivity by varying the effective Mg^{2+} concentration in the determination of $P_{\text{unblocked}}$. We have shown that NR1/NR2B-NMDARs are the most mechanosensitive,

with triheteromeric NMDARs having intermediate sensitivity, and NR1/NR2A-NMDARs having very limited sensitivity (Chapter 2). Based on these findings and past work showing the stretch-induced loss of the magnesium block, we modeled the effect of mechanical injury by using a Mg^{2+} concentration of 0mM for NR1/NR2B-NMDARs, 0.1mM for triheteromeric NMDARs, and 0.8mM for NR1/NR2A-NMDARs (Zhang et al 1996). We compared these conditions to simulations of synapses not mechanically injured, where we used a Mg^{2+} concentration of 0.8mM was used for all subtypes. Membrane potential (V_m) was calculated at each time step by finding the incremental change in V_m dictated by total ionic flux through AMPARs and NMDARs by

$$\Delta V_m = \frac{(I_{AMPA} + I_{NMDA} - I_{leak})}{C_m} \Delta t,$$

where I_{AMPA} , I_{NMDA} , and I_{leak} are calculated using

$$I_{AMPA} = g_{AMPA} (V_m - E_{AMPA}) N_{AMPA}$$

$$I_{NMDA} = g_{NMDA} (V_m - E_{NMDA}) N_{NMDA}$$

$$I_{leak} = g_{leak} (V_m - E_{leak})$$

N_{AMPA} and N_{NMDA} are the number of open receptors of each receptor type. It was assumed that g_{AMPA} and g_{NMDA} , the single channel conductance for each receptor, was 12pS and 45pS respectively. The reversal potentials, E_{AMPA} and E_{NMDA} , for both AMPARs and NMDARs were assumed to be 0mV. In computing a generalized leak current, a leak conductance, g_{leak} , was assumed to be 10nS, with a reversal potential of -60mV which establishes equilibrium V_m at -60mV. Finally, the membrane capacitance (C_m) of the

spine was found using a reported capacitance density of $1\mu\text{F}/\text{cm}^2$ (Dolowy 1984). The probability for a receptor to be unblocked by magnesium ($P_{unblocked}$) was then used to determine if each individual activated NMDAR, as defined by Smoldyn simulations, was able to conduct calcium in that time step. The number of calcium ions entered per open NMDAR per time step was calculated using a probability distribution of ions entered given by

$$p(n) = \frac{(N_{Ca})^n}{n!} e^{-N_{Ca}}$$

Here, N_{Ca} is the average number of calcium ions entered during this time step and is computed by

$$N_{Ca} = \frac{\gamma_{NMDA,Ca} \cdot V_m}{Z_{Ca} \cdot e_c} \Delta t ,$$

where the single channel calcium conductance for NMDARs, $\gamma_{NMDA,Ca}$, is assumed to be 4.5pS, Z_{Ca} is the valence for Ca^{2+} ($z = 2$), and e_c is the elementary charge ($1.6 \times 10^{-19}\text{C}$). To match with stochastic simulations, a time step of 0.01ms was used. In our examination of calcium entry with and without the added effect of mechanosensitivity, identical glutamate receptor activation profiles, for each glutamate release profile, were analyzed allowing for direct comparison between groups.

Calmodulin activation model: Calmodulin (CaM) activation was modeled using a reaction scheme accounting for the binding of calcium ions to four independent binding sites, 2 on the N lobe and 2 on the C lobe (Keller et al 2008). Calcium influx (see above

section) appeared at discrete receptor locations along the presynaptic face, and the calcium was allowed to diffuse freely throughout the spine. Precise quantity and localization of CaM within the dendritic spine is not yet understood. Estimates place neuronal CaM concentration in the range of 10-100 μM (Xia and Storm 2005). Here, we placed 1200 CaM molecules, equivalent to 20 μM , within the spine head. Molecules were allowed to freely diffuse, with a diffusion constant of $0.01\mu\text{m}^2\text{ms}^{-1}$ (Sanabria et al 2008). Calcium binding to the four sites was defined using a previously described reaction scheme (Keller et al 2008). Consistent with the Keller model, additional calcium buffering proteins (CBPs) were placed within the spine head, including 45 μM Calbindin-D28k, which binds calcium at two high affinity and two medium affinity sites, and 5 μM of endogenous CBP with fast kinetics. All the reaction rates for these proteins are given in Table 1.

Simulations and analysis: All stochastic models were run in Smoldyn 1.84, a stochastic simulator for biomolecular reaction networks (Andrews and Bray 2004, Andrews 2009). Based on convergence studies, a time step of 0.01ms was used for all simulations. Unless otherwise noted, simulations were terminated at 1 second. Total amounts of activated species were tracked throughout the entire timecourse of the simulation. Numbers of entered calcium ions and calcium flux were found using a user created MATLAB script. Significance between multiple conditions was detected through either ANOVA, and post hoc Tukey's Test, or with student's t-test.

Parameter	Value
Calcium diffusion rate	$0.22\mu\text{m}^2\text{ms}^{-1}$
CaM concentration	$20\mu\text{M}$
CaM diffusion rate (Sanabria et al 2008)	$0.01\mu\text{m}^2\text{ms}^{-1}$
CaM C-lobe first association rate	$11,288\text{nm}^3\text{ms}^{-1}$
CaM C-lobe first dissociation rate	0.068ms^{-1}
CaM C-lobe second association rate	$11,288\text{nm}^3\text{ms}^{-1}$
CaM C-lobe second dissociation rate	0.010ms^{-1}
CaM N-lobe first association rate	$179,280\text{nm}^3\text{ms}^{-1}$
CaM N-lobe first dissociation rate	4.150ms^{-1}
CaM N-lobe second association rate	$179,280\text{nm}^3\text{ms}^{-1}$
CaM N-lobe second dissociation rate	0.8ms^{-1}
Calbindin concentration	$45\mu\text{M}$
Calbindin diffusion rate	$0.028\mu\text{m}^2\text{ms}^{-1}$
Calbindin medium affinity association rate	$72210\text{nm}^3\text{ms}^{-1}$
Calbindin medium affinity dissociation rate	0.0358ms^{-1}
Calbindin high affinity association rate	$9130\text{nm}^3\text{ms}^{-1}$
Calbindin high affinity dissociation rate	0.0026ms^{-1}
Fast calcium-binding protein concentration	$5\mu\text{M}$
Fast calcium-binding protein diffusion rate	$0\mu\text{m}^2\text{ms}^{-1}$
Fast calcium-binding protein association rate	$99600\text{nm}^3\text{ms}^{-1}$
Fast calcium-binding protein dissociation rate	1.2ms^{-1}

Table 1: Reaction rates and other model parameters for simulations of intracellular CaM activation.
Taken from Keller et al (2008) unless otherwise noted.

RESULTS

Mechanical injury to cultured cortical neurons shows a strong association with NMDAR activation and requires presynaptic glutamate release

We first focused on developing the necessary experimental data to frame any subsequent simulations of the immediate and delayed synaptic response to mechanical injury. We mechanically injured cortical neurons at one of two different peak stretch injury levels (50%, 80% peak), based on previous studies that showed 50% peak stretch did not cause cell death 24 h after traumatic injury, while 80% peak stretch caused a significant increase in cell death at the same time point (Spaethling et al 2008). Using a calcium indicator dye to measure the immediate response after mechanical injury, we observed the initial peak calcium transient significantly differed between these two injury levels. Moreover, activation of the NMDA receptor was critical in this immediate response after injury for both stretch injury conditions, as inhibiting the activation of NMDARs with APV pretreatment reduced the peak calcium increase by 90-95%, to a level only slightly higher than control, uninjured cultures (Fig 2A). We used an experimental protocol to isolate extrasynaptic NMDARs, and found that the highest stretch injury level studied produced a relatively large fraction of calcium influx through extrasynaptic NMDARs. Alternatively, the same pretreatment protocol showed only a modest contribution by extrasynaptic NMDARs to the resulting peak calcium increase after 50% stretch injury. We used a second experimental approach – blocking NR1/NR2B NMDARs with the highly selective antagonist Ro 25-6981 – to show that the

activation of these NMDAR subtypes contributes little after 50% stretch but has a more prominent role after 80% stretch (Fig 2A). Together, these data show that the NMDARs are critical mediators of the initial response to traumatic mechanical injury across the spectrum of injury, and that the relative activation of receptors expands to include extrasynaptic NMDARs at higher injury levels.

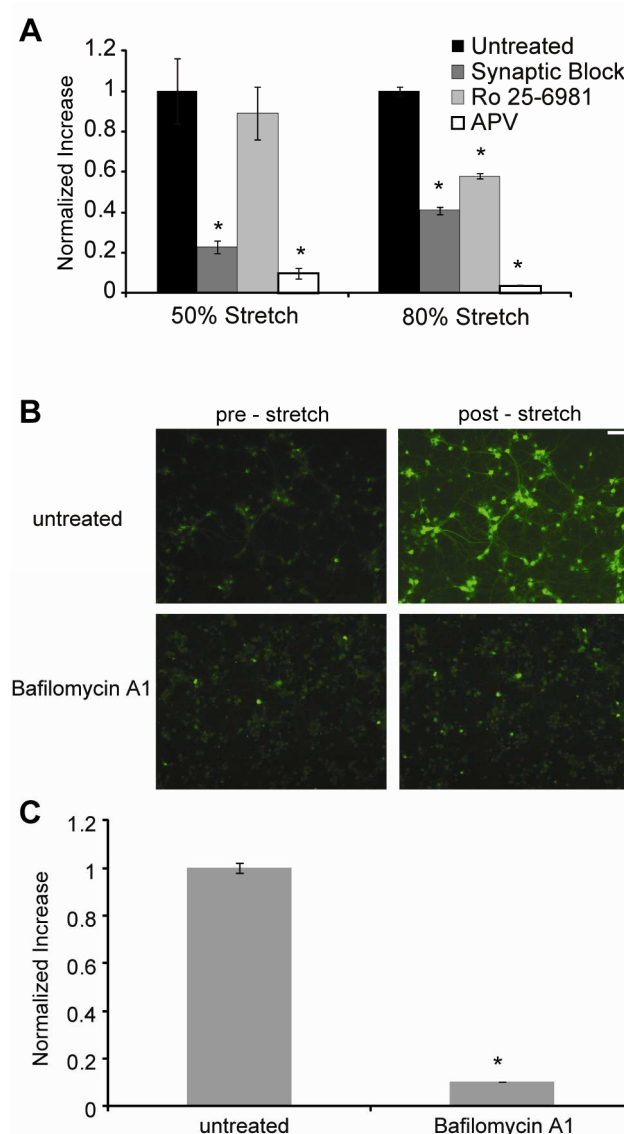


Figure 2: Injury induced calcium influx dependent on NMDAR activation and glutamate vesicle release. (A) Immediate calcium influx following *in vitro* stretch is significantly reduced by alternatively blocking NR1/NR2B-NMDARs or the extrasynaptic pool of NMDARs. APV treatment demonstrates that stretch induced calcium is almost completely eliminated by blocking glutamate binding to NMDARs. (B) Primary cortical neurons, loaded with calcium sensitive dye Fluo-4, were stretch injured with or without pre-treatment with Bafilomycin A1, a compound that inhibits the transport of glutamate into vesicles. Bafilomycin A1 treated cells do not experience a visible calcium rise following stretch (scale bar = 50 μ m). (C) Quantified, Bafilomycin A1 significantly reduces the peak increase in calcium after *in vitro* stretch injury. (* $p < 0.05$ compared to untreated)

Although these data demonstrate the importance of the NMDAR in the response of primary neurons to mechanical injury, they do not directly indicate how these glutamate receptors are activated from stretch. Some stretch activated channels do not require the action of an agonist to exhibit stretch sensitivity (Kung 2005), but our data with APV pretreatment show that the agonist binding is necessary for neurons to respond following mechanical injury. The most likely mechanism is that the mechanical stretch event triggers the release of glutamate from the readily releasable pool of vesicles in the presynaptic bouton. We incubated primary cortical neurons with bafilomycin A to prevent glutamate loading into presynaptic vesicles, as a means to test the relative role that presynaptic vesicular release has on the primary response to mechanical injury (Fig 2B). Following stretch, there was a significant reduction in the primary calcium influx with bafilomycin treatment, with a minimal observed rise in intracellular calcium following stretch (Fig 2C). Therefore, presynaptic release of glutamate is a critical component of the immediate response to mechanical injury, and represents an essential component of the model we developed to study synaptic receptor activation profiles following mechanical injury.

Presynaptic release caused by mechanical injury causes a significant shift in the profile of NMDAR activation

Although our experimental data showed that mechanical injury activated both synaptic and extrasynaptic NMDAR populations, it was not possible to estimate the relative fraction of triheteromeric and diheteromeric receptors activated with a single

stretch event. It is increasingly clear that NMDAR subtypes will preferentially activate different signaling pathways (Waxman and Lynch 2005, Liu et al 2007), but the pharmacological control of these receptor subpopulations remains difficult (Neyton and Paoletti 2006). As an alternative to pharmacology, we utilized our computational model of glutamatergic receptor activation at a single dendritic spine to examine how injury induced glutamate release results in differential patterns of NMDAR subtype activation. We simulated injury in our computational model as a simultaneous release of single or multiple vesicles – 1, 5 or 15 vesicles - to span the range reported for the size of the readily releasable pool of vesicle in the presynaptic bouton (Schikorski and Stevens 2001). Each single vesicle contained 1500 glutamate molecules, and the postsynaptic receptor face was populated with a physiological representation of synaptic NMDAR content – 8 NR2A-NMDARs, 8 NR2A/NR2B-NMDARs, and 4 NR2B-NMDARs – and 10 extrasynaptic NR2B-NMDARs (see methods). Single vesicle release resulted in the activation of primarily synaptically located NMDARs, and synaptic NR2A-NMDARs showed significantly higher activation than synaptically located triheteromeric NMDARs and NR2B-NMDARs (Fig 3A). The simultaneous release of more than one vesicle significantly enhanced receptor activation of all receptor subtypes (Fig 3B), with the total receptor activated time for all NMDARs increased nearly fourfold, for a release of 15 vesicles compared to a single vesicular release event. Interestingly, the most dramatic difference is predicted in the extrasynaptic NR2B-NMDAR population. Although almost no activation was predicted after release of a single vesicle, there was significant activation of extrasynaptic receptors following the release of either 5 or 15 vesicles (Fig

3A), with total receptor activated time increasing from 0.355ms after physiologic release to 106.1ms after release of 15 vesicles (Fig 3B). Across the same range of vesicular release conditions, NR2A-NMDAR activation was not significantly different. As a result, the relative contribution of NR2A-NMDARs significantly decreased from 91.6% during univesicular release to 36.3% following the release of 15 vesicles, while the contribution of all other subtypes increased after injury (Fig 3C). Intriguingly, extrasynaptic NR2B-NMDARs contributed only 0.2% during physiologic release, but rose to 23% when 15 vesicles were released.

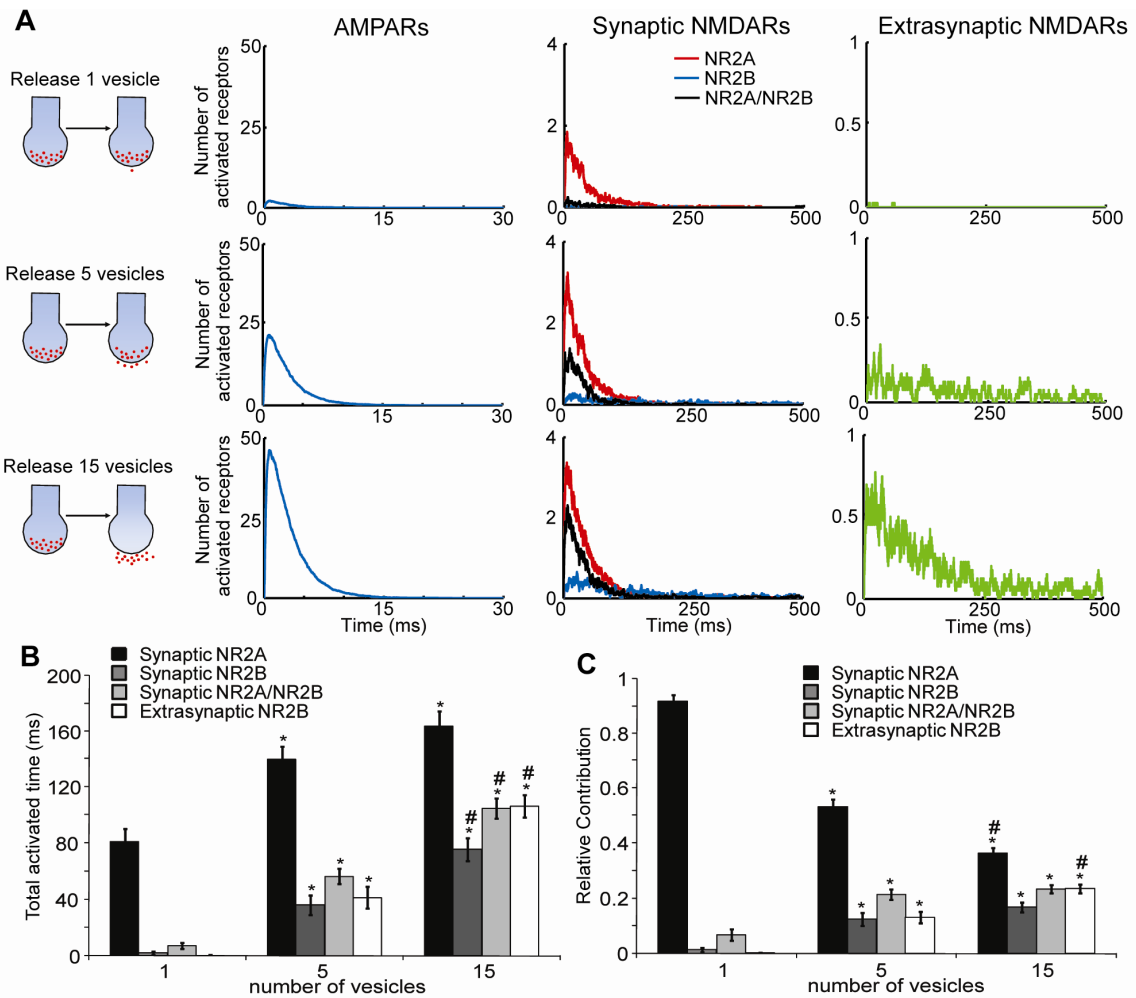


Figure 3: Injury mediated glutamate release alters both the extent and patterns of NMDAR subtype activation. The biochemical component of injury was simulated as an instantaneous release of 5 or 15 glutamate vesicles onto a dendritic spine containing 80 AMPARs, a physiological mix of 20 synaptic NMDARs (8 NR1/NR2A-NMDARs, 8 NR1/NR2A/NR2B-NMDARs, 4 NR1/NR2B-NMDARs), and 10 NR1/NR2B extrasynaptic NMDARs. (A) The average traces of activated AMPARs and synaptically and extrasynaptically located NMDAR subtypes demonstrate that activation of all receptors increases in injury conditions. (B) The average activated time for NMDAR subtypes again shows injury mediated increases in activation. (C) The relative contribution of each subtype to the total NMDAR response demonstrates that the overall pattern of NMDAR subtype activation is significantly altered after injury, with increased in contribution of NR2B containing NMDARs and decreased contribution of synaptic NR1/NR2A-NMDARs. (n = 40 simulations, * p < 0.05 compared to release of 1 vesicle, # p < 0.05 compared to release of 5 vesicles)

Although our simulations predict the total time of receptor activation for a given NMDAR subtype, calcium influx through activated receptors is frequently cited as a necessary proximal event for triggering the activation of signaling systems within the spine. Calcium influx through NMDARs is dependent upon the Mg^{2+} block of the pore, relieved when the membrane is sufficiently depolarized (Dingledine et al 1999). We iteratively calculated membrane potential based on the NMDAR and AMPAR activation profiles, calculated the corresponding Mg^{2+} block at this membrane potential, and computed calcium influx through distinct NMDARs on the postsynaptic surface. As expected, cumulative calcium entry and calcium flux significantly increased as the number of released vesicles was increased (Fig 4A). Furthermore, we observed large increases in calcium entry and calcium flux among the NR2B containing NMDAR subtypes, particularly the extrasynaptic NR2B-NMDARs (Fig 4B), with increasing levels of glutamate release. A similar injury induced shift in contribution of subtypes to calcium influx occurred, with decreased contribution of NR2A-NMDARs and increased contribution of NR2B containing NMDARs (data not shown). The relative amount of calcium influx through extrasynaptic NMDARs following 50% injury best matched our simulations releasing 5 vesicles from the presynaptic bouton. In comparison, we did not match the more enhanced influx from extrasynaptic NMDARs following 80% peak stretch injury, even if we compared the measurements with predicted the release of 15 vesicles (Fig 4C).

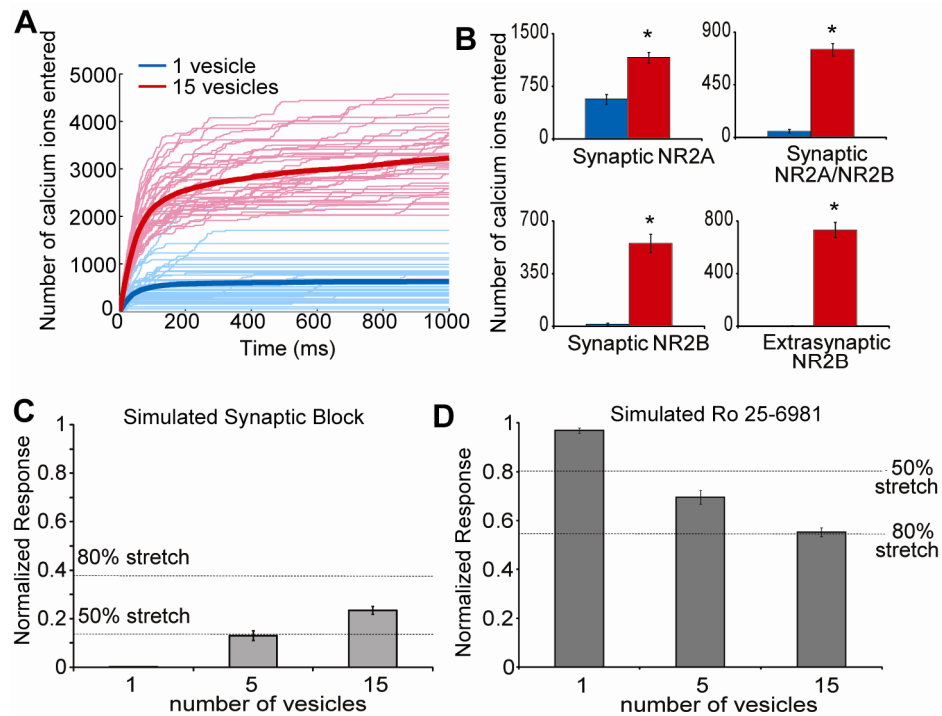


Figure 4: Injury induced glutamate release enhances calcium entry through NMDAR subtypes. (A) Overall calcium entry and (B) calcium entry through specific NMDAR subtypes is significantly increased after injury mediated release of 15 vesicles (pink-individual simulations, red-average), compared to release of a single vesicle (light blue-individual simulations, blue-average) (* $p < 0.01$ compared to single vesicle release). The estimated normalized calcium entry in which certain NMDAR populations were “blocked” simulating pharmacological manipulations of (C) Synaptic NMDAR block and (D) Ro 25-6981 treatment, compared to responses measured following *in vitro* stretch injury.

Stretch-induced loss of the Mg^{2+} block significantly enhances calcium influx

Following mechanical injury, published reports show a sustained loss of the magnesium block (Zhang et al 1996) that can alter the post acute calcium homeostasis (Fig 5A). Our past work (see Chapter 3) shows the importance of the NR2B subunit in conferring mechanosensitivity to the NMDAR. To examine how both glutamate release and NMDAR mechanosensitivity work in concert, we modulated the probability of Mg^{2+} block for each receptor subtype during simulations of NMDAR activation following

injury mediated glutamate release. Probability of the magnesium block for the NMDAR depends upon both the membrane potential and Mg^{2+} concentration (Jahr and Stevens 1990). We simulated a complete loss of the magnesium block for NR1/NR2B-NMDARs (simulated with 0 mM magnesium concentration), and a partial loss of the block for NR1/NR2A/NR2B-NMDARs (0.1 mM) to match the response from stretched neurons. With a simulated loss in the magnesium block for all NR2B-containing NMDARs, the number of entered calcium ions was nearly two orders of magnitude larger than in simulations without a selective loss in Mg^{2+} block (Fig 5B). Predictably, the increase was due to enhanced calcium through NR2B-NMDARs and NR2A/NR2B-NMDARs (Fig 5D). In conditions of injury with a loss in Mg^{2+} block in NR2B-NMDARs, extrasynaptic NR2B-NMDARs account for approximately 55% of the total calcium influx, compared to 25% when Mg^{2+} block is intact (Fig 5E). The release of 5 or 15 vesicles did not significantly change the expected contribution of extrasynaptic NMDARs to the initial calcium influx following injury (Fig 5F). Both release conditions were similar to the measured contribution of extrasynaptic NMDARs after 80% peak stretch injury, but was not similar to the measured response after 50% stretch injury.

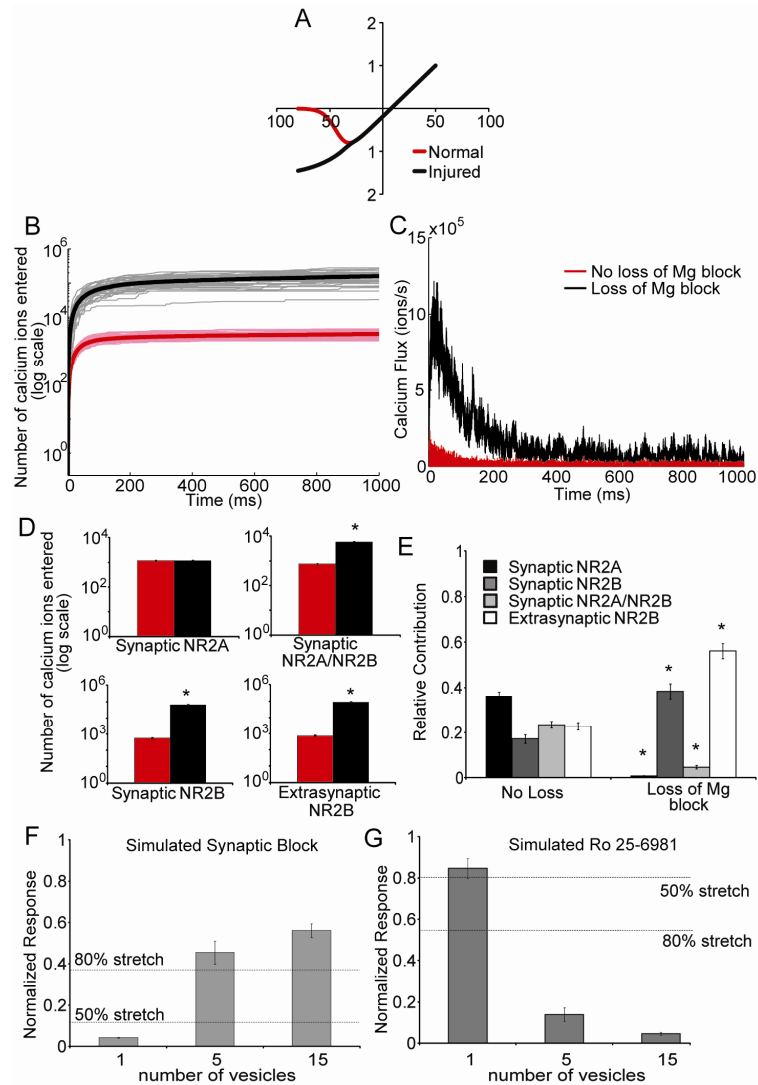


Figure 5: Selective mechanosensitivity and loss of Mg²⁺ block in NR2B containing NMDARs greatly enhances injury induced calcium influx. (A) Schematic describing the stretch induced observed loss of the typical “J-shaped” curve, depicting native voltage dependent Mg²⁺ block (Zhang et al 1996). (B) The total number of entered calcium ions and (C) calcium flux was increased in conditions of injury glutamate release with NR2B mechanosensitivity (gray – individual simulations, black – average), compared to injury release of 15 vesicles alone (pink – individual simulations, red – average). (D) The number of calcium ions through each subtype is increased for NR2B containing NMDARs, but not different for NR1/NR2A, in conditions of combined 15 vesicle injury release and mechanosensitivity. (E) The relative contribution of each subtype to the total calcium is significantly altered by the institution of NR2B mechanosensitivity, with extrasynaptic NMDAR – sourced calcium accounting for more than half of the total calcium entry. The estimated normalized calcium entry in which certain NMDAR populations were “blocked” simulating pharmacological manipulations of (F) Synaptic NMDAR block and (G) Ro 25-6981 treatment, compared to responses measured following *in vitro* stretch injury.

Injury mediated calcium influx controls the activation of calmodulin

These simulations, supported by our measurements of the response in cortical neurons, indicate that both the release of glutamate and partial loss of the magnesium block of the NMDAR are critical aspects of the post acute calcium response following traumatic mechanical injury. To gauge the extent of synaptic signaling under these possible conditions, we developed a model of calmodulin (CaM) activation within the spine (Fig 6A). Calcium bound CaM binding is the major precursor which links calcium entry to the initiation of numerous signaling pathways within the spine (Xia and Storm 2005). Activation of CaM effectors, such as CaMKII and calcineurin, is dependent on its binding with CaM, where the binding rates increase as the calcium occupancy of CaM increases. For this reason, we monitored the various calcium occupancy states of CaM (CaM-Ca1, CaM-Ca2, CaM-Ca3, and CaM-Ca4) following univesicular and multivesicular (15 vesicles) release, in combination with the loss of magnesium block for NR2B-containing NMDARs. Univesicular release produced a brief calcium influx that led to little binding of calmodulin, whereas injury induced glutamate release led to only a modest increase in the number of single and double calcium bound calmodulin molecules. Neither release paradigm resulted in significant activation of CaM-Ca3 and CaM-Ca4, the states with greatest ability to bind and activate CaM effectors (Fig 6B). In comparison, the combined effects of injury induced glutamate release and selective loss in Mg^{2+} block resulted in a peak number of CaM-Ca4 that was nearly 95% of total CaM species, representing a significant increase in the extent of signaling that would be

observed after injury with a loss in Mg^{2+} block (Fig 6B). This initial response to injury highlights a key role of injury induced loss in the magnesium block in altering postsynaptic signaling, providing a much stronger stimulus for altering signaling when compared to the enhanced release of glutamate from the presynaptic bouton.

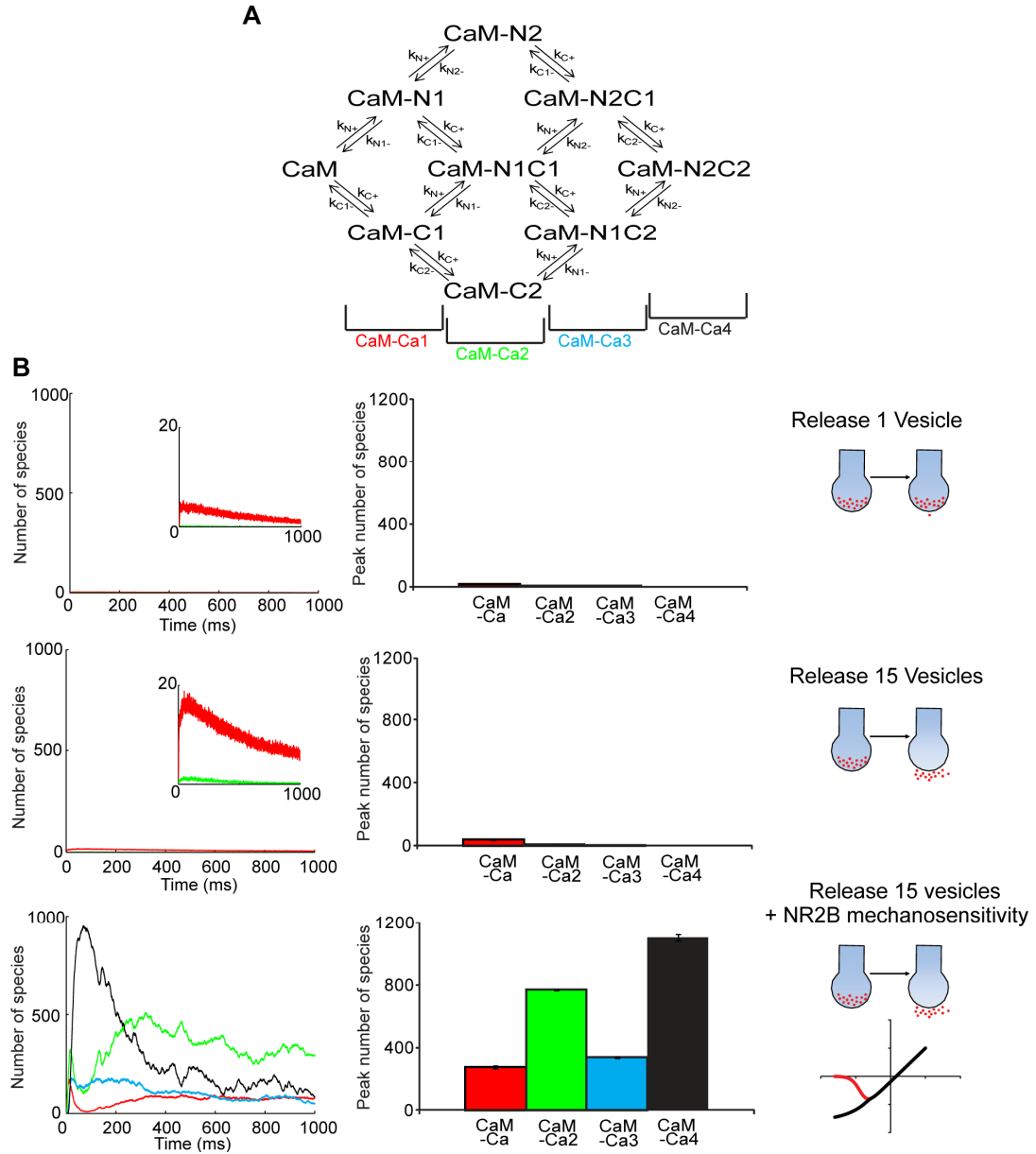


Figure 6: CaM activation is potentiated by injury release with a concurrent loss of Mg^{2+} block in NR2B. (A) Calmodulin (CaM) activation was modeled through calcium binding to two sites on the N-lobe and two sites on the C-lobe. Total numbers of CaM bound to specific numbers of calcium ions (CaM-Ca1 through CaM-Ca4) were observed for (B) three calcium entry conditions: release of a single vesicle, injury induced release of 15 vesicles, and release of 15 vesicles with NR2B mechanosensitivity. Neither release of 1 nor 15 vesicles alone produces fully bound CaM, although 15 vesicle release slightly enhances levels of CaM-Ca1 (see insets) compared to single vesicular release. Peak numbers of calcium bound species demonstrates that the added mechanical effect of a loss of Mg^{2+} block in NR2B significantly increases CaM activation.

Prolonged loss of Mg^{2+} block alters NMDAR signaling in the post acute period after injury

TBI results in both primary cell death, initiated at the initial time of injury, and secondary cell death, a progressive death in the time periods following injury. Thus, the hours immediately after injury are a critical time period in the determination of the overall health of neuronal circuits. The observed loss of Mg^{2+} block in stretched cultures is seen to persist for up to 6 hours (Zhang et al 1996). This suggests that altered calcium entry, particularly from NR2B containing receptors, exists well past the initial injury insult which can significantly influence postsynaptic responses in this critical period. Using the identical glutamate receptor activation patterns from stochastic simulations of univesicular release, we evaluated how sustained relief of the Mg^{2+} block in NR2B containing NMDARs in an injured spine affects the resultant calcium entry. We quickly noticed that a sustained loss in Mg^{2+} block in the “injured” spine resulted in two types of calcium entry phenotypes (Fig 7A). A majority of simulations resulted in calcium entry that was not different from “pre-injury” simulations in which the Mg^{2+} block was intact. However, in several (4 out of 40) simulations, calcium entry was drastically enhanced in the “injured” spine. These two unique subsets of responses suggest a reduction in the fidelity of signaling following injury, which may contribute to long lasting network dysfunction. Interestingly, the subset of enhanced calcium correlated with the rare simulations which resulted in NR1/NR2B-NMDAR activation (6 out of 40) (Fig 7C).

Not surprisingly, all 4 cases of enhanced calcium entry resulted from a receptor activation pattern that included NR1/NR2B-NMDAR activation.

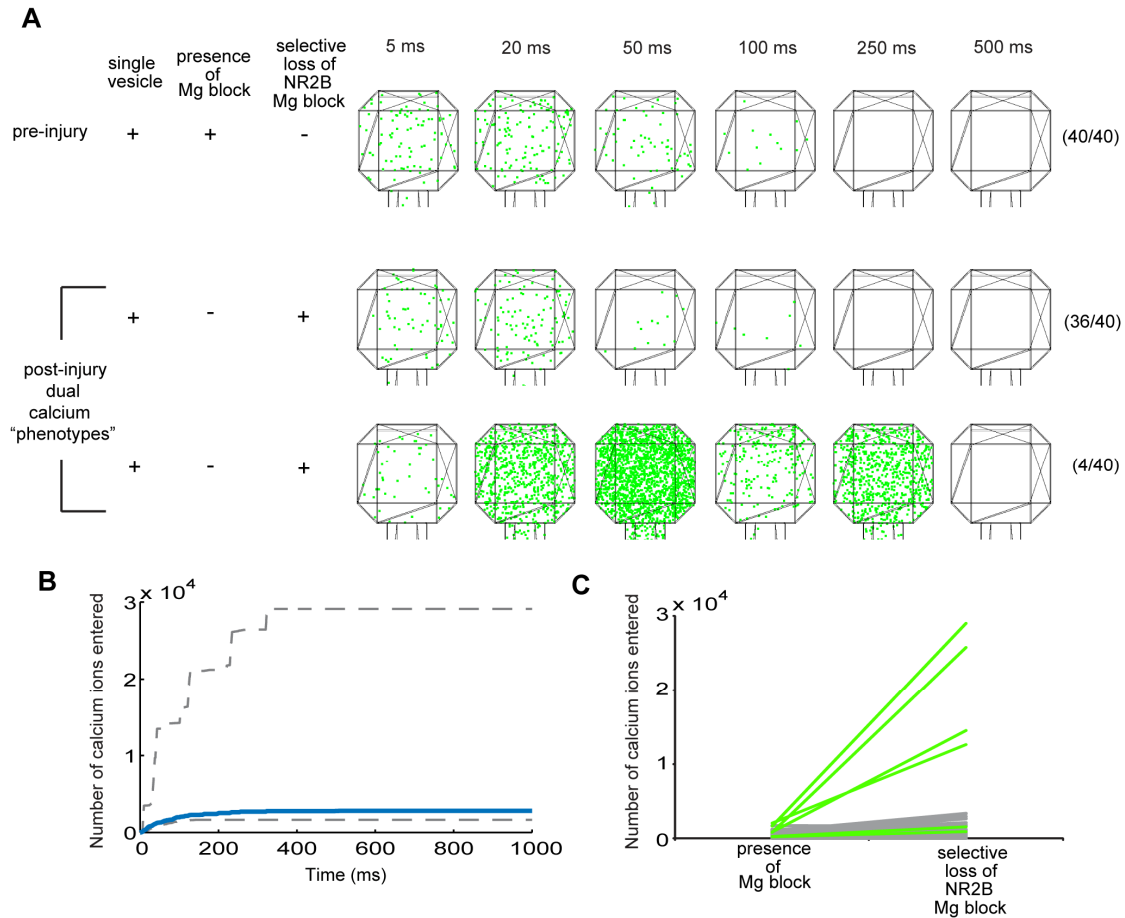


Figure 7: Persistent loss of Mg^{2+} block in the post acute period results in two distinct phenotypes of calcium response to univesicular release in injured spines. Physiological signaling in the post-acute period following injury was modeled by calculating calcium entry following univesicular release in spines in which there is a persistent loss of Mg^{2+} block in NR2B containing NMDARs. (A) Calcium ions (green) present at distinct time points following univesicular release shows that two distinct calcium phenotypes exist in the simulation of calcium entry at an injured spine: one subset of simulations in which calcium dynamics is similar to that seen pre-injury (with an intact Mg^{2+} block) and another subset of drastically enhanced calcium entry. (B) The cumulative number of calcium ions entering the spine for the two post-injury calcium entry patterns shown in A (grey dashed lines) illustrates the separation of these two phenotypes (blue – average of cumulative calcium entry following single vesicle release in all injured spines, $n = 40$). (C) Paired calcium entry for identical NMDAR subtype activation patterns, pre-injury (intact Mg^{2+} block) and post-injury (loss of block in NR2B), where a small subset (4 out of 40) experience enhanced calcium entry. Simulations in which at least one synaptic or extrasynaptic NR1/NR2B-NMDAR is activated (6 out of 40 - green) account for all of simulations within the enhanced calcium entry subset.

Given the correlation of enhanced calcium entry and NR2B activation, we separately analyzed the “post injury” postsynaptic responses and resultant signaling for the two receptor activation subsets: (1) responses with no NR1/NR2B-NMDAR activation (34 out of 40) and (2) responses with at least one NR1/NR2B-NMDAR activated (6 out of 40). Calcium entry through NR1/NR2A-NMDARs was not different among the “pre-injury” and two “post-injury” subsets, while entry through triheteromeric NMDARs was slightly increased in the post injury subsets due to a partial sustained loss in the Mg^{2+} block for these receptors (Fig 8A). Further, calcium entry through synaptic and extrasynaptic NR1/NR2B-NMDARs was significantly increased in the post injury subset that included NR1/NR2B-NMDAR activation. The enhancement of NR2B mediated calcium entry significantly shifts the relative contributions of subtypes to the total calcium response (Fig 8B), with NR1/NR2B-NMDARs, when activated, contributing to over half of the calcium influx. This suggests that the extent and fidelity of subtype specific signaling may be altered in a subset of responses. Intracellular signaling in this post acute period is also predicted to be altered, as CaM activation is significantly increased in the “post-injury” spine when NR1/NR2B-NMDARs are activated (Fig 8C). Together this data shows that the mechanical sensitivity of NR2B, through its loss of Mg^{2+} block, can significantly alter the postsynaptic responses and intracellular signaling in the post acute period. These changes can influence network dysfunction and ultimately secondary cell death following mechanical injury.

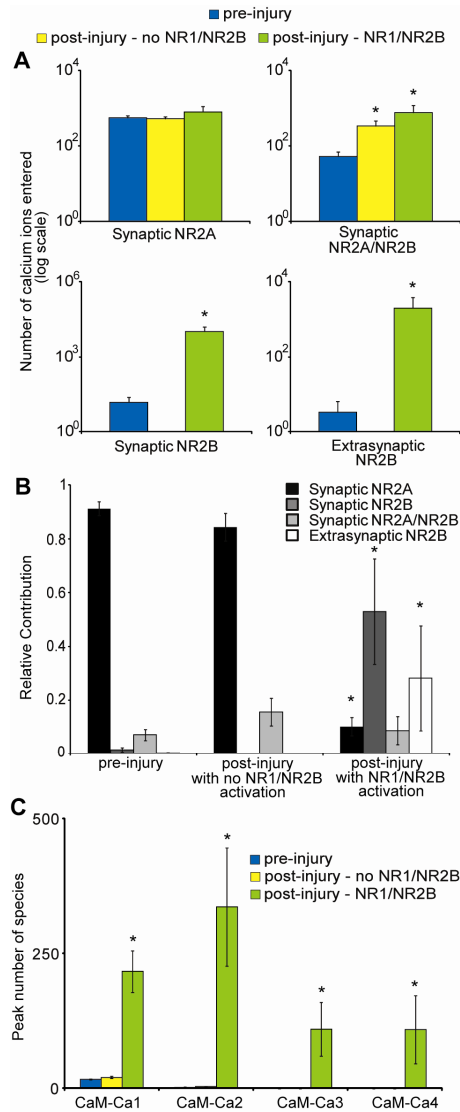


Figure 8: Persistent loss of Mg^{2+} block increases calcium entry and CaM activation in the subset of physiologic postsynaptic responses that result in NR1/NR2B activation. Responses to univesicular release in the post-acute period after injury, with a persistent loss of Mg^{2+} block in NR2B containing NMDARs, were separated by whether release resulted in NR1/NR2B activation. (A) Calcium entry through specific NMDAR subtypes show that, when NR1/NR2B is activated by a single glutamate vesicle post-injury, significantly more calcium enters through NR2B containing subtypes, with no difference in calcium entry in NR1/NR2A-NMDARs. (B) The relative contribution of subtypes to the total calcium influx is significantly shifted by persistent loss of block, particularly when NR1/NR2B-NMDARs are activated. (C) CaM-calcium binding is enhanced when NR1/NR2B-NMDARs are activated post-injury suggesting that a persistent change in Mg^{2+} block in the post acute period after injury can significantly influence intracellular signaling mediated by physiologic glutamate stimuli. (* $p < 0.05$ compared to “pre-injury”)

DISCUSSION

In this chapter, we used a computational model and investigated the patterns of NMDAR activation, calcium entry, and calmodulin (CaM) activation following traumatic mechanical injury in a single dendritic spine. Traumatic mechanical injury is a unique disease paradigm with two distinct mechanisms that contribute to NMDAR mediated neuronal dysfunction – excessive glutamate release and stretch-induced loss of the NMDAR Mg^{2+} block. The use of an *in silico* model provides insight not currently possible using traditional experimental models. The initial calcium influx predicted from our model, confirmed with experiments on cultured neurons, shows that both glutamate release and selective mechanosensitivity of the NMDARs are necessary components of the response following mechanical injury. The combined response of chemical activation and mechanically-induced augmentation of the receptor yields a unique postsynaptic response with a more significant contribution of synaptic and extrasynaptic NR2B containing NMDARs. One consequence of this altered receptor activation profile after injury is a shift in the activation of CaM, which is a key calcium-binding protein involved in many enzymes regulating synaptic plasticity. We find that the stretch-induced loss of the NMDAR Mg^{2+} block is a critical factor in activating CaM. Further, we illustrate that persisting loss of Mg^{2+} block in the post acute period following injury can enhance calcium entry and CaM activation, but only in a subset of spines. Together, these results highlight how the mechanical injury yields a diverse response in single spines, and this diversity extends into activation of important signaling networks within some, but not all, spines.

The primary effect of mechanical injury occurring at the time of insult is remarkably difficult to examine experimentally, especially in single spines, given the spatial and temporal resolutions necessary to visualize the immediate injury effect. We used our simulations to examine the possible circumstances that drive the immediate response after mechanical injury, and to infer the relative role of glutamate vesicular release and alterations in the NMDAR physiology across the spectrum of injury. Our results suggest at least two phases form the spectrum of the response: a phase involving the release of presynaptic glutamate vesicles that appears to closely match the response measured in cortical neurons after moderate (50% stretch) mechanical injury, and a second phase at more severe injury (80% stretch) that includes a more prominent contribution from extrasynaptic NMDARs, primarily from the loss of the Mg^{2+} block in this receptor subpopulation. Although we do not know the precise number of vesicles released from the presynaptic bouton during injury, the relative role of the extrasynaptic NMDARs in contributing to the calcium influx appears relatively insensitive to the number of glutamate vesicles released when a loss in the Mg^{2+} block of the NMDAR is modeled after injury (Fig 5). Therefore, at severe injury levels, the number of released vesicles appears less critical. The number of glutamate vesicles released appears more important in modeling the response of synaptic NMDARs to injury when no loss in Mg^{2+} block occurs, as this response will scale in proportion to the glutamate released from the presynaptic face.

One feature of the model that will likely influence subsequent signaling through any of the spine signaling networks is the relative composition of the NMDAR subtypes

along the postsynaptic face. In our current work, we assumed the subtype content of the synaptic NMDARs to contain all three subtypes (8 NR2A-NMDARs, 8 NR2A/NR2B-NMDARs, and 4 NR2B-NMDARs), based on reported relative amounts of NR2 protein within the postsynaptic density (Cheng et al 2006). However, there continues to be considerable debate as to the subtype content of receptors at synaptic sites. Although NR2A replaces NR2B at synaptic sites during maturation, there are several reports that demonstrate that a majority of receptors are of the triheteromeric subtype (Tovar and Westbrook 1999, Rauner and Kohr 2010), while other reports suggest a mixture of NR1/NR2A and triheteromeric receptors. Our data shows that the content of receptors at these sites is particularly important in cases of injury, where mechanosensitivity is restricted to NR2B containing receptors. In spines where NR1/NR2A-NMDARs dominate, overall calcium load would be significantly less than spines containing significant NR1/NR2B receptors. In contrast, a spine dominated by NR1/NR2B-NMDARs would show a more pronounced change in calcium influx relative to spines with triheteromeric NMDARs. Thus, subtype content at individual spines is an important variable that can impact the postsynaptic response and resultant signaling during injury. Further investigation into the regulatory mechanisms to direct subtype content at the synapse would provide some insight into how development, as well as alterations at the synapse after injury, would play a role in mediating both physiological and pathological signaling after injury. Thus, while this model represents an accurate starting point in simulating the postsynaptic response to injury, future investigations are necessary to assess the dynamic range of the synapse to better replicate primary injury.

Injury induced activation patterns of NMDAR subtypes

While there is substantial evidence of multiple sources of injury induced increases in extracellular glutamate *in vivo*, we show that glutamate release via synaptic vesicular release represents the primary source that initiates immediate calcium influx in our *in vitro* model of injury. Further, as the observed glutamate increase in experimental models is correlated with injury severity (Faden et al 1989, Palmer et al 1993), we modulated simulated injury with the release of different numbers of vesicles. Our results show that the activation patterns of NMDAR subtypes is significantly altered during injury mediated glutamate release. While univesicular release primarily activates synaptic NR1/NR2A-NMDARs and rarely activates extrasynaptic NR1/NR2B-NMDARs, injury induced glutamate release produced significant synaptic and extrasynaptic NR1/ NR2B-NMDAR activation. These predictions, supported by experimental data collected in mechanically injured primary neurons, show that NR1/NR2B-NMDARs are uniquely suited to transmit the excitotoxic glutamate stimuli during injury. The implications of this alteration in NMDAR subtype activation are important, as several studies show that activating this extrasynaptic receptor pool is linked to pro-death signaling seen during models of excitotoxicity (Hardingham et al 2002, Zhang et al 2007, Xu et al 2009, Hardingham and Bading 2010). The activation of extrasynaptic NMDARs after mechanical injury is critical for determining cell fate, as blocking this specific receptor subpopulation will protect against neuronal death caused by mechanical injury (DeRidder et al 2006). In combination with past studies showing the importance of activating specific synaptic receptor subpopulations to trigger either

long-term potentiation or long-term depression, these results reveal that the use of computational simulations to reveal the precise “fingerprint” of the postsynaptic response is valuable for precisely understanding the similarities and differences among the extent and temporal dynamics of NMDAR activation for stimuli that range from physiologic to pathophysiological.

Selective NR2B mechanosensitivity functions as a pathological sensor switch

Mechanical injury produces a unique change in the physiology of the NMDAR, with the physical stretching of the neuron leading to a loss of Mg^{2+} block, significantly potentiating NMDAR mediated calcium influx at resting membrane potential (Zhang et al 1996). This loss in the Mg^{2+} block is one part of the mechanosensitivity reported for the NMDAR (Paoletti and Ascher 1994, Casado and Ascher 1998), and our past work showed that this stretch sensitivity is restricted to the NR2B subunit (Chapter 2). Understanding the specific role of this stretch-induced change in the physiology of the NMDAR is not straightforward experimentally, as distinguishing between the effects of injury mediated glutamate release and mechanosensitivity is difficult to discern as they occur simultaneously. Computationally, we showed that injury induced glutamate release resulted in enhanced calcium on its own, but incorporating a loss in the Mg^{2+} block greatly increased the extent of calcium entry and further altered the balance of signaling toward NR2B containing NMDARs. Our data suggests that mechanical sensitivity results in calcium influx that is two orders larger than what would be seen during excitotoxic NMDAR activation alone. As calcium overload is commonly attributed to

neuronal damage in numerous models of disease through the activation of proteases, phospholipases, and other harmful enzymes (Choi 1988), we propose that these simulations show the combined effects of injury induced glutamate and selective loss of Mg^{2+} block in NR2B containing receptors flip a pathological ‘switch’. There is mounting evidence that this switch may play a role in neuronal outcome, as several studies demonstrate that extrasynaptic NMDAR activation – primarily NR2B-NMDARs – is responsible for mitochondrial dysfunction, calpain activation, and inhibition of pro-survival transcription (Hardingham et al 2002, Zhang et al 2007, Xu et al 2009). Furthermore, disruption of the NR2B subunit from its signaling complexes eliminates elements of pro-death signaling, suggesting that NR2B mediated nanodomain signaling strongly influences cell death (Soriano et al 2008). This is the first evidence at the synaptic scale which supports experimental studies showing NR2B specific antagonists significantly reduce damage after both *in vivo* (Okiyama et al 1997, Dempsey et al 2000, Yurkewicz et al 2005) and *in vitro* models of traumatic brain injury (DeRidder et al 2006). Thus, the specific targeting of NR2B-NMDARs and NR2B mediated signaling remain intriguing options for the development of potential therapeutic strategies for TBI. One consideration in these therapeutic approaches should be the consequence of this altered activation scheme on synaptic signaling, and whether this change in synaptic signaling produces new therapeutic targets. In our simulations, we predict that stretch-induced changes in the NMDAR will produce robust changes in activated CaM, and this activation was critically dependent upon the loss in the Mg^{2+} block of the receptor. The strong association of CaM with the selective change in the physiology of the NMDAR

means that this activated molecule may be the important proximal synaptic sensor which, in turn, will activate signaling networks within either nanodomains surrounding the receptor or within the spine. Although not explicitly examined in detail for this study, future simulations will include more defined NMDAR signaling domains to determine how injury induced NMDAR activity directs the specificity of signaling.

Stretch-induced changes in NMDAR alter physiological synaptic signaling and enhance synaptic ‘noise’

TBI can significantly impact glutamatergic signaling at the synapse in the periods following injury, with reported injury induced effects on both AMPARs and NMDARs. Stretch injury removes AMPAR desensitization (Goforth et al 1999, Goforth et al 2004) and modifies the subunit composition of AMPARs, promoting the aberrant surface expression of calcium permeable AMPARs (Spaethling et al 2008). Along with a loss in Mg^{2+} block (Zhang et al 1996) NMDAR subtype content at the synapse is altered by injury, with a reported increase in the ratio of NR2B:NR2A expressed subunits (Giza et al 2006). These changes, coupled with injury mediated impairment of glutamate transporters on nearby astrocytes (Rao et al 1998, Yi and Hazell 2006), significantly influence the postsynaptic responses at single synapses, potentially leading to network dysfunction and secondary cell death. Among the most intriguing aspects of this work is the effect of persistent loss of Mg^{2+} block to normal glutamatergic transmission. Zhang et al. demonstrate that their observed loss in Mg^{2+} block can last for up to 6 hours post stretch. This implies that once the initial calcium transient associated with mechanical

injury subsides (Lusardi et al 2004, Spaethling et al 2008), physiologic glutamatergic signaling following injury could augment the primary injury mechanisms and influence secondary cell death. Secondary cell death, which we define as all the injury induced damage not caused by the primary insult, is a major source of the continuing neurological defects of the injured patient and represents the pathology that can be targeted by potential therapeutic interventions (McIntosh et al 1998, Kochanek et al 2000, Loane and Faden 2010). Our data shows that a persisting loss of Mg^{2+} block in the NR2B containing receptors causes reduced fidelity in synaptic communication, by producing a subset of responses to univesicular release that far exceed the “normal” response. This instability or ‘noise’ in the synaptic response leads to a corresponding division in intracellular signaling, as measured by CaM activation, potentially contributing to abnormal network behavior. It is not clear, though, if this induced noise in the synaptic signaling reaches a threshold to affect neuronal fate or alter normal synaptic signaling. The relative infrequency of this predicted behavior – occurring in approximately 10% of the univesicular release simulations – will undoubtedly be influenced by the rate of vesicular release. Our past work shows a more consistent activation of NR2B-containing NMDARs when presynaptic stimulation frequencies exceed 5-10 Hz (Chapter 3). This suggests that this pathological change in synaptic signaling will be activated more robustly and consistently across spines in physiological stimulations, perhaps altering either the threshold of LTP and LTD in mechanically injured cultures or, alternatively, converting a physiological stimulation into a pathological stimulation. Moreover, we do not consider the potential regulation on the presynaptic neuron, where injury mediated

modulation of vesicular release may directly impact post injury network excitability. Our computational model was used to investigate one of these injury induced modifications in the post acute period – selective mechanosensitivity – but provides a unique model system to examine the individual and collective effects of all potential injury induced changes at the synapse.

In this chapter, we used our computational model of a single dendritic spine to examine how the specific paradigm of TBI affects glutamatergic signaling during and post injury. The unique injury effect of mechanosensitivity and resultant loss of Mg^{2+} block distinguishes injury from other models of excitotoxicity by further altering the balance of source specific calcium entry towards NR2B containing NMDARs. Furthermore, as this effect can persist into the post acute period after injury, we predict that postsynaptic responses and neuronal network behavior is significantly disrupted by injury leading to potential secondary damage. Finally, our model represents a unique system to examine injury mediated modifications at scales which are currently difficult to obtain experimentally, and will aid in future identification of potential therapeutic targets which can best restore healthy synaptic communication.

Chapter 5: Summary and Conclusions

The goal of this work was to further examine how NMDAR subtypes contribute to the neuronal response to TBI. Our lab has previously demonstrated that NMDARs are responsible for the immediate calcium influx seen after stretch injury (Geddes-Klein et al 2006), and that activity of specific subtypes can dictate differential functional outcomes post injury (DeRidder et al 2006). Here, we built upon these studies to examine how two unique aspects of TBI, (1) NMDAR stretch sensitivity and (2) increased extracellular glutamate concentration, differentially modulate the activity of specific NMDAR subtypes. We were able to utilize both *in vitro* and *in silico* models to demonstrate that TBI preferentially acts upon NR2B containing NMDARs, producing an effective pathological switch in NMDAR mediated signaling.

Despite the wealth of evidence pointing to NMDARs as a critical mediator of TBI induced pathology (Faden et al 1989, McIntosh et al 1990, Smith et al 1993, Rao et al 2001), it has remained difficult to evaluate the roles of specific NMDAR subtypes. Here, we have used two unique model systems that have enabled us to effectively discriminate the actions of specific subtypes. Through the expression of recombinant NMDARs in HEK 293 cells, we demonstrated that NMDAR mechanosensitivity is dependent on NMDAR subtype, and that this property is regulated at specific C-terminal domains. Additionally, we developed a novel stochastic model of glutamatergic signaling at a single dendritic spine in which we were able to model the activation of AMPARs and NMDAR subtypes in response to unique signaling paradigms. This model has proved useful in determining distinct activation patterns among subtypes during both physiologic

and pathologic signaling. Again, NR2B acted as a unique switch whose activation was particularly enhanced following simulated injury mediated glutamate release and its differential signaling is predicted to last long after the acute injury. Together, our data has demonstrated that injury produces a unique microenvironment which is particularly suited for the activation of NR2B containing NMDARs – a class of receptors whose activation has been linked to pro-death signaling (Liu et al 2007, Poddar et al 2010). Given the knowledge that these NMDAR subtypes can mediate different, and often opposing, signaling pathways, the ability for injury to differentially impact specific subtypes is an intriguing discovery that may direct the identification of novel therapeutic options.

SUMMARY OF FINDINGS

Selective mechanosensitivity of NR2B containing NMDARs

NMDARs have been previously shown to be sensitive to stretch through a persistent loss of its native voltage dependent Mg^{2+} block (Zhang et al 1996). However, until now, the subtype dependence of this mechanosensitive property had not been studied. Using a recombinant system of transfected NMDAR subunits expressed in HEK 293 cells, we created the dual benefit of eliminating the need for unreliable antagonists and removing the receptor from the synaptic architecture. This allowed us to evaluate the mechanosensitivity of expressed receptors without the confounding factors of injury induced glutamate release from presynaptic sites. We demonstrated that NMDAR

mechanosensitivity was primarily directed by the NR2B subunit. While NR1/NR2B expressing cells responded with an immediate stretch induced rise in intracellular calcium, NR1/NR2A expressing cells produced no such response. Additionally, we provided evidence that triheteromeric NR1/NR2A/NR2B-NMDARs display an intermediate level of stretch sensitivity. Strikingly, this is opposite of the NMDAR activation profiles of subtypes following agonist stimulation, where NR1/NR2A-NMDARs are more readily activated than triheteromeric and NR1/NR2B-NMDARs. This selective mechanosensitivity has significant potential implications in both the extent and type of TBI induced signaling. Recently, numerous studies have demonstrated that extrasynaptic NMDARs, which are primarily of the NR1/NR2B subtype, are preferentially linked to pro-death signaling pathways (Hardingham et al 2002, Zhang et al 2007, Xu et al 2009), whereas synaptic NMDARs are linked to pro-survival signaling (Hardingham et al 2002, Zhang et al 2007). Further, a recent report suggests that NR2B containing NMDARs, regardless of localization, can induce pro-death signaling (Liu et al 2007). These studies highlight the importance of the precise balance of signaling between NMDAR subtypes in the determination of cell fate, and together with our data suggest that selective mechanosensitivity can have significant influence on injury induced intracellular signaling.

Selective mechanosensitivity may also play a role in dendritic sprouting and neurite outgrowth which has recently been shown to be dependent on the mechanical properties of the substrate (Jiang et al 2008, Jiang et al 2010). Furthermore, the activity

of NR2B containing receptors is crucial for outgrowth (Georgiev et al 2008, Espinosa et al 2009). Thus the mechanosensitivity of NR2B may be of particular advantage during development and repair, two conditions in which NR2B expression is known to dominate.

Differential effectiveness of NMDAR antagonists in mitigating NR2B mechanosensitivity

In our observation of NR2B mechanosensitivity, we also evaluated the ability for traditional NMDAR antagonists, APV and MK801 to mitigate stretch induced calcium influx. These two antagonists have no subunit specificity but have very different and important modes of action. APV competitively binds the glutamate binding site, preventing glutamate binding to the receptor, while MK801 is a high affinity blocker of the receptor pore, physically blocking ionic flux. We found that while both antagonists decreased the stretch response, APV was more effective in completely eliminating the observed rise in calcium. This provides the important observation that glutamate binding is still needed for observed stretch response. Thus, our data taken with the observed loss of Mg^{2+} block reported by Zhang et al (1996), suggests that stretch in neuronal culture induces a selective loss in Mg^{2+} block in NR2B containing receptors allowing for enhanced calcium entry when bound and activated by glutamate. Supporting this thought is the fact that MK801 is not as effective as APV in mitigating the NR1/NR2B stretch response. MK801 and Mg^{2+} both block conductance through binding of a well defined region of the NMDAR pore (Kashiwagi et al 2002), and thus stretch may induce a change

in the pore region that could alter both the inherent Mg^{2+} block as well as MK801 effectiveness. It is also important to point out that this does not suggest that NR1/NR2A-NMDARs have no role in the neuronal response to injury. Although insensitive to a loss in Mg^{2+} block, they can still be activated by synaptically released glutamate and contribute to the overall signaling seen after injury.

Influence of C-terminal NR2B in its mechanosensitivity

With the expression of NR2B truncation mutants, we were able to demonstrate that the cytoplasmic C-terminal tail of NR2B is integral in NR2B mechanosensitivity. Elimination of the region distal to amino acid 1036 significantly reduced observed NR2B mechanosensitivity at 40% stretch. This region is rich with phosphorylation sites, protein binding sites, and anchoring sites for cytoskeletal elements. While we were unable to investigate the role of cytoskeletal anchoring in this model, it remains an intriguing potential mediator of NMDAR mechanosensitivity. Our lab has previously demonstrated that primary cortical cultures display an almost complete elimination of immediate stretch response when pretreated with latrunculin A, to destabilize the cytoskeleton (Geddes-Klein et al 2006). However, it remains unknown whether the mechanism of this reduction acts on the postsynaptic receptors, or at presynaptic sites of glutamate release. NR2B has a stronger linkage to the actin cytoskeleton than NR2A, primarily through binding sites of spectrin and α -actinin-2 located in the distal region of the NR2B C-terminus. Thus, force transfer through the cytoskeleton to the NR2B subunit may play an important role in its mechanosensitivity. Interestingly, elimination of the C-terminal tail

distal to amino acid 1433 produced no difference in stretch response. This region notably contains a binding site for PSD95, suggesting that NR2B association with this essential scaffolding protein does not play a large role in mechanosensitivity. This highlights the potential for synaptic and extrasynaptic NR2B containing receptors to have similar mechanosensitivity, although more experiments would be necessary to fully examine this point.

PKC activity and Ser-1323 on NR2B regulates NR2B mechanosensitivity

Consistent with the previously reported role of PKC activity in loss of Mg^{2+} block in stretched neurons (Zhang et al 1996), we demonstrate that PKC inhibition significantly attenuates stretch induced calcium influx in NR1/NR2B transfected HEKs and primary cortical cultures. Further, by utilizing NR2B point mutations, mutated at known PKC phosphorylation sites, we have shown that NR2B mechanosensitivity is regulated by a single critical residue, Ser-1323. Expression of NR2B-S1323A significantly reduced NR2B mechanosensitivity, while not affecting response to NMDA stimulation.

Together, this suggests that PKC activity upon this residue on NR2B can dynamically control receptor mechanosensitivity. This provides an intriguing mechanism in which the mechanical tone of a given neuron can be manipulated. While the precise mechanism of how this residue can control mechanosensitivity remains unknown, there is past evidence that PKC activity can influence the state of the Mg^{2+} block (Chen and Huang 1992).

Together, this data suggests that the intricate interplay between PKC activity and stretch

can influence the extent of neuronal calcium entry during TBI, potentially impacting both primary and secondary cell death.

Development of computational model of stochastic glutamatergic signaling at a single dendritic spine

Investigations of NMDAR subtype specific roles in both physiological and pathologic function has primarily relied upon the use of subtype specific antagonists. However, there has recently been considerable debate on the specificity of these tools, which has made these particular studies difficult to interpret (Neyton and Paoletti 2006). Thus, we have developed a new stochastic model of glutamatergic signaling at a single dendritic spine in which we were able to better examine differences in activation patterns between NMDAR subtypes. While past computational models have been able to examine NMDAR saturation (Franks et al 2003, Raghavachari and Lisman 2004) and the effect of glutamate spillover (Ruskov and Kullmann 1998, Pankratov and Krishtal 2003, Mitchell et al. 2007), the recent discovery of subtype specific reaction rates has only now allowed for the examination of specific subtypes. Using this model, we have made three major conclusions about subtype activation during physiological neurotransmission: (1) Differential dynamic range among subtypes, (2) Frequency dependent shifts in the pattern of NMDAR subtype activation, and (3) Synaptic subtype content influences extent and fidelity of NMDAR activation.

Differential dynamic ranges of activation among NMDAR subtypes

We have shown that the different NMDAR subtypes display unique ranges in activation to varied amounts of glutamate release. At low levels of presynaptic glutamate release (500-1500 molecules), the range seen during release of a single vesicle, NR1/NR2A-NMDARs are primarily activated, while there is little to no activation of triheteromeric or NR1/NR2B-NMDARs. Furthermore, the activation of NR1/NR2A-NMDARs significantly increases throughout this range, but saturates at releases of greater than 3000 molecules. In contrast, activation of triheteromeric and NR1/NR2B-NMDARs scales within the larger levels of glutamate release. This data suggests that NR1/NR2A-NMDARs are the primary mediator of univesicular release, while NR2B-containing NMDARs are more suited to discriminate between signals at multivesicular release. There have recently been extensive investigations on the preponderance of univesicular or multivesicular release at specific synapses, with evidence demonstrating that both types of glutamate release occur throughout the CNS (Gulyas et al 1993, Hanse and Gustafsson 2001a, Hanse and Gustafsson 2001b, Christie and Jahr 2006). Here we show that differences in the activation kinetics of NMDAR subtypes allow for the ability for synapses to generate unique postsynaptic responses to these different presynaptic glutamate signals

Frequency of presynaptic stimulation alters patterns of NMDAR subtype activation

Presynaptic stimulation, at varied frequencies, is traditionally the most common model to induce different forms of synaptic plasticity including LTD and LTP. There is currently considerable debate within the literature regarding the role of subtypes in governing both LTD and LTP induction (Liu et al 2004, Massey et al 2004, Barria and Malinow 2005, Bartlett et al 2007). Using our computational model, we showed that frequency of stimulation significantly impacts the pattern of NMDAR subtype activation. Most functional synapses contain a diverse set of NMDAR subtypes at defined synaptic and extrasynaptic sites. Using an idealized population of NMDAR subtypes, we observed that increasing frequency significantly increases the contribution of NR2B containing NMDARs to the total postsynaptic response with a concurrent decrease in the contribution of NR1/NR2A-NMDARs. Thus, while increased frequency also increases the overall NMDAR activation, changes in the balance of subtype specific signaling are likely to impact long term changes at the synapse. Our finding supports both major hypotheses of synaptic plasticity that alternatively argue that either overall calcium load or subtype specific activation directs plasticity. However, we feel that our model provides an additional tool in future examinations of how specific subtypes respond to different models of plasticity induction.

Synaptic subtype content influences extent and fidelity of signaling

The identity of synaptic NMDARs changes through development, with NR1/NR2B-NMDARs being replaced by NR2A. However, there has yet to be a consensus on the relative content synaptic NMDAR subtypes at mature spines (Tovar and Westbrook 1999, Al-Hallaq et al 2007, Rauner and Kohr 2010). By using two additional models of synaptic plasticity induction, chemical LTP and spike-timing dependent plasticity, we demonstrated that particular content of these synaptic NMDARs drastically impacts both the overall extent as well as the fidelity of postsynaptic responses. Both a 5Hz release of glutamate, as seen during chemical LTP, and spike-timed postsynaptic depolarization fail to generate consistent calcium entry in immature, NR1/NR2B-NMDAR dominated synapses. However, recent evidence suggests that NR2B in immature cultures retain the ability to transmit a number of LTD and LTP inducing pathways (Martel et al 2009). This suggests that other compensatory mechanisms, including increased receptor number or multivesicular release, may be necessary for proper signaling at younger spines. Furthermore, we showed that postsynaptic responses produced by spines with 100% NR1/NR2A-NMDARs at synaptic sites, a configuration that is often thought of as the prototypical mature spine, are significantly enhanced and more consistent than spines with a reported “physiological” mix of subtypes. Together, this data demonstrates that increased NR2A content significantly improves the extent and fidelity of postsynaptic responses to glutamate stimuli.

Simulated injury mediated glutamate release enhances contribution of NR2B containing NMDARs

A hallmark of TBI has been the observation of increased extracellular glutamate, which can lead to over-activation of glutamate receptors, including NMDARs, and eventually to cell death and network dysfunction (Faden et al 1989, Nilsson et al 1994). While it is expected that excessive glutamate will potentiate the activation of all NMDARs, we used our computational model to examine if the patterns of subtype activation are significantly altered by the immediate glutamate release seen during injury. Indeed, we demonstrated that simulated injury, modeled as the release of 5 or 15 synaptic glutamate vesicles, significantly increases NMDAR activation and the contribution of NR2B containing NMDARs, compared to univesicular release. Strikingly, the largest increase was seen in the contribution of extrasynaptic NR1/NR2B-NMDARs, whose activation is extremely rare during univesicular release. This data suggests that the activation of this pool of receptors during injury may represent a unique pathologic switch.

Combined effects of injury mediated glutamate release and selective mechanosensitivity

We have argued that TBI represents a unique disease state as it contains the dual effects of injury mediated glutamate release combined with NMDAR mechanosensitivity. We used our computational model to examine calcium influx during simulated injury,

with or without the added effect of selective NR2B mechanosensitivity. As expected, the modeled loss or reduction of Mg^{2+} block in NR2B containing NMDARs drastically increased the extent of the immediate calcium influx and resultant calmodulin activation occurring at the time of injury. However, potentially more importantly, the contribution of extrasynaptic NR1/NR2B-NMDARs is significantly greater in conditions of selective mechanosensitivity. Interestingly, the contribution of extrasynaptic NMDARs to the overall calcium load in the injury mediated glutamate + mechanosensitivity simulations is in agreement with the observed contribution of extrasynaptic NMDARs to calcium influx following *in vitro* stretch injury of primary cortical neurons. Our simulations showed that the added effect of mechanosensitivity during the mechanical insult potentiates overall calcium load and shifts the balance of NMDAR source specific signaling towards that mediated by extrasynaptic NMDARs. Both of these consequences will exacerbate pro-death signaling stemming from the injury, and thus have major influence on the extent of primary damage seen after injury.

Persistent loss of Mg^{2+} block can alter fidelity of network signaling

Among the most intriguing observations made through these studies is the potential for persistent dysfunction in the activity of postsynaptic spines caused by NR2B mechanosensitivity. Zhang et al (1996) has shown that the loss of Mg^{2+} block lasts up to 6 hours post stretch injury. This suggests that responses to physiological levels of glutamate signaling in this post acute period following injury may be significantly

altered. Using our model, we demonstrated that calcium influx following a physiological univesicular release at “injured” spines produces two unique phenotypes, with most simulations exhibiting calcium influx that is not different from the uninjured case while several simulations result in significantly enhanced calcium. Not surprisingly, increased calcium was found in simulations with NR1/NR2B-NMDAR activation. Given that the kinetics of NR1/NR2B-NMDAR activation make activation of this subtype rare during single vesicle release, our model predicted that persistent loss of Mg^{2+} block in NR2B containing receptors results in enhanced calcium in only a small subset of univesicular release simulations. However, enhanced calcium entry, specifically through NR2B containing receptors, has the potential to aberrantly activate pro-death signaling pathways and thus contribute to secondary cell death. Furthermore, the observation of inconsistency or reduction of fidelity in physiological glutamatergic signaling has the potential to disrupt network communication. It should be noted that while NR2B activation is rare following single vesicle release, it is predicted to be more predominant in coordinated network communication, thus allowing NR2B dysfunction to have a larger influence in aberrant signaling following these stimulation paradigms. Network dysfunction following injury has been recently reported (Goforth et al 2011), and is currently being explored in our lab. It remains an open question as to the particular consequences of this observed network dysfunction as to a role in secondary cell death or behavioral deficits. However, the manipulation and potential restoration of proper network communication in the post acute therapeutic window represents an intriguing

therapeutic strategy in mitigating secondary damage following TBI. Here, our data suggest that the selective and persistent loss of Mg^{2+} block in NR2B containing NMDARs represents a mechanism for sustained network dysfunction, and thus the NR2B subunit may be an intriguing therapeutic target.

LIMITATIONS AND FUTURE DIRECTIONS

In our studies, we used two alternative models to examine the role of NMDAR subtypes in TBI, partly due to the drawbacks and limitations of currently used experimental tools. While we believe that using these models has enabled us to ask and answer questions that would be otherwise difficult or impossible to study, they come with their own set of inherent limitations that could require further study. In spite of these potential caveats, our data has revealed several key features of NMDAR subtype function which can lead to some intriguing future research, with the eventual goal of directing the strategy of TBI therapeutics.

In evaluating NMDAR mechanosensitivity, we were eager to isolate the receptor from the synaptic architecture so that receptor activity would not be greatly influenced from glutamate release from nearby sites. While we believe that this technique allowed us to demonstrate the selective mechanosensitivity of NR2B containing NMDARs, it is possible that other components of the synapse can influence receptor mechanosensitivity. While we expressed the most common scaffolding protein, PSD95, along with NMDAR subunits, it is likely that it does not completely replicate the intracellular scaffolding

network seen in neurons. The environment within a dendritic spine is rich with scaffolding proteins, aside from PSD95, which include the MAGUKs PSD93, SAP97, and SAP102 (Montgomery et al 2004). These scaffolds and associated protein complexes may play a role in the transfer of force to surface NMDARs, and thus mechanosensitivity is likely to be more complex in the neuronal architecture compared to that observed in HEKs. Thus, while using a recombinant system allows for unique manipulation and interpretation, the inherent drawback of a lack of physiological complexity necessitates the validation in higher order models.

We are currently working towards creating AAV-plasmids which encode truncation and point mutations of NR2B. These plasmids will provide increased transfection efficiency in neuronal culture, and thus we can effectively investigate the role of Ser-1323 in the stretch response in primary neurons. Expression of mutant and potentially stretch resistant NR2B can thus be used to evaluate changes in cell viability as well as network dysfunction following *in vitro* stretch. Additionally, we have engaged in preliminary studies that examined the potential beneficial effects of tamoxifen pretreatment in *in vivo* injury. One of the primary reasons for choosing tamoxifen as the PKC antagonist in our studies to was that it is a compound already used clinically, for its therapeutic effects in treating cancer. Thus, if shown effective in treating TBI in animal models, it would provide a relatively quick route to clinical use. With this in mind, future studies are planned to evaluate if tamoxifen treatment can improve learning and

memory, as measured by Morris water maze, following cortical impact or fluid percussion injuries in mice.

In our investigation of mechanosensitivity, we evaluated the stretch response only at 40% stretch, as stretch at higher levels was seen to cause calcium influx in non NMDAR transfected HEKs, presumably through shearing of the plasma membrane. Thus, it is quite possible that the stretch sensitivity of NR2A may not be observed until higher levels of mechanical stretch. Indeed NR2A contains two PKC phosphorylation sites, at Ser-1291 and Ser-1312, analogous to Ser-1303 and Ser-1323 on NR2B, and thus a similar PKC regulated mechanosensitivity of NR2A is quite possible. The precise level of stretch is of importance in the determination of cell fate, where cell death 24 hours post stretch in dissociated cortical cultures is only apparent above 80% stretch (Spaethling et al 2008). Thus, if we assume that stretch levels scale between HEKs and dissociated neurons, selective NR2B mechanosensitivity may not play a large role in the amount of cell death seen during TBI. However, there has been increasing importance paid to the effects of mild injury, where cell death may not be as evident. Thus, NR2B mechanosensitivity may play a larger role in the aberrant postsynaptic signaling in surviving neurons, a prediction also made by our injury simulations. Given this possibility, potential changes in the neural network dynamics of stretch injured cultures is currently being explored by our lab and others. Together, our data suggests that NR2B may play a larger role in signaling seen after injury – potentially competing with NR2A mediated signaling. Further, there is debate as to whether synaptic NR2B mediates pro-

survival (Martel et al 2009) or pro-death (Liu et al 2007) signaling. Further clarification on the role of this subtype will help elucidate whether enhanced calcium entry through these receptors can potentially compete with pro-death signaling from extrasynaptic receptors or alternatively simply add to the calcium overload. Thus, data from both our *in vitro* and *in silico* models leads to several more additional questions regarding how NMDAR subtypes, and their resultant signaling, impact network behavior and neuronal damage in the critical post acute period after injury.

As with most computational models, specific parameters must be assumed from published data in order to simulate the best possible representation of the physiological system. In this work, we used prior work to guide our decisions on the number and localization of AMPARs and NMDAR subtypes. With the knowledge that these parameters are likely to vary from region to region within the brain, and even from spine to spine on a single dendrite, we kept these values constant for better comparison between the activities of NMDAR subtypes. Given our observed scalability of the activation of individual receptors to predict the total activation of a population of receptors, it is possible to use distributions of receptor number to simulate the activation profiles among a variety of spines with different NMDAR subtype content. Using this technique will enable future work in which we can use the stochastic model of signaling at a single spine as a basis for simulating the activity of all spines on a cell, and eventually scaling to the entire neural network.

Again, similar to the drawback of limited complexity in HEKs, model simulations are limited by the presence of only a portion of the elements seen physiologically. Here, we focused our simulations on the activity of AMPARs and NMDARs. Future work may include the activation of metabotropic glutamate receptors, and include calcium entry from voltage dependent sources. Similarly, when simulating CaM activation we attempted to make our simulations more realistic by including other potential calcium buffering proteins. However, realistically, the spine is rich numerous buffers, proteins, and protein complexes, all of which can impact diffusion rates, calcium dynamics, and CaM activation. With this in mind, we hope that our model represents a framework in which future elements or conditions can be easily added and evaluated. For instance, we demonstrate that loss of Mg^{2+} block in the NR2B containing receptors in the post acute period results in reduced fidelity of the postsynaptic response by creating a subset of responses with greatly enhanced calcium entry. However, we are aware that TBI has numerous consequences which can also impact glutamatergic signaling at the synapse. Work in our lab and others has shown that AMPAR activity is significantly altered after injury, with a reported loss of desensitization (Goforth et al 1999, Goforth et al 2004) and increased expression of aberrant calcium permeable AMPARs (Spaethling et al 2008). NMDAR expression is also known to be altered, with reported preferential decreases in NR2A expression (Giza et al 2006). Astrocytic function may also be compromised, with actions on glutamate transporter activity (Yi and Hazell 2006), and potentially the release of astrocytic glutamate directly onto extrasynaptic NMDARs. Finally, we have

preliminary evidence that spine shape may be transiently altered by stretch. All of these additional characteristics of the injured spine in the post acute period can be added to our model to determine their influence on the extent and reliability of postsynaptic signaling. In this way, our model can be used in concert with traditional experimental methods for more complete investigations of activity in the injured neuron.

CONCLUSION

TBI is a devastating injury which can have detrimental short term and long term effects on the neurologic function and quality of life for many patients. Despite the recent advances made in the understanding of the neuronal response to injury, and the increased attention to TBI in the past several years, an effective therapeutic strategy is lacking. The NMDAR is now well established to be the primary mediator of cell death and dysfunction following injury, but the lack of success in clinical trials may have taken the attention away from NMDAR-centric strategies for TBI intervention. The observed diversity in NMDAR function has led to considerable confusion within the field on how the activity of these receptors can be manipulated to best treat pathological conditions while promoting physiological function. In this report we used unique models to provide additional information on how the multiple subtypes of NMDARs are uniquely suited to transmit different stimuli, and are differentially impacted by injury. Collectively, our data demonstrates that the NR2B subunit can act as an effective pathological switch, whose activation is preferentially influenced by the biomechanical components of TBI.

Finally, this work provides a new model system for the future investigation of injury induced modifications of synaptic communication, and further argues for a stronger look at targeting the NR2B subunit, and associated signaling, in strategies for protection and treatment for brain injuries.

Bibliography

- Adesnik, H., G. Li, et al. (2008). "NMDA receptors inhibit synapse unsilencing during brain development." Proc Natl Acad Sci U S A **105**(14): 5597-602.
- Al-Hallaq, R. A., T. P. Conrads, et al. (2007). "NMDA di-heteromeric receptor populations and associated proteins in rat hippocampus." J Neurosci **27**(31): 8334-43.
- Anderson, T., M. Heitger, et al. (2006). "Concussion and mild head injury." Pract Neurol **6**(6): 342-357.
- Andrews, S. S. (2009). "Accurate particle-based simulation of adsorption, desorption and partial transmission." Phys Biol **6**(4): 046015.
- Andrews, S. S. and D. Bray (2004). "Stochastic simulation of chemical reactions with spatial resolution and single molecule detail." Phys Biol **1**(3-4): 137-51.
- Aoki, C., S. Fujisawa, et al. (2003). "NMDA receptor blockade in intact adult cortex increases trafficking of NR2A subunits into spines, postsynaptic densities, and axon terminals." Brain Res **963**(1-2): 139-49.
- Arnold, F. J., F. Hofmann, et al. (2005). "Microelectrode array recordings of cultured hippocampal networks reveal a simple model for transcription and protein synthesis-dependent plasticity." J Physiol **564**(Pt 1): 3-19.
- Arundine, M., G. K. Chopra, et al. (2003). "Enhanced vulnerability to NMDA toxicity in sublethal traumatic neuronal injury in vitro." J Neurotrauma **20**(12): 1377-95.
- Arundine, M. and M. Tymianski (2004). "Molecular mechanisms of glutamate-dependent neurodegeneration in ischemia and traumatic brain injury." Cell Mol Life Sci **61**(6): 657-68.
- Auberson, Y. P., H. Allgeier, et al. (2002). "5-Phosphonomethylquinoxalinediones as competitive NMDA receptor antagonists with a preference for the human 1A/2A, rather than 1A/2B receptor composition." Bioorg Med Chem Lett **12**(7): 1099-102.
- Barria, A. and R. Malinow (2005). "NMDA receptor subunit composition controls synaptic plasticity by regulating binding to CaMKII." Neuron **48**(2): 289-301.
- Bartlett, T. E., N. J. Bannister, et al. (2007). "Differential roles of NR2A and NR2B-containing NMDA receptors in LTP and LTD in the CA1 region of two-week old rat hippocampus." Neuropharmacology **52**(1): 60-70.
- Bear, M. F. and R. C. Malenka (1994). "Synaptic plasticity: LTP and LTD." Curr Opin Neurobiol **4**(3): 389-99.

- Berberich, S., V. Jensen, et al. (2007). "The role of NMDAR subtypes and charge transfer during hippocampal LTP induction." Neuropharmacology **52**(1): 77-86.
- Berberich, S., P. Punnakal, et al. (2005). "Lack of NMDA receptor subtype selectivity for hippocampal long-term potentiation." J Neurosci **25**(29): 6907-10.
- Biegon, A., P. A. Fry, et al. (2004). "Dynamic changes in N-methyl-D-aspartate receptors after closed head injury in mice: Implications for treatment of neurological and cognitive deficits." Proc Natl Acad Sci U S A **101**(14): 5117-22.
- Bigford, G. E., O. F. Alonso, et al. (2009). "A novel protein complex in membrane rafts linking the NR2B glutamate receptor and autophagy is disrupted following traumatic brain injury." J Neurotrauma **26**(5): 703-20.
- Boeckman, F. A. and E. Aizenman (1994). "Stable transfection of the NR1 subunit in Chinese hamster ovary cells fails to produce a functional N-methyl-D-aspartate receptor." Neurosci Lett **173**(1-2): 189-92.
- Boeckman, F. A. and E. Aizenman (1996). "Pharmacological properties of acquired excitotoxicity in Chinese hamster ovary cells transfected with N-methyl-D-aspartate receptor subunits." J Pharmacol Exp Ther **279**(2): 515-23.
- Bradshaw, J. M., Y. Kubota, et al. (2003). "An ultrasensitive Ca²⁺/calmodulin-dependent protein kinase II-protein phosphatase 1 switch facilitates specificity in postsynaptic calcium signaling." Proc Natl Acad Sci U S A **100**(18): 10512-7.
- Buchanan, K. A. and J. R. Mellor (2010). "The activity requirements for spike timing-dependent plasticity in the hippocampus." Front Synaptic Neurosci **2**: 11.
- Bullock, R., A. Zauner, et al. (1995). "Evidence for prolonged release of excitatory amino acids in severe human head trauma. Relationship to clinical events." Ann N Y Acad Sci **765**: 290-7; discussion 298.
- Burger, P. M., E. Mehl, et al. (1989). "Synaptic vesicles immunisolated from rat cerebral cortex contain high levels of glutamate." Neuron **3**(6): 715-20.
- Casado, M. and P. Ascher (1998). "Opposite modulation of NMDA receptors by lysophospholipids and arachidonic acid: common features with mechanosensitivity." J Physiol **513** (Pt 2): 317-30.
- Chen, B. S. and K. W. Roche (2007). "Regulation of NMDA receptors by phosphorylation." Neuropharmacology **53**(3): 362-8.
- Chen, L. and L. Y. Huang (1992). "Protein kinase C reduces Mg²⁺ block of NMDA-receptor channels as a mechanism of modulation." Nature **356**(6369): 521-3.

- Chen, M., T. J. Lu, et al. (2008). "Differential roles of NMDA receptor subtypes in ischemic neuronal cell death and ischemic tolerance." Stroke **39**(11): 3042-8.
- Cheng, A., S. Wang, et al. (2003). "Calmodulin mediates brain-derived neurotrophic factor cell survival signaling upstream of Akt kinase in embryonic neocortical neurons." J Biol Chem **278**(9): 7591-9.
- Cheng, D., C. C. Hoogenraad, et al. (2006). "Relative and absolute quantification of postsynaptic density proteome isolated from rat forebrain and cerebellum." Mol Cell Proteomics **5**(6): 1158-70.
- Choi, D. W. (1988). "Glutamate neurotoxicity and diseases of the nervous system." Neuron **1**(8): 623-34.
- Choi, D. W., M. Maulucci-Gedde, et al. (1987). "Glutamate neurotoxicity in cortical cell culture." J Neurosci **7**(2): 357-68.
- Christie, J. M. and C. E. Jahr (2006). "Multivesicular release at Schaffer collateral-CA1 hippocampal synapses." J Neurosci **26**(1): 210-6.
- Cohen, O., E. Feinstein, et al. (1997). "DAP-kinase is a Ca²⁺/calmodulin-dependent, cytoskeletal-associated protein kinase, with cell death-inducing functions that depend on its catalytic activity." Embo J **16**(5): 998-1008.
- Conti, R. and J. Lisman (2003). "The high variance of AMPA receptor- and NMDA receptor-mediated responses at single hippocampal synapses: evidence for multiquantal release." Proc Natl Acad Sci U S A **100**(8): 4885-90.
- Cull-Candy, S., S. Brickley, et al. (2001). "NMDA receptor subunits: diversity, development and disease." Curr Opin Neurobiol **11**(3): 327-35.
- Cull-Candy, S. G. and D. N. Leszkiewicz (2004). "Role of distinct NMDA receptor subtypes at central synapses." Sci STKE **2004**(255): re16.
- Dempsey, R. J., M. K. Baskaya, et al. (2000). "Attenuation of brain edema, blood-brain barrier breakdown, and injury volume by ifenprodil, a polyamine-site N-methyl-D-aspartate receptor antagonist, after experimental traumatic brain injury in rats." Neurosurgery **47**(2): 399-404; discussion 404-6.
- DeRidder, M. N., M. J. Simon, et al. (2006). "Traumatic mechanical injury to the hippocampus in vitro causes regional caspase-3 and calpain activation that is influenced by NMDA receptor subunit composition." Neurobiol Dis **22**(1): 165-76.
- Dingledine, R., K. Borges, et al. (1999). "The glutamate receptor ion channels." Pharmacol Rev **51**(1): 7-61.

- Dolowy, K. (1984). "Bioelectrochemistry of cell surfaces." Prog Surf Sci **15**: 245-368.
- Dugan, L. L., S. L. Sensi, et al. (1995). "Mitochondrial production of reactive oxygen species in cortical neurons following exposure to N-methyl-D-aspartate." J Neurosci **15**(10): 6377-88.
- Ehlers, M. D., E. T. Fung, et al. (1998). "Splice variant-specific interaction of the NMDA receptor subunit NR1 with neuronal intermediate filaments." J Neurosci **18**(2): 720-30.
- Erreger, K., S. M. Dravid, et al. (2005). "Subunit-specific gating controls rat NR1/NR2A and NR1/NR2B NMDA channel kinetics and synaptic signalling profiles." J Physiol **563**(Pt 2): 345-58.
- Espinosa, J. S., D. G. Wheeler, et al. (2009). "Uncoupling dendrite growth and patterning: single-cell knockout analysis of NMDA receptor 2B." Neuron **62**(2): 205-17.
- Ewald, R. C., K. R. Van Keuren-Jensen, et al. (2008). "Roles of NR2A and NR2B in the development of dendritic arbor morphology in vivo." J Neurosci **28**(4): 850-61.
- Faden, A. I., P. Demediuk, et al. (1989). "The role of excitatory amino acids and NMDA receptors in traumatic brain injury." Science **244**(4906): 798-800.
- Fedulov, V., C. S. Rex, et al. (2007). "Evidence that long-term potentiation occurs within individual hippocampal synapses during learning." J Neurosci **27**(30): 8031-9.
- Foster, K. A., N. McLaughlin, et al. (2010). "Distinct roles of NR2A and NR2B cytoplasmic tails in long-term potentiation." J Neurosci **30**(7): 2676-85.
- Franks, K. M., T. M. Bartol, Jr., et al. (2002). "A Monte Carlo model reveals independent signaling at central glutamatergic synapses." Biophys J **83**(5): 2333-48.
- Franks, K. M., C. F. Stevens, et al. (2003). "Independent sources of quantal variability at single glutamatergic synapses." J Neurosci **23**(8): 3186-95.
- Gallagher, M. J., H. Huang, et al. (1996). "Interactions between ifenprodil and the NR2B subunit of the N-methyl-D-aspartate receptor." J Biol Chem **271**(16): 9603-11.
- Geddes-Klein, D. M., G. Serbest, et al. (2006). "Pharmacologically induced calcium oscillations protect neurons from increases in cytosolic calcium after trauma." J Neurochem **97**(2): 462-74.
- Georgiev, D., H. Taniura, et al. (2008). "A critical importance of polyamine site in NMDA receptors for neurite outgrowth and fasciculation at early stages of P19 neuronal differentiation." Exp Cell Res **314**(14): 2603-17.

- Ghajar, J. (2000). "Traumatic brain injury." Lancet **356**(9233): 923-9.
- Giza, C. C., N. S. Maria, et al. (2006). "N-methyl-D-aspartate receptor subunit changes after traumatic injury to the developing brain." J Neurotrauma **23**(6): 950-61.
- Goforth, P. B., E. F. Ellis, et al. (1999). "Enhancement of AMPA-mediated current after traumatic injury in cortical neurons." J Neurosci **19**(17): 7367-74.
- Goforth, P. B., E. F. Ellis, et al. (2004). "Mechanical injury modulates AMPA receptor kinetics via an NMDA receptor-dependent pathway." J Neurotrauma **21**(6): 719-32.
- Goforth, P. B., J. Ren, et al. (2011). "Excitatory synaptic transmission and network activity are depressed following mechanical injury in cortical neurons." J Neurophysiol.
- Gogas, K. R. (2006). "Glutamate-based therapeutic approaches: NR2B receptor antagonists." Curr Opin Pharmacol **6**(1): 68-74.
- Grant, E. R., B. J. Bacskai, et al. (1998). "Opposing contributions of NR1 and NR2 to protein kinase C modulation of NMDA receptors." J Neurochem **71**(4): 1471-81.
- Gulyas, A. I., R. Miles, et al. (1993). "Hippocampal pyramidal cells excite inhibitory neurons through a single release site." Nature **366**(6456): 683-7.
- Guttmann, R. P., D. L. Baker, et al. (2001). "Specific proteolysis of the NR2 subunit at multiple sites by calpain." J Neurochem **78**(5): 1083-93.
- Hanse, E. and B. Gustafsson (2001). "Factors explaining heterogeneity in short-term synaptic dynamics of hippocampal glutamatergic synapses in the neonatal rat." J Physiol **537**(Pt 1): 141-9.
- Hanse, E. and B. Gustafsson (2001). "Quantal variability at glutamatergic synapses in area CA1 of the rat neonatal hippocampus." J Physiol **531**(Pt 2): 467-80.
- Hardingham, G. E. (2006). "Pro-survival signalling from the NMDA receptor." Biochem Soc Trans **34**(Pt 5): 936-8.
- Hardingham, G. E. (2009). "Coupling of the NMDA receptor to neuroprotective and neurodestructive events." Biochem Soc Trans **37**(Pt 6): 1147-60.
- Hardingham, G. E. and H. Bading (2003). "The Yin and Yang of NMDA receptor signalling." Trends Neurosci **26**(2): 81-9.

- Hardingham, G. E. and H. Bading (2010). "Synaptic versus extrasynaptic NMDA receptor signalling: implications for neurodegenerative disorders." Nat Rev Neurosci **11**(10): 682-96.
- Hardingham, G. E., Y. Fukunaga, et al. (2002). "Extrasynaptic NMDARs oppose synaptic NMDARs by triggering CREB shut-off and cell death pathways." Nat Neurosci **5**(5): 405-14.
- Harris, A. Z. and D. L. Pettit (2007). "Extrasynaptic and synaptic NMDA receptors form stable and uniform pools in rat hippocampal slices." J Physiol **584**(Pt 2): 509-19.
- Harris, K. M., F. E. Jensen, et al. (1992). "Three-dimensional structure of dendritic spines and synapses in rat hippocampus (CA1) at postnatal day 15 and adult ages: implications for the maturation of synaptic physiology and long-term potentiation." J Neurosci **12**(7): 2685-705.
- Hatton, C. J. and P. Paoletti (2005). "Modulation of triheteromeric NMDA receptors by N-terminal domain ligands." Neuron **46**(2): 261-74.
- Hetman, M. and G. Kharebava (2006). "Survival signaling pathways activated by NMDA receptors." Curr Top Med Chem **6**(8): 787-99.
- Hoge, C. W., D. McGurk, et al. (2008). "Mild traumatic brain injury in U.S. Soldiers returning from Iraq." N Engl J Med **358**(5): 453-63.
- Holmes, W. R. (1995). "Modeling the effect of glutamate diffusion and uptake on NMDA and non-NMDA receptor saturation." Biophys J **69**(5): 1734-47.
- Huang, C. Y. and J. E. Ferrell, Jr. (1996). "Ultrasensitivity in the mitogen-activated protein kinase cascade." Proc Natl Acad Sci U S A **93**(19): 10078-83.
- Huerta, P. T., L. D. Sun, et al. (2000). "Formation of temporal memory requires NMDA receptors within CA1 pyramidal neurons." Neuron **25**(2): 473-80.
- Ikonomidou, C., F. Bosch, et al. (1999). "Blockade of NMDA receptors and apoptotic neurodegeneration in the developing brain." Science **283**(5398): 70-4.
- Ikonomidou, C., V. Stefovskaja, et al. (2000). "Neuronal death enhanced by N-methyl-D-aspartate antagonists." Proc Natl Acad Sci U S A **97**(23): 12885-90.
- Ikonomidou, C. and L. Turski (2002). "Why did NMDA receptor antagonists fail clinical trials for stroke and traumatic brain injury?" Lancet Neurol **1**(6): 383-6.
- Iwasaki, S. and T. Takahashi (2001). "Developmental regulation of transmitter release at the calyx of Held in rat auditory brainstem." J Physiol **534**(Pt 3): 861-71.

- Jahr, C. E. and C. F. Stevens (1990). "Voltage dependence of NMDA-activated macroscopic conductances predicted by single-channel kinetics." J Neurosci **10**(9): 3178-82.
- Jiang, F. X., B. Yurke, et al. (2008). "Neurite outgrowth on a DNA crosslinked hydrogel with tunable stiffnesses." Ann Biomed Eng **36**(9): 1565-79.
- Jiang, F. X., B. Yurke, et al. (2010). "Effect of dynamic stiffness of the substrates on neurite outgrowth by using a DNA-crosslinked hydrogel." Tissue Eng Part A **16**(6): 1873-89.
- Jin, S. X. and L. A. Feig (2010). "Long-term potentiation in the CA1 hippocampus induced by NR2A subunit-containing NMDA glutamate receptors is mediated by Ras-GRF2/Erk map kinase signaling." PLoS One **5**(7): e11732.
- Jonas, P., G. Major, et al. (1993). "Quantal components of unitary EPSCs at the mossy fibre synapse on CA3 pyramidal cells of rat hippocampus." J Physiol **472**: 615-63.
- Jones, M. L. and J. P. Leonard (2005). "PKC site mutations reveal differential modulation by insulin of NMDA receptors containing NR2A or NR2B subunits." J Neurochem **92**(6): 1431-8.
- Kandaswamy, U., P. Y. Deng, et al. (2010). "The role of presynaptic dynamics in processing of natural spike trains in hippocampal synapses." J Neurosci **30**(47): 15904-14.
- Kashiwagi, K., T. Masuko, et al. (2002). "Channel blockers acting at N-methyl-D-aspartate receptors: differential effects of mutations in the vestibule and ion channel pore." Mol Pharmacol **61**(3): 533-45.
- Keller, D. X., K. M. Franks, et al. (2008). "Calmodulin activation by calcium transients in the postsynaptic density of dendritic spines." PLoS One **3**(4): e2045.
- Kendrick, S. J., D. R. Lynch, et al. (1996). "Characterization of glutamate binding sites in receptors assembled from transfected NMDA receptor subunits." J Neurochem **67**(2): 608-16.
- Kim, M. J., A. W. Dunah, et al. (2005). "Differential roles of NR2A- and NR2B-containing NMDA receptors in Ras-ERK signaling and AMPA receptor trafficking." Neuron **46**(5): 745-60.
- Kinney, J. W., C. N. Davis, et al. (2006). "A specific role for NR2A-containing NMDA receptors in the maintenance of parvalbumin and GAD67 immunoreactivity in cultured interneurons." J Neurosci **26**(5): 1604-15.

- Kochanek, P. M., R. S. Clark, et al. (2000). "Biochemical, cellular, and molecular mechanisms in the evolution of secondary damage after severe traumatic brain injury in infants and children: Lessons learned from the bedside." *Pediatr Crit Care Med* **1**(1): 4-19.
- Kohr, G., V. Jensen, et al. (2003). "Intracellular domains of NMDA receptor subtypes are determinants for long-term potentiation induction." *J Neurosci* **23**(34): 10791-9.
- Krapivinsky, G., L. Krapivinsky, et al. (2003). "The NMDA receptor is coupled to the ERK pathway by a direct interaction between NR2B and RasGRF1." *Neuron* **40**(4): 775-84.
- Kung, C. (2005). "A possible unifying principle for mechanosensation." *Nature* **436**(7051): 647-54.
- Lawrence, J. J., Z. M. Grinspan, et al. (2004). "Quantal transmission at mossy fibre targets in the CA3 region of the rat hippocampus." *J Physiol* **554**(Pt 1): 175-93.
- Lee, S. J., Y. Escobedo-Lozoya, et al. (2009). "Activation of CaMKII in single dendritic spines during long-term potentiation." *Nature* **458**(7236): 299-304.
- Li, S., X. Tian, et al. (2006). "Distinct roles for Ras-guanine nucleotide-releasing factor 1 (Ras-GRF1) and Ras-GRF2 in the induction of long-term potentiation and long-term depression." *J Neurosci* **26**(6): 1721-9.
- Liao, G. Y., D. A. Wagner, et al. (2001). "Evidence for direct protein kinase-C mediated modulation of N-methyl-D-aspartate receptor current." *Mol Pharmacol* **59**(5): 960-4.
- Lipton, S. A. and P. A. Rosenberg (1994). "Excitatory amino acids as a final common pathway for neurologic disorders." *N Engl J Med* **330**(9): 613-22.
- Lisman, J. E., S. Raghavachari, et al. (2007). "The sequence of events that underlie quantal transmission at central glutamatergic synapses." *Nat Rev Neurosci* **8**(8): 597-609.
- Liu, L., T. P. Wong, et al. (2004). "Role of NMDA receptor subtypes in governing the direction of hippocampal synaptic plasticity." *Science* **304**(5673): 1021-4.
- Liu, X. B., K. D. Murray, et al. (2004). "Switching of NMDA receptor 2A and 2B subunits at thalamic and cortical synapses during early postnatal development." *J Neurosci* **24**(40): 8885-95.
- Liu, Y., T. P. Wong, et al. (2007). "NMDA receptor subunits have differential roles in mediating excitotoxic neuronal death both in vitro and in vivo." *J Neurosci* **27**(11): 2846-57.

- Loane, D. J. and A. I. Faden (2010). "Neuroprotection for traumatic brain injury: translational challenges and emerging therapeutic strategies." Trends Pharmacol Sci **31**(12): 596-604.
- Lusardi, T. A., J. Rangan, et al. (2004). "A device to study the initiation and propagation of calcium transients in cultured neurons after mechanical stretch." Ann Biomed Eng **32**(11): 1546-58.
- Lynch, D. R. and R. P. Guttman (2001). "NMDA receptor pharmacology: perspectives from molecular biology." Curr Drug Targets **2**(3): 215-31.
- Lynch, D. R. and R. P. Guttman (2002). "Excitotoxicity: perspectives based on N-methyl-D-aspartate receptor subtypes." J Pharmacol Exp Ther **300**(3): 717-23.
- Malenka, R. C., J. A. Kauer, et al. (1989). "An essential role for postsynaptic calmodulin and protein kinase activity in long-term potentiation." Nature **340**(6234): 554-7.
- Martel, M. A., D. J. Wyllie, et al. (2009). "In developing hippocampal neurons, NR2B-containing N-methyl-D-aspartate receptors (NMDARs) can mediate signaling to neuronal survival and synaptic potentiation, as well as neuronal death." Neuroscience **158**(1): 334-43.
- Massey, P. V., B. E. Johnson, et al. (2004). "Differential roles of NR2A and NR2B-containing NMDA receptors in cortical long-term potentiation and long-term depression." J Neurosci **24**(36): 7821-8.
- Matsuda, S. and H. Hirai (1999). "The clustering of NMDA receptor NR1 subunit is regulated by the interaction between the C-terminal exon cassettes and the cytoskeleton." Neurosci Res **34**(3): 157-63.
- McIntosh, T. K., M. Juhler, et al. (1998). "Novel pharmacologic strategies in the treatment of experimental traumatic brain injury: 1998." J Neurotrauma **15**(10): 731-69.
- McIntosh, T. K., R. Vink, et al. (1990). "Effect of noncompetitive blockade of N-methyl-D-aspartate receptors on the neurochemical sequelae of experimental brain injury." J Neurochem **55**(4): 1170-9.
- Mitchell, C. S., S. S. Feng, et al. (2007). "An analysis of glutamate spillover on the N-methyl-D-aspartate receptors at the cerebellar glomerulus." J Neural Eng **4**(3): 276-82.
- Montgomery, J. M., P. L. Zamorano, et al. (2004). "MAGUKs in synapse assembly and function: an emerging view." Cell Mol Life Sci **61**(7-8): 911-29.

- Monyer, H., N. Burnashev, et al. (1994). "Developmental and regional expression in the rat brain and functional properties of four NMDA receptors." *Neuron* **12**(3): 529-40.
- Monyer, H., R. Sprengel, et al. (1992). "Heteromeric NMDA receptors: molecular and functional distinction of subtypes." *Science* **256**(5060): 1217-21.
- Morishita, W., W. Lu, et al. (2007). "Activation of NR2B-containing NMDA receptors is not required for NMDA receptor-dependent long-term depression." *Neuropharmacology* **52**(1): 71-6.
- Morris, G. F., R. Bullock, et al. (1999). "Failure of the competitive N-methyl-D-aspartate antagonist Selfotel (CGS 19755) in the treatment of severe head injury: results of two phase III clinical trials. The Selfotel Investigators." *J Neurosurg* **91**(5): 737-43.
- Morris, R. G., E. Anderson, et al. (1986). "Selective impairment of learning and blockade of long-term potentiation by an N-methyl-D-aspartate receptor antagonist, AP5." *Nature* **319**(6056): 774-6.
- Mulkey, R. M., C. E. Herron, et al. (1993). "An essential role for protein phosphatases in hippocampal long-term depression." *Science* **261**(5124): 1051-5.
- Muller, T., D. Albrecht, et al. (2009). "Both NR2A and NR2B subunits of the NMDA receptor are critical for long-term potentiation and long-term depression in the lateral amygdala of horizontal slices of adult mice." *Learn Mem* **16**(6): 395-405.
- Nelson, T. J., M. K. Sun, et al. (2008). "Insulin, PKC signaling pathways and synaptic remodeling during memory storage and neuronal repair." *Eur J Pharmacol* **585**(1): 76-87.
- Neyton, J. and P. Paoletti (2006). "Relating NMDA receptor function to receptor subunit composition: limitations of the pharmacological approach." *J Neurosci* **26**(5): 1331-3.
- Nilsson, P., E. Ronne-Engstrom, et al. (1994). "Epileptic seizure activity in the acute phase following cortical impact trauma in rat." *Brain Res* **637**(1-2): 227-32.
- Okamoto, H. and K. Ichikawa (2000). "Switching characteristics of a model for biochemical-reaction networks describing autophosphorylation versus dephosphorylation of Ca²⁺/calmodulin-dependent protein kinase II." *Biol Cybern* **82**(1): 35-47.
- Okiyama, K., D. H. Smith, et al. (1997). "Effects of the novel NMDA antagonists CP-98,113, CP-101,581 and CP-101,606 on cognitive function and regional cerebral

- edema following experimental brain injury in the rat." J Neurotrauma **14**(4): 211-22.
- Olney, J. W. (1969). "Brain lesions, obesity, and other disturbances in mice treated with monosodium glutamate." Science **164**(880): 719-21.
- Palmer, A. M., D. W. Marion, et al. (1993). "Traumatic brain injury-induced excitotoxicity assessed in a controlled cortical impact model." J Neurochem **61**(6): 2015-24.
- Pankratov, Y. V. and O. A. Krishtal (2003). "Distinct quantal features of AMPA and NMDA synaptic currents in hippocampal neurons: implication of glutamate spillover and receptor saturation." Biophys J **85**(5): 3375-87.
- Paoletti, P. and P. Ascher (1994). "Mechanosensitivity of NMDA receptors in cultured mouse central neurons." Neuron **13**(3): 645-55.
- Papadia, S., P. Stevenson, et al. (2005). "Nuclear Ca²⁺ and the cAMP response element-binding protein family mediate a late phase of activity-dependent neuroprotection." J Neurosci **25**(17): 4279-87.
- Poddar, R., I. Deb, et al. (2010). "NR2B-NMDA receptor mediated modulation of the tyrosine phosphatase STEP regulates glutamate induced neuronal cell death." J Neurochem **115**(6): 1350-62.
- Racca, C., F. A. Stephenson, et al. (2000). "NMDA receptor content of synapses in stratum radiatum of the hippocampal CA1 area." J Neurosci **20**(7): 2512-22.
- Raghavachari, S. and J. E. Lisman (2004). "Properties of quantal transmission at CA1 synapses." J Neurophysiol **92**(4): 2456-67.
- Rao, V. L., M. K. Baskaya, et al. (1998). "Traumatic brain injury down-regulates glial glutamate transporter (GLT-1 and GLAST) proteins in rat brain." J Neurochem **70**(5): 2020-7.
- Rao, V. L., A. Dogan, et al. (2001). "Neuroprotection by memantine, a non-competitive NMDA receptor antagonist after traumatic brain injury in rats." Brain Res **911**(1): 96-100.
- Rauner, C. and G. Kohr (2010). "Triheteromeric NR1/NR2A/NR2B receptors constitute the major N-methyl-D-aspartate (NMDA) receptor population in adult hippocampal synapses." J Biol Chem.
- Ricci-Tersenghi, F., F. Minneci, et al. (2006). "Multivesicular release at developing Schaffer collateral-CA1 synapses: an analytic approach to describe experimental data." J Neurophysiol **96**(1): 15-26.

- Rusakov, D. A. (2001). "The role of perisynaptic glial sheaths in glutamate spillover and extracellular Ca(2+) depletion." Biophys J **81**(4): 1947-59.
- Rusakov, D. A. and D. M. Kullmann (1998). "Extrasynaptic glutamate diffusion in the hippocampus: ultrastructural constraints, uptake, and receptor activation." J Neurosci **18**(9): 3158-70.
- Saftenu, E. E. (2005). "Modeling of slow glutamate diffusion and AMPA receptor activation in the cerebellar glomerulus." J Theor Biol **234**(3): 363-82.
- Sakimura, K., T. Kutsuwada, et al. (1995). "Reduced hippocampal LTP and spatial learning in mice lacking NMDA receptor epsilon 1 subunit." Nature **373**(6510): 151-5.
- Salter, M. W. and L. V. Kalia (2004). "Src kinases: a hub for NMDA receptor regulation." Nat Rev Neurosci **5**(4): 317-28.
- Sanabria, H., M. A. Digman, et al. (2008). "Spatial diffusivity and availability of intracellular calmodulin." Biophys J **95**(12): 6002-15.
- Santucci, D. M. and S. Raghavachari (2008). "The effects of NR2 subunit-dependent NMDA receptor kinetics on synaptic transmission and CaMKII activation." PLoS Comput Biol **4**(10): e1000208.
- Sarvey, J. M., E. C. Burgard, et al. (1989). "Long-term potentiation: studies in the hippocampal slice." J Neurosci Methods **28**(1-2): 109-24.
- Sattler, R., Z. Xiong, et al. (1999). "Specific coupling of NMDA receptor activation to nitric oxide neurotoxicity by PSD-95 protein." Science **284**(5421): 1845-8.
- Schikorski, T. and C. F. Stevens (1997). "Quantitative ultrastructural analysis of hippocampal excitatory synapses." J Neurosci **17**(15): 5858-67.
- Schikorski, T. and C. F. Stevens (2001). "Morphological correlates of functionally defined synaptic vesicle populations." Nat Neurosci **4**(4): 391-5.
- Shapira, Y., G. Yadid, et al. (1990). "Protective effect of MK801 in experimental brain injury." J Neurotrauma **7**(3): 131-9.
- Sheng, M. and C. C. Hoogenraad (2007). "The postsynaptic architecture of excitatory synapses: a more quantitative view." Annu Rev Biochem **76**: 823-47.
- Shi, S. H., Y. Hayashi, et al. (1999). "Rapid spine delivery and redistribution of AMPA receptors after synaptic NMDA receptor activation." Science **284**(5421): 1811-6.

- Shirasaki, Y., Y. Kanazawa, et al. (2006). "Involvement of calmodulin in neuronal cell death." Brain Res **1083**(1): 189-95.
- Shouval, H. Z., M. F. Bear, et al. (2002). "A unified model of NMDA receptor-dependent bidirectional synaptic plasticity." Proc Natl Acad Sci U S A **99**(16): 10831-6.
- Shouval, H. Z., S. S. Wang, et al. (2010). "Spike timing dependent plasticity: a consequence of more fundamental learning rules." Front Comput Neurosci **4**.
- Silver, R. A., S. G. Cull-Candy, et al. (1996). "Non-NMDA glutamate receptor occupancy and open probability at a rat cerebellar synapse with single and multiple release sites." J Physiol **494 (Pt 1)**: 231-50.
- Smith, D. H., K. Okiyama, et al. (1993). "Magnesium and ketamine attenuate cognitive dysfunction following experimental brain injury." Neurosci Lett **157**(2): 211-4.
- Smith, D. H., J. A. Wolf, et al. (1999). "High tolerance and delayed elastic response of cultured axons to dynamic stretch injury." J Neurosci **19**(11): 4263-9.
- Soriano, F. X., M. A. Martel, et al. (2008). "Specific targeting of pro-death NMDA receptor signals with differing reliance on the NR2B PDZ ligand." J Neurosci **28**(42): 10696-710.
- Spaethling, J. M., D. M. Geddes-Klein, et al. (2007). "Linking impact to cellular and molecular sequelae of CNS injury: modeling in vivo complexity with in vitro simplicity." Prog Brain Res **161**: 27-39.
- Spaethling, J. M., D. M. Klein, et al. (2008). "Calcium-permeable AMPA receptors appear in cortical neurons after traumatic mechanical injury and contribute to neuronal fate." J Neurotrauma **25**(10): 1207-16.
- Storm, D. R., C. Hansel, et al. (1998). "Impaired cerebellar long-term potentiation in type I adenylyl cyclase mutant mice." Neuron **20**(6): 1199-210.
- Sun, L. and S. June Liu (2007). "Activation of extrasynaptic NMDA receptors induces a PKC-dependent switch in AMPA receptor subtypes in mouse cerebellar stellate cells." J Physiol **583**(Pt 2): 537-53.
- Tovar, K. R. and G. L. Westbrook (1999). "The incorporation of NMDA receptors with a distinct subunit composition at nascent hippocampal synapses in vitro." J Neurosci **19**(10): 4180-8.
- Tsien, J. Z., P. T. Huerta, et al. (1996). "The essential role of hippocampal CA1 NMDA receptor-dependent synaptic plasticity in spatial memory." Cell **87**(7): 1327-38.

- Umemiya, M., M. Senda, et al. (1999). "Behaviour of NMDA and AMPA receptor-mediated miniature EPSCs at rat cortical neuron synapses identified by calcium imaging." J Physiol **521 Pt 1**: 113-22.
- Ventriglia, F. and V. Di Maio (2003). "Stochastic fluctuations of the quantal EPSC amplitude in computer simulated excitatory synapses of hippocampus." Biosystems **71**(1-2): 195-204.
- Vicini, S., J. F. Wang, et al. (1998). "Functional and pharmacological differences between recombinant N-methyl-D-aspartate receptors." J Neurophysiol **79**(2): 555-66.
- von Engelhardt, J., I. Coserea, et al. (2007). "Excitotoxicity in vitro by NR2A- and NR2B-containing NMDA receptors." Neuropharmacology **53**(1): 10-7.
- von Engelhardt, J., B. Doganci, et al. (2009). "Synaptic NR2A- but not NR2B-Containing NMDA Receptors Increase with Blockade of Ionotropic Glutamate Receptors." Front Mol Neurosci **2**: 19.
- Waxman, E. A. and D. R. Lynch (2005). "N-methyl-D-aspartate receptor subtype mediated bidirectional control of p38 mitogen-activated protein kinase." J Biol Chem **280**(32): 29322-33.
- Waxman, E. A. and D. R. Lynch (2005). "N-methyl-D-aspartate receptor subtypes: multiple roles in excitotoxicity and neurological disease." Neuroscientist **11**(1): 37-49.
- Weber, J. T., B. A. Rzigalinski, et al. (1999). "Alterations in calcium-mediated signal transduction after traumatic injury of cortical neurons." Cell Calcium **26**(6): 289-99.
- Wechsler, A. and V. I. Teichberg (1998). "Brain spectrin binding to the NMDA receptor is regulated by phosphorylation, calcium and calmodulin." Embo J **17**(14): 3931-9.
- Werner, C. and K. Engelhard (2007). "Pathophysiology of traumatic brain injury." Br J Anaesth **99**(1): 4-9.
- Wiegert, J. S., F. Hofmann, et al. (2009). "A transcription-dependent increase in miniature EPSC frequency accompanies late-phase plasticity in cultured hippocampal neurons." BMC Neurosci **10**: 124.
- Williams, K. (1993). "Ifenprodil discriminates subtypes of the N-methyl-D-aspartate receptor: selectivity and mechanisms at recombinant heteromeric receptors." Mol Pharmacol **44**(4): 851-9.

- Williams, K., S. L. Russell, et al. (1993). "Developmental switch in the expression of NMDA receptors occurs in vivo and in vitro." Neuron **10**(2): 267-78.
- Wilson, N. R., J. Kang, et al. (2005). "Presynaptic regulation of quantal size by the vesicular glutamate transporter VGLUT1." J Neurosci **25**(26): 6221-34.
- Wolf, J. A., P. K. Stys, et al. (2001). "Traumatic axonal injury induces calcium influx modulated by tetrodotoxin-sensitive sodium channels." J Neurosci **21**(6): 1923-30.
- Wu, H. Y., F. C. Hsu, et al. (2007). "Fyn-mediated phosphorylation of NR2B Tyr-1336 controls calpain-mediated NR2B cleavage in neurons and heterologous systems." J Biol Chem **282**(28): 20075-87.
- Wu, X. S., L. Xue, et al. (2007). "The origin of quantal size variation: vesicular glutamate concentration plays a significant role." J Neurosci **27**(11): 3046-56.
- Wyszynski, M., J. Lin, et al. (1997). "Competitive binding of alpha-actinin and calmodulin to the NMDA receptor." Nature **385**(6615): 439-42.
- Xia, Z. and D. R. Storm (2005). "The role of calmodulin as a signal integrator for synaptic plasticity." Nat Rev Neurosci **6**(4): 267-76.
- Xu, J., P. Kurup, et al. (2009). "Extrasynaptic NMDA receptors couple preferentially to excitotoxicity via calpain-mediated cleavage of STEP." J Neurosci **29**(29): 9330-43.
- Yang, C. H., C. C. Huang, et al. (2005). "Behavioral stress enhances hippocampal CA1 long-term depression through the blockade of the glutamate uptake." J Neurosci **25**(17): 4288-93.
- Yang, S. N., Y. G. Tang, et al. (1999). "Selective induction of LTP and LTD by postsynaptic [Ca²⁺]_i elevation." J Neurophysiol **81**(2): 781-7.
- Yi, J. H. and A. S. Hazell (2006). "Excitotoxic mechanisms and the role of astrocytic glutamate transporters in traumatic brain injury." Neurochem Int **48**(5): 394-403.
- Yurkewicz, L., J. Weaver, et al. (2005). "The effect of the selective NMDA receptor antagonist traxoprodil in the treatment of traumatic brain injury." J Neurotrauma **22**(12): 1428-43.
- Zhang, L., B. A. Rzigalinski, et al. (1996). "Reduction of voltage-dependent Mg²⁺ blockade of NMDA current in mechanically injured neurons." Science **274**(5294): 1921-3.

- Zhang, S. J., M. N. Steijaert, et al. (2007). "Decoding NMDA receptor signaling: identification of genomic programs specifying neuronal survival and death." Neuron **53**(4): 549-62.
- Zhou, M. and M. Baudry (2006). "Developmental changes in NMDA neurotoxicity reflect developmental changes in subunit composition of NMDA receptors." J Neurosci **26**(11): 2956-63.
- Zhou, Y., E. Takahashi, et al. (2007). "Interactions between the NR2B receptor and CaMKII modulate synaptic plasticity and spatial learning." J Neurosci **27**(50): 13843-53.
- Zhou, Y. D., C. D. Acker, et al. (2005). "Increasing Ca²⁺ transients by broadening postsynaptic action potentials enhances timing-dependent synaptic depression." Proc Natl Acad Sci U S A **102**(52): 19121-5.
- Zohar, O., R. Lavy, et al. (2011). "PKC activator therapeutic for mild traumatic brain injury in mice." Neurobiol Dis **41**(2): 329-37.

Appendix A: Smoldyn code: Activation of AMPARs and NMDAR subtypes

```
## EXAMPLE SMOLDYN CODE FOR ACTIVATION OF AMPARS AND NMDAR
##SUBTYPES

graphics none
graphic_iter 10
dim 3

#Define each molecule species
names gl AR ARA ARA2 ARA2F ARA2S ARA2FS AD1 AD2 BR BRA BRA2 BRA2F
BRA2S BRA2FS BD1 BD2 R S T open Sdes Tdes opensdes trans GT GT2 ABR ABRAA
ABRAB ABRA2 ABRA2F ABRA2S ABRA2FS ABD1 ABD2

#cmd b pause
max_mol 2000000

#Define color and size for defined molecules
color gl(all) 1 0 0 #red
color AR(all) 0.6 0 0.6 #purple
color ARA(all) 0 0 1 #blue
color ARA2(all) 0 0 1 #blue
color ARA2F(all) 0 0 1
color ARA2S(all) 0 0 1
color ARA2FS(all) 0 1 0 #green
color AD1(all) 0 0 0 #black
color AD2(all) 0 0 0
color BR(all) 0.8 0.9 0 #yellow
color BRA(all) 0 0 1 #blue
color BRA2(all) 0 0 1 #blue
color BRA2F(all) 0 0 1
color BRA2S(all) 0 0 1
color BRA2FS(all) 0 1 0 #green
color BD1(all) 0 0 0 #black
color BD2(all) 0 0 0
color ABR(all) 0 0.6 0.5 #blue-green
color ABRAA(all) 0 0 1 #blue
color ABRAB(all) 0 0 1 #blue
color ABRA2(all) 0 0 1 #blue
color ABRA2F(all) 0 0 1
color ABRA2S(all) 0 0 1
color ABRA2FS(all) 0 1 0 #green
```

```
color ABD1(all) 0 0 0 #black
color ABD2(all) 0 0 0
color R(all) 1 0 0 #red
color S(all) 1 0.4 0 #redorange
color T(all) 1 0.7 0 #orange
color open(all) 0.8 0.9 0 #yellow
color Sdes(all) 0.7 0.7 0.7 #lightgrey
color Tdes(all) 0.4 0.4 0.4 #grey
color opendes(all) 0 0 0 #black
color trans(all) 0 1 0
color GT(all) 0 0 1
color GT2(all) 1 0 0
```

```
display_size gl(all) 2
display_size AR(all) 10
display_size ARA(all) 10
display_size ARA2(all) 10
display_size ARA2F(all) 10
display_size ARA2S(all) 10
display_size ARA2FS(all) 10
display_size AD1(all) 10
display_size AD2(all) 10
display_size BR(all) 10
display_size BRA(all) 10
display_size BRA2(all) 10
display_size BRA2F(all) 10
display_size BRA2S(all) 10
display_size BRA2FS(all) 10
display_size BD1(all) 10
display_size BD2(all) 10
display_size ABR(all) 10
display_size ABRAA(all) 10
display_size ABRAB(all) 10
display_size ABRA2(all) 10
display_size ABRA2F(all) 10
display_size ABRA2S(all) 10
display_size ABRA2FS(all) 10
display_size ABD1(all) 10
display_size ABD2(all) 10
display_size R(all) 10
display_size S(all) 10
display_size T(all) 10
```

```
display_size open(all) 10
display_size Sdes(all) 10
display_size Tdes(all) 10
display_size opendes(all) 10
display_size trans(all) 10
display_size GT(all) 10
display_size GT2(all) 10
```

```
low_wall 0 -2000 r
high_wall 0 2000 r
low_wall 1 -2000 r
high_wall 1 2000 r
low_wall 2 -2000 r
high_wall 2 2000 r
```

```
#set start time, end time, and time steps
time_start 0
time_stop 1000
time_step 0.01
```

```
# Define glutamate release and diffusion
mol 1500 gl 0 265 0
difc gl(all) 200000
```

```
##DEFINE SURFACES
```

```
max_surface 20
start_surface
name synapticface
action both gl r
action both AR r
action both ARA r
action both ARA2 r
action both ARA2F r
action both ARA2S r
action both ARA2FS r
action both AD1 r
action both AD2 r
action both BR r
action both BRA r
```

```
action both BRA2 r
action both BRA2F r
action both BRA2S r
action both BRA2FS r
action both BD1 r
action both BD2 r
action both ABR r
action both ABRAA r
action both ABRAB r
action both ABRA2 r
action both ABRA2F r
action both ABRA2S r
action both ABRA2FS r
action both ABD1 r
action both ABD2 r
action both R r
action both S r
action both T r
action both open r
action both Sdes r
action both Tdes r
action both opendes r
#color all 1 0 0 0.5
max_panels r 30
max_panels tri 50
polygon both edge
panel r +1 -150 250 -150 300 300 synapticface
end_surface

start_surface
name perisynaptic
action both gl r
action both AR r
action both ARA r
action both ARA2 r
action both ARA2F r
action both ARA2S r
action both ARA2FS r
action both AD1 r
action both AD2 r
action both BR r
action both BRA r
```

```
action both BRA2 r
action both BRA2F r
action both BRA2S r
action both BRA2FS r
action both BD1 r
action both BD2 r
action both ABR r
action both ABRAA r
action both ABRAB r
action both ABRA2 r
action both ABRA2F r
action both ABRA2S r
action both ABRA2FS r
action both ABD1 r
action both ABD2 r
action both R r
action both S r
action both T r
action both open r
action both Sdes r
action both Tdes r
action both opendes r

#color all 1 0 0 0.5
max_panels r 30
max_panels tri 50
polygon both edge
panel tri -150 250 150 -250 150 150 -250 150 -150 peri1
panel tri -150 250 150 -250 150 -150 -150 250 -150 peri2
panel tri -150 250 150 -150 150 250 -250 150 150 peri3
panel tri -150 250 150 -150 150 250 150 150 250 peri4
panel tri -150 250 150 150 250 150 150 150 250 peri5
panel tri 150 250 150 150 150 250 250 150 150 peri6
panel tri 150 250 150 250 150 150 250 150 -150 peri7
panel tri 150 250 150 150 250 -150 250 150 -150 peri8
panel tri 150 250 -150 250 150 -150 150 150 -250 peri9
panel tri 150 250 -150 150 150 -250 -150 150 -250 peri10
panel tri 150 250 -150 -150 250 -150 -150 150 -250 peri11
panel tri -150 250 -150 -150 150 -250 -250 150 -150 peri12
end_surface

start_surface
```

```
name extrasynaptic
action both gl r
action both AR r
action both ARA r
action both ARA2 r
action both ARA2F r
action both ARA2S r
action both ARA2FS r
action both AD1 r
action both AD2 r
action both BR r
action both BRA r
action both BRA2 r
action both BRA2F r
action both BRA2S r
action both BRA2FS r
action both BD1 r
action both BD2 r
action both ABR r
action both ABRAA r
action both ABRAB r
action both ABRA2 r
action both ABRA2F r
action both ABRA2S r
action both ABRA2FS r
action both ABD1 r
action both ABD2 r
action both R r
action both S r
action both T r
action both open r
action both Sdes r
action both Tdes r
action both opendes r

#color all 0 1 0 0.5
max_panels r 30
max_panels tri 50
polygon both edge
panel r -0 -250 150 -150 -300 300 extra1
panel r +0 250 150 -150 -300 300 extra2
panel r +2 -150 -150 -250 300 300 extra3
```

```
panel r +2 -150 -150 250 300 300 extra4
panel tri -150 150 250 -250 150 150 -250 -150 150 extra5
panel tri -150 150 250 -150 -150 250 -250 -150 150 extra6
panel tri 150 150 250 250 150 150 250 -150 150 extra7
panel tri 150 150 250 150 -150 250 250 -150 150 extra8
panel tri 250 150 -150 150 150 -250 150 -150 -250 extra9
panel tri 250 150 -150 250 -150 -150 150 -150 -250 extra10
panel tri -150 150 -250 -250 150 -150 -250 -150 -150 extra11
panel tri -150 150 -250 -150 -150 -250 -250 -150 -150 extra12
end_surface
```

```
start_surface
name spinebottom
action both gl r
action both AR r
action both ARA r
action both ARA2 r
action both ARA2F r
action both ARA2S r
action both ARA2FS r
action both AD1 r
action both AD2 r
action both BR r
action both BRA r
action both BRA2 r
action both BRA2F r
action both BRA2S r
action both BRA2FS r
action both BD1 r
action both BD2 r
action both ABR r
action both ABRAA r
action both ABRAB r
action both ABRA2 r
action both ABRA2F r
action both ABRA2S r
action both ABRA2FS r
action both ABD1 r
action both ABD2 r
action both R r
action both S r
action both T r
```



```
action both open r
action both Sdes r
action both Tdes r
action both opendes r

#color all 1 0 0 0.5
max_panels r 30
max_panels tri 50
polygon both edge
panel tri -250 -150 150 -250 -150 -150 -150 -250 150
panel tri -150 -250 150 -150 -250 -150 -250 -150 -150
panel tri -250 -150 150 -150 -150 250 -150 -250 150
panel tri -150 -250 150 -150 -150 250 150 -150 250
panel tri -150 -250 150 150 -250 150 150 -150 250
panel tri 150 -250 150 150 -150 250 250 -150 150
panel tri 250 -150 150 150 -250 150 150 -250 -150
panel tri 250 -150 150 250 -150 -150 150 -250 -150
panel tri 150 -250 -150 250 -150 -150 150 -150 -250
panel tri 150 -150 -250 -150 -150 -250 -150 -250 -150
panel tri 150 -150 -250 150 -250 -150 -150 -250 -150
panel tri -150 -250 -150 -250 -150 -150 -150 -150 -250
panel r +1 -150 -250 -150 50 300
panel r +1 100 -250 -150 50 300
panel r +1 -100 -250 -150 200 50
panel r +1 -100 -250 100 200 50
panel tri -100 -250 -100 -50 -250 -100 -100 -250 -50
panel tri 50 -250 -100 100 -250 -100 100 -250 -50
panel tri -100 -250 50 -100 -250 100 -50 -250 100
panel tri 50 -250 100 100 -250 100 100 -250 50
panel r +0 -100 -250 -50 -500 100
panel r -0 100 -250 -50 -500 100
panel r -2 -50 -750 -100 100 500
panel r -2 -50 -750 100 100 500
panel tri -50 -250 100 -50 -750 100 -100 -750 50
panel tri -50 -250 100 -100 -250 50 -100 -750 50
panel tri 50 -250 100 50 -750 100 100 -750 50
panel tri 50 -250 100 100 -250 50 100 -750 50
panel tri -50 -250 -100 -50 -750 -100 -100 -750 -50
panel tri -50 -250 -100 -100 -250 -50 -100 -750 -50
panel tri 50 -250 -100 50 -750 -100 100 -750 -50
panel tri 50 -250 -100 100 -250 -50 100 -750 -50
end_surface
```

```
start_surface
name presynaptic
action both gl r
action both AR r
action both ARA r
action both ARA2 r
action both ARA2F r
action both ARA2S r
action both ARA2FS r
action both AD1 r
action both AD2 r
action both BR r
action both BRA r
action both BRA2 r
action both BRA2F r
action both BRA2S r
action both BRA2FS r
action both BD1 r
action both BD2 r
action both ABR r
action both ABRAA r
action both ABRAB r
action both ABRA2 r
action both ABRA2F r
action both ABRA2S r
action both ABRA2FS r
action both ABD1 r
action both ABD2 r
action both R r
action both S r
action both T r
action both open r
action both Sdes r
action both Tdes r
action both opendes r

#color all 0.8 0.9 0
max_panels r 30
max_panels tri 50
polygon both edge
panel tri -250 370 150 -250 370 -150 -150 270 150
```

```
panel tri -150 270 150 -150 270 -150 -250 370 -150
panel tri -250 370 150 -150 370 250 -150 270 150
panel tri -150 270 150 -150 370 250 150 370 250
panel tri -150 270 150 150 270 150 150 370 250
panel tri 150 270 150 150 370 250 250 370 150
panel tri 250 370 150 150 270 150 150 270 -150
panel tri 250 370 150 250 370 -150 150 270 -150
panel tri 150 270 -150 250 370 -150 150 370 -250
panel tri 150 370 -250 -150 370 -250 -150 270 -150
panel tri 150 370 -250 150 270 -150 -150 270 -150
panel tri -150 270 -150 -250 370 -150 -150 370 -250
panel tri -150 670 250 -250 670 150 -250 370 150
panel tri -150 670 250 -150 370 250 -250 370 150
panel tri 150 670 250 250 670 150 250 370 150
panel tri 150 670 250 150 370 250 250 370 150
panel tri 250 670 -150 150 670 -250 150 370 -250
panel tri 250 670 -150 250 370 -150 150 370 -250
panel tri -150 670 -250 -250 670 -150 -250 370 -150
panel tri -150 670 -250 -150 370 -250 -250 370 -150
panel r +0 -250 670 -150 -300 300
panel r -0 250 670 -150 -300 300
panel r -1 -150 770 -150 300 300
panel r +1 -150 270 -150 300 300
panel r -2 -150 370 -250 300 300
panel r -2 -150 370 250 300 300
panel tri -150 770 150 -250 670 150 -250 670 -150
panel tri -150 770 150 -250 670 -150 -150 770 -150
panel tri -150 770 150 -150 670 250 -250 670 150
panel tri -150 770 150 -150 670 250 150 670 250
panel tri -150 770 150 150 770 150 150 670 250
panel tri 150 770 150 150 670 250 250 670 150
panel tri 150 770 150 250 670 150 250 670 -150
panel tri 150 770 150 150 770 -150 250 670 -150
panel tri 150 770 -150 250 670 -150 150 670 -250
panel tri 150 770 -150 150 670 -250 -150 670 -250
panel tri 150 770 -150 -150 770 -150 -150 670 -250
panel tri -150 770 -150 -150 670 -250 -250 670 -150
end_surface

start_surface
name leftbackast
action both gl r
```

```
action both AR r
action both ARA r
action both ARA2 r
action both ARA2F r
action both ARA2S r
action both ARA2FS r
action both AD1 r
action both AD2 r
action both BR r
action both BRA r
action both BRA2 r
action both BRA2F r
action both BRA2S r
action both BRA2FS r
action both BD1 r
action both BD2 r
action both ABR r
action both ABRAA r
action both ABRAB r
action both ABRA2 r
action both ABRA2F r
action both ABRA2S r
action both ABRA2FS r
action both ABD1 r
action both ABD2 r
action both R r
action both S r
action both T r
action both open r
action both Sdes r
action both Tdes r
action both opendes r

color all 0 1 0 0.5
max_panels r 100
max_panels tri 100
polygon both edge
panel r +0 -270 150 -150 -300 300
panel r -2 -150 -150 -270 300 300
panel tri -160 260 150 -270 150 150 -270 150 -150
panel tri -160 260 150 -270 150 -150 -160 260 -150
panel tri -160 260 150 -150 150 270 -270 150 150
```

```
panel tri 150 260 -160 150 150 -270 -150 150 -270
panel tri 150 260 -160 -160 260 -150 -150 150 -270
panel tri -160 260 -150 -150 150 -270 -270 150 -150
panel tri -150 150 270 -270 150 150 -270 -150 150
panel tri -150 150 270 -150 -150 270 -270 -150 150
panel tri -150 150 -270 -270 150 -150 -270 -150 -150
panel tri -150 150 -270 -150 -150 -270 -270 -150 -150
panel tri -270 -150 150 -270 -150 -150 -150 -270 150
panel tri -150 -270 150 -150 -270 -150 -270 -150 -150
panel tri -270 -150 150 -150 -150 270 -150 -270 150
panel tri 150 -150 -270 -150 -150 -270 -150 -270 -150
panel tri 150 -150 -270 150 -270 -150 -150 -270 -150
panel tri -150 -270 -150 -270 -150 -150 -150 -150 -270
panel r +0 -270 670 -150 -300 300
panel r -2 -150 370 -270 300 300
panel tri -270 370 150 -270 370 -150 -160 260 150
panel tri -160 260 150 -160 260 -150 -270 370 -150
panel tri -270 370 150 -150 370 250 -160 260 150
panel tri 150 370 -270 -150 370 -270 -160 260 -150
panel tri 150 370 -270 150 260 -160 -160 260 -150
panel tri -160 260 -150 -270 370 -150 -150 370 -270
panel tri -150 670 250 -270 670 150 -270 370 150
panel tri -150 670 250 -150 370 250 -270 370 150
panel tri -150 670 -270 -270 670 -150 -270 370 -150
panel tri -150 670 -270 -150 370 -270 -270 370 -150
panel tri -150 790 150 -270 670 150 -270 670 -150
panel tri -150 790 150 -270 670 -150 -150 790 -150
panel tri -150 790 150 -150 670 250 -270 670 150
panel tri 150 790 -150 150 670 -270 -150 670 -270
panel tri 150 790 -150 -150 790 -150 -150 670 -270
panel tri -150 790 -150 -150 670 -270 -270 670 -150
end_surface
```

```
start_surface
name frontrightast
action both gl r
action both AR r
action both ARA r
action both ARA2 r
action both ARA2F r
action both ARA2S r
action both ARA2FS r
```

action both AD1 r
action both AD2 r
action both BR r
action both BRA r
action both BRA2 r
action both BRA2F r
action both BRA2S r
action both BRA2FS r
action both BD1 r
action both BD2 r
action both ABR r
action both ABRAA r
action both ABRAB r
action both ABRA2 r
action both ABRA2F r
action both ABRA2S r
action both ABRA2FS r
action both ABD1 r
action both ABD2 r
action both R r
action both S r
action both T r
action both open r
action both Sdes r
action both Tdes r
action both opendes r

color all 0 0 1 0.5
max_panels r 100
max_panels tri 100
polygon both edge
panel r -0 270 150 -150 -300 300
panel r -2 -150 -150 270 300 300
panel tri -150 260 160 -150 150 270 150 150 270
panel tri -150 260 160 160 260 150 150 150 270
panel tri 160 260 150 150 150 270 270 150 150
panel tri 160 260 150 270 150 150 270 150 -150
panel tri 160 260 150 160 260 -150 270 150 -150
panel tri 160 260 -150 270 150 -150 150 150 -270
panel tri 150 150 270 270 150 150 270 -150 150
panel tri 150 150 270 150 -150 270 270 -150 150
panel tri 270 150 -150 150 150 -270 150 -150 -270

```

panel tri 270 150 -150 270 -150 -150 150 -150 -270
panel tri -150 -270 150 -150 -150 270 150 -150 270
panel tri -150 -270 150 150 -270 150 150 -150 270
panel tri 150 -270 150 150 -150 270 270 -150 150
panel tri 270 -150 150 150 -270 150 150 -270 -150
panel tri 270 -150 150 270 -150 -150 150 -270 -150
panel tri 150 -270 -150 270 -150 -150 150 -150 -270
panel tri -150 260 160 -150 370 270 150 370 270
panel tri -150 260 160 160 260 150 150 370 270
panel tri 160 260 150 150 370 270 270 370 150
panel tri 270 370 150 160 260 150 160 260 -150
panel tri 270 370 150 270 370 -150 160 260 -150
panel tri 160 260 -150 270 370 -150 150 370 -270
panel tri 150 670 270 270 670 150 270 370 150
panel tri 150 670 270 150 370 270 270 370 150
panel tri 270 670 -150 150 670 -270 150 370 -270
panel tri 270 670 -150 270 370 -150 150 370 -270
panel r -0 270 670 -150 -300 300
panel r -2 -150 370 270 300 300
panel tri -150 790 150 -150 670 270 150 670 270
panel tri -150 790 150 150 790 150 150 670 270
panel tri 150 790 150 150 670 270 270 670 150
panel tri 150 790 150 270 670 150 270 670 -150
panel tri 150 790 150 150 790 -150 270 670 -150
panel tri 150 790 -150 270 670 -150 150 670 -270
end_surface

```

```

start_surface
name square
action both all absorb
max_panels r 6
polygon both edge
panel r +0 -400 +1000 -500 -2000 1000
panel r +0 +400 +1000 -500 -2000 1000
panel r +1 +400 -1000 -500 -800 1000
panel r +1 +400 +1000 -500 -800 1000
panel r +2 +400 -1000 -500 -800 2000
panel r +2 +400 -1000 +500 -800 2000
end_surface

```

```

#Define the number and localization of receptors R=AMPAR, AR=NR2A, BR=NR2B,
#ABR=NR2A/NR2B

```

```

surface_mol 80 R(up) synapticface all all
surface_mol 8 AR(up) synapticface all all
surface_mol 8 ABR(up) synapticface all all
surface_mol 4 BR(up) synapticface all all
surface_mol 10 BR(up) extrasynaptic all all
#surface_mol 9900 trans(up) leftbackast all all
#surface_mol 9900 trans(up) frontrightast all all

```

```

#DEFINE ALL REACTION:  REACTANTS -> PRODUCTS RATE
reaction 2Bfirstdebind BRA2(all) -> BRA(up) + gl(fsoln) 0.0762
reaction 2Bseconddebind BRA(all) -> BR(up) + gl(fsoln) 0.0381
reaction 2Bopenslow BRA2(all) -> BRA2S(up) 0.048
reaction 2Bopenfast BRA2(all) -> BRA2F(up) 2.836
reaction 2Bopen2ndfast BRA2S(all) -> BRA2FS(up) 2.836
reaction 2Bopen2ndslow BRA2F(all) -> BRA2FS(up) 0.048
reaction 2Bclose2ndslow BRA2FS(all) -> BRA2F(up) 0.230
reaction 2Bclose2ndfast BRA2FS(all) -> BRA2S(up) 0.175
reaction 2Bclosefast BRA2F(all) -> BRA2(up) 0.175
reaction 2Bcloseslow BRA2S(all) -> BRA2(up) 0.230
reaction 2Bdesens1 BRA2(all) -> BD1(up) 0.550
reaction 2Bdesens2 BRA2(all) -> BD2(up) 0.112
reaction 2Bresens1 BD1(all) -> BRA2(up) 0.0814
reaction 2Bresens2 BD2(all) -> BRA2(up) 0.00091
reaction ABfirstBdebind ABRA2(all) -> ABRAA(up) 0.0381
reaction ABsecondBdebind ABRAB(all) -> ABR(up) + gl(fsoln) 0.0381
reaction ABfirstAdebind ABRA2(all) -> ABRAB(up) + gl(fsoln) 1.010
reaction ABsecondAdebind ABRAA(all) -> ABR(up) + gl(fsoln) 1.01
reaction ABopenslow ABRA2(all) -> ABRA2S(up) 0.139
reaction ABopenfast ABRA2(all) -> ABRA2F(up) 2.988
reaction ABopen2ndfast ABRA2S(all) -> ABRA2FS(up) 2.988
reaction ABopen2ndslow ABRA2F(all) -> ABRA2FS(up) 0.139
reaction ABclose2ndslow ABRA2FS(all) -> ABRA2F(up) 0.204
reaction ABclose2ndfast ABRA2FS(all) -> ABRA2S(up) 0.1745
reaction ABclosefast ABRA2F(all) -> ABRA2(up) 0.1745
reaction ABcloseslow ABRA2S(all) -> ABRA2(up) 0.204
reaction ABdesens1 ABRA2(all) -> ABD1(up) 0.3175
reaction ABdesens2 ABRA2(all) -> ABD2(up) 0.171
reaction ABresens1 ABD1(all) -> ABRA2(up) 0.05555
reaction ABresens2 ABD2(all) -> ABRA2(up) 0.00096
reaction 2Afirstdebind ARA2(all) -> ARA(up) + gl(fsoln) 2.02

```


reaction 2Aseconddebind ARA(all) -> AR(up) + gl(fsoln) 1.01
 reaction 2Aopenslow ARA2(all) -> ARA2S(up) 0.230
 reaction 2Aopenfast ARA2(all) -> ARA2F(up) 3.140
 reaction 2Aopen2ndfast ARA2S(all) -> ARA2FS(up) 3.140
 reaction 2Aopen2ndslow ARA2F(all) -> ARA2FS(up) 0.230
 reaction 2Aclose2ndslow ARA2FS(all) -> ARA2F(up) 0.178
 reaction 2Aclose2ndfast ARA2FS(all) -> ARA2S(up) 0.174
 reaction 2Aclosefast ARA2F(all) -> ARA2(up) 0.174
 reaction 2Acloseslow ARA2S(all) -> ARA2(up) 0.178
 reaction 2Adesens1 ARA2(all) -> AD1(up) 0.0851
 reaction 2Adesens2 ARA2(all) -> AD2(up) 0.230
 reaction 2Aresens1 AD1(all) -> ARA2(up) 0.0297
 reaction 2Aresens2 AD2(all) -> ARA2(up) 0.00101
 reaction Aseconddebind S(all) -> R(up) + gl(fsoln) 4.26
 reaction Afirstdebind T(all) -> S(up) + gl(fsoln) 3.26
 reaction Aopening T(all) -> open(up) 4.24
 reaction Aclosing open(all) -> T(up) 0.9
 reaction opendesens open(all) -> opendes(up) 0.0177
 reaction openresens opendes(all) -> open(up) 0.004
 reaction Tdesens T(all) -> Tdes(up) 0.172
 reaction Tresens Tdes(all) -> T(up) 0.000727
 reaction Sdesens S(all) -> Sdes(up) 2.89
 reaction Sresens Sdes(all) -> S(up) 0.0392
 reaction TdestoSdes Tdes(all) -> Sdes(up) + gl(fsoln) 0.0457
 reaction Tdestoopendes Tdes(all) -> opendes(up) 0.0168
 reaction opendestoTdes opendes(all) -> Tdes(up) 0.1904
 reaction Transcont GT(all) -> GT2(up) 0.180
 reaction Transdebind GT(all) -> trans(up) + gl(bsoln)
 reaction Transport GT2(all) -> trans(up) 0.0257
 reaction ABfirstAbind gl + ABR(all) -> ABRAA(up) 52456
 reaction ABfirstBbind gl + ABR(all) -> ABRAB(up) 4698
 reaction ABsecondAbind ABRAB(all) + gl -> ABRA2(up) 52456
 reaction ABsecondBbind ABRAA(all) + gl -> ABRA2(up) 4698
 reaction 2Bfirstbind gl + BR(all) -> BRA(up) 9396
 reaction 2Bsecondbind gl + BRA(all) -> BRA2(up) 4698
 reaction 2Afistbind gl + AR(all) -> ARA(up) 104912
 reaction 2Asecondbind gl + ARA(all) -> ARA2(up) 52446
 reaction Afirstbind gl + R(all) -> S(up) 7619
 reaction Asecondbind gl + S(all) -> T(up) 47144
 reaction Adesbind gl + Sdes(all) -> Tdes(up) 2108
 reaction Transbind trans(all) + gl -> GT(up) 29880

```
output_files example_syn example_ex example_sg example_g example_box  
example_2Bo example_2Ao example_2A2Bo example_AMPAo
```

```
#Define output files
```

```
output_file_number example_syn i  
output_file_number example_ex i  
output_file_number example_sg i  
output_file_number example_g i  
output_file_number example_box i  
output_file_number example_2Bo i  
output_file_number example_2Ao i  
output_file_number example_2A2Bo i  
output_file_number example_AMPAo i
```

```
#Define writing of output files
```

```
cmd e molcountonsurf synapticface example_syn  
cmd e molcountonsurf extrasynaptic example_ex  
cmd e molcount example_g  
cmd e molcountinbox -150 150 250 270 -150 150 example_box  
cmd e molpos BRA2FS(all) example_2Bo  
cmd e molpos ARA2FS(all) example_2Ao  
cmd e molpos ABRA2FS(all) example_2A2Bo  
cmd e molpos open(all) example_AMPAo
```

```
end_file
```

Appendix B: Matlab code: Calculations of the sites and times of calcium entry following simulations of NMDAR activation

```
%Extracts activation time periods for distinct receptors, as defined by
%smoldyn simulations. Calculates calcium entry (Jahr et al 1990) by
%iteratively calculating AMPAR and NMDAR current and membrane
potential.
%Calcium entry dependent on Punblocked, as determined by the Mg
%concentration. The effect of selective mechanosensitivity can be
built
%into this calculation by reducing the effective Mg concentration for
the
%calculation of Punblocked for NR2Bs and Tris (triheteromeric)

clear all

tic;
allVmem=zeros(1,(100000*10));
allP=zeros(1,(100000*10));
timeforplot=zeros(1,(100000*10));
allIampa=zeros(1,(100000*10));
allInmda=zeros(1,(100000*10));
allInmda_mg=zeros(1,(100000*10));
allItwoA=zeros(1,(100000*10));
allItri=zeros(1,(100000*10));
allIsyn_twoB=zeros(1,(100000*10));
allIex_twoB=zeros(1,(100000*10));
allItwoA_mg=zeros(1,(100000*10));
allItri_mg=zeros(1,(100000*10));
allIsyn_twoB_mg=zeros(1,(100000*10));
allIex_twoB_mg=zeros(1,(100000*10));

avg_all_twoAca=0;
avg_all_trica=0;
avg_all_ex_twoBca=0;
avg_all_syn_twoBca=0;
avg_all_ca=0;
avg_Inmda=0;
avg_allVmem=0;
for n=1:40

    n
    clear ampasets ampaopens trisets triopens twoAsets twoAopen
twoBsets twoBopens
filename=['example'];

%Calls functions which extract the coordinates and activation times for
%activated receptors for AMPARs and NMDAR subtypes
[ampasets, ampaopens]=ampaopen(filename,n);
[trisets, triopens]=triopen(filename,n);
```

```

[twoAsets,twoAopens]=twoAopen(filename,n);
[twoBsets,twoBopens]=twoBopen(filename,n);

[row,column]=size(ampaopens);
ampaopens=ampaopens((2:row),:);

[row,column]=size(ampasets);
ampasets=ampasets((2:row),:);

[row,column]=size(twoAopens);
twoAopens=twoAopens((2:row),:);
twoAopentime=sum(sum(twoAopens));
twoArand=rand(row-1,column).*twoAopens;
twoAca=zeros(row-1,column);
twoAca_cumulative=zeros(row-1,column);
twoAca_rand=zeros(row-1,column);
twoAca_rand_cumulative=zeros(row-1,column);

[row,column]=size(twoAsets);
twoAsets=twoAsets((2:row),:);
%alters coordinates of receptor to ensure it is inside the spine
surface.
twoAsets=twoAsets-0.1.*(twoAsets./abs(twoAsets));

[row,column]=size(twoBsets);
[row,column]=size(twoBopens);

%Separates NR2B open sets into synaptic NR2Bs and extrasynaptic NR2Bs

syn_twoBsets=[0,0,0];
syn_twoBopens=zeros(1,column);
ex_twoBsets=[];
ex_twoBopens=[];
for x=1:row
    if twoBsets(x,2)==250
        syn_twoBsets=[syn_twoBsets;twoBsets(x,:)];
        syn_twoBopens=[syn_twoBopens;twoBopens(x,:)];
    else
        ex_twoBsets=[ex_twoBsets;twoBsets(x,:)];
        ex_twoBopens=[ex_twoBopens;twoBopens(x,:)];
    end
end
end
[row,column]=size(syn_twoBopens);
syn_twoBopens=syn_twoBopens((2:row),:);
syn_twoBopentime=sum(sum(syn_twoBopens));
syn_twoBrand=rand(row-1,column).*syn_twoBopens;
syn_twoBca=zeros(row-1,column);
syn_twoBca_cumulative=zeros(row-1,column);
syn_twoBca_rand=zeros(row-1,column);

```

```

syn_twoBca_rand_cumulative=zeros(row-1,column);

[row,column]=size(syn_twoBsets);
syn_twoBsets=syn_twoBsets((2:row),:);
syn_twoBsets=syn_twoBsets-0.1.*(syn_twoBsets./abs(syn_twoBsets));
%alters coordinates of receptor to ensure it is inside the spine
surface.

[row,column]=size(ex_twoBopens);
ex_twoBopens=ex_twoBopens((2:row),:);
ex_twoBopentime=sum(sum(ex_twoBopens));
ex_twoBrand=rand(row-1,column).*ex_twoBopens;
ex_twoBca=zeros(row-1,column);
ex_twoBca_cumulative=zeros(row-1,column);
ex_twoBca_rand=zeros(row-1,column);
ex_twoBca_rand_cumulative=zeros(row-1,column);

[row,column]=size(ex_twoBsets);
ex_twoBsets=ex_twoBsets((2:row),:);
ex_twoBsets=ex_twoBsets-0.1.*(ex_twoBsets./abs(ex_twoBsets)); %alters
coordinates of receptor to ensure it is inside the spine surface.

[row,column]=size(triopens);
triopens=triopens((2:row),:);
triopentime=sum(sum(triopens));
trirand=rand(row-1,column).*triopens;
trica=zeros(row-1,column);
trica_cumulative=zeros(row-1,column);
trica_rand=zeros(row-1,column);
trica_rand_cumulative=zeros(row-1,column);

[row,column]=size(trisets);
trisets=trisets((2:row),:);
trisets=trisets-0.1.*(trisets./abs(trisets)); %alters coordinates of
receptor to ensure it is inside the spine surface.

Vmem=-60e-3;
gampa=-12e-12; %single channel conductance (AMPA)
gnmda=-45e-12; %single channel conductance (NMDA)

[numberofopenampars,totaltime]=size(ampaopens);
Cmem=1e-6*(4*pi*(500e-7)^2); %Membrane capacitance

gleak=10e-9; %leak conductance
timestep=0.001e-3;
smoldtime=0.01e-3*(1:1:totaltime);
time=0;
s=1;
iter=1;

```

```

%Start iterative calculations
while time <1000e-3

    time=time+timestep;
    if time > smoldtime(s)
        s=s+1;
    end
    ampas=sum(ampaopens(:,s));

    if size(triopens,1)>0
        for q=1:size(triopens,1)
            if s>1

                if trirand(q,s)>Punblocked_tri
                    triopens(q,s)=0;
                end

                trica(q,s)=triopens(q,s)*((4.5e-12*Vmem)/(2*-1.6e-
19))*0.01e-3;
                if trica(q,s)>0.5
                    possible=1:1:(5*round(trica(q,s)));
                    prob=poisscdf(possible,trica(q,s));
                    random=rand(1);
                    if random > prob(length(prob))
                        trica_rand(q,s)=length(prob)+1;
                    else
                        trica_rand(q,s)=find(random<=prob,1);
                    end
                end
            end

            trica_cumulative(q,s)=trica(q,s)+trica_cumulative(q,s-1);
            trica_rand_cumulative(q,s)=trica_rand(q,s)+trica_rand_cumulative(q,s-
1);
        end
    end
    tris=sum(triopens(:,s));

    if size(syn_twoBopens,1)>0
        for q=1:size(syn_twoBopens,1)
            if s>1

                if syn_twoBrand(q,s)>Punblocked_twoB
                    syn_twoBopens(q,s)=0;
                end
            end
        end
    end
end

```

```

        syn_twoBca(q,s)=syn_twoBopens(q,s)*((4.5e-
12*Vmem)/(2*-1.6e-19))*0.01e-3;
        if syn_twoBca(q,s)>0.5
            possible=1:1:(5*round(syn_twoBca(q,s)));
            prob=poisscdf(possible,syn_twoBca(q,s));
            random=rand(1);
            if random > prob(length(prob))
                syn_twoBca_rand(q,s)=length(prob)+1;
            else
                syn_twoBca_rand(q,s)=find(random<=prob,1);
            end
        end
    end

syn_twoBca_cumulative(q,s)=syn_twoBca(q,s)+syn_twoBca_cumulative(q,s-
1);

syn_twoBca_rand_cumulative(q,s)=syn_twoBca_rand(q,s)+syn_twoBca_rand_cu
mulative(q,s-1);

        end
    end
end
syn_twoBs=sum(syn_twoBopens(:,s));

if size(ex_twoBopens,1)>0
    for q=1:size(ex_twoBopens,1)
        if s>1

            if ex_twoBrand(q,s)>Punblocked_twoB
                ex_twoBopens(q,s)=0;
            end

            ex_twoBca(q,s)=ex_twoBopens(q,s)*((4.5e-
12*Vmem)/(2*-1.6e-19))*0.01e-3;
            if ex_twoBca(q,s)>0.5
                possible=1:1:(5*round(ex_twoBca(q,s)));
                prob=poisscdf(possible,ex_twoBca(q,s));
                random=rand(1);
                if random > prob(length(prob))
                    ex_twoBca_rand(q,s)=length(prob)+1;
                else
                    ex_twoBca_rand(q,s)=find(random<=prob,1);
                end
            end
        end

ex_twoBca_cumulative(q,s)=ex_twoBca(q,s)+ex_twoBca_cumulative(q,s-1);

ex_twoBca_rand_cumulative(q,s)=ex_twoBca_rand(q,s)+ex_twoBca_rand_cumul
ative(q,s-1);

```

```

        end
    end
end
ex_twoBs=sum(ex_twoBopens(:,s));

if size(twoAopens,1)>0
    for q=1:size(twoAopens,1)
        if s>1

            if twoArand(q,s)>Punblocked
                twoAopens(q,s)=0;
            end

            twoAca(q,s)=twoAopens(q,s)*((4.5e-12*Vmem)/(2*-
1.6e-19))*0.01e-3;
            if twoAca(q,s)>0.5
                possible=1:1:(5*round(twoAca(q,s)));
                prob=poisscdf(possible,twoAca(q,s));
                random=rand(1);
                if random > prob(length(prob))
                    twoAca_rand(q,s)=length(prob)+1;
                else
                    twoAca_rand(q,s)=find(random<=prob,1);
                end
            end
        end

twoAca_cumulative(q,s)=twoAca(q,s)+twoAca_cumulative(q,s-1);

twoAca_rand_cumulative(q,s)=twoAca_rand(q,s)+twoAca_rand_cumulative(q,s
-1);

        end

    end
end
twoAs=sum(twoAopens(:,s));

allampas(iter)=ampas;
ItwoA=twoAs*gnmda*Vmem;
Itri=tris*gnmda*Vmem;
Isyn_twoB=syn_twoBs*gnmda*Vmem;
Iex_twoB=ex_twoBs*gnmda*Vmem;

Inmda=ItwoA+Itri+Isyn_twoB+Iex_twoB;
allItwoA(iter)=ItwoA;
allItri(iter)=Itri;
allIsyn_twoB(iter)=Isyn_twoB;

```



```

allIex_twoB(iter)=Iex_twoB;

allInmda(iter)=Inmda;

Iampa=ampas*gampa*Vmem;
allIampa(iter)=Iampa;
Ileak=gleak*(Vmem-(-60e-3));
delVmem=((Inmda+Iampa)-Ileak)*timestep/Cmem);

allVmem(iter)=Vmem;
%timeforplot(1,iter)=time;
Vmem=Vmem+delVmem;

%calculation of Punblocked for each subtype
%vary Mg concentration to add mechano-effect

Punblocked=1/(1+2.718^(-0.062*(Vmem*1000))*(0.8*3.57));
Punblocked_twoB=1/(1+2.718^(-0.062*(Vmem*1000))*(0.8*3.57));
Punblocked_tri=1/(1+2.718^(-0.062*(Vmem*1000))*(0.8*3.57));

allP(iter)=Punblocked;
iter=iter+1;
end
charge_ampa(n)=trapz(allIampa).*timestep;
charge_nmda(n)=trapz(allInmda).*timestep;
charge_nmda_mg(n)=trapz(allInmda_mg).*timestep;
charge_twoA(n)=trapz(allItwoA).*timestep;
charge_twoA_mg(n)=trapz(allItwoA_mg).*timestep;
charge_tri(n)=trapz(allItri).*timestep;
charge_tri_mg(n)=trapz(allItri_mg).*timestep;
charge_syn_twoB(n)=trapz(allIsyn_twoB).*timestep;
charge_syn_twoB_mg(n)=trapz(allIsyn_twoB_mg).*timestep;
charge_ex_twoB(n)=trapz(allIex_twoB).*timestep;
charge_ex_twoB_mg(n)=trapz(allIex_twoB_mg).*timestep;

avg_Inmda=avg_Inmda+allInmda;
all_twoAca=sum(twoAca_rand_cumulative,1);
avg_all_twoAca=avg_all_twoAca+all_twoAca;
all_trica=sum(trica_rand_cumulative,1);
avg_all_trica=avg_all_trica+all_trica;
all_ex_twoBca=sum(ex_twoBca_rand_cumulative,1);
avg_all_ex_twoBca=avg_all_ex_twoBca+all_ex_twoBca;
all_syn_twoBca=sum(syn_twoBca_rand_cumulative,1);
avg_all_syn_twoBca=avg_all_syn_twoBca+all_syn_twoBca;

all_ca=all_twoAca+all_trica+all_syn_twoBca+all_ex_twoBca;
avg_all_ca=avg_all_ca+all_ca;
avg_allVmem=avg_allVmem+allVmem;

```

```

total_twoAca(n)=max(all_twoAca);
total_trica(n)=max(all_trica);
total_ex_twoBca(n)=max(all_ex_twoBca);
total_syn_twoBca(n)=max(all_syn_twoBca);
total_all_ca(n)=max(all_ca);

avg_voltchange(n)=max(allVmem);

%PLOT cumulative calcium entry
figure(1)
plot(smoldtime(1:100000),all_ca(1:100000),'b')
hold on
figure(2)
subplot(2,2,1)
plot(smoldtime(1:100000),all_twoAca(1:100000),'b')
hold on
subplot(2,2,2)
plot(smoldtime(1:100000),all_trica(1:100000),'b')
hold on
subplot(2,2,3)
plot(smoldtime(1:100000),all_syn_twoBca(1:100000),'b')
hold on
subplot(2,2,4)
plot(smoldtime(1:100000),all_ex_twoBca(1:100000),'b')
hold on

%%Opens and writes calcium entry data and smoldyn code specifying
calcium entry sites and times for future intracellular signaling
smoldyn models

A=fopen(['twoA_example_Ca_',num2str(n),'.txt'],'wt');
sB=fopen(['syn_twoB_example_Ca_',num2str(n),'.txt'],'wt');
eB=fopen(['ex_twoB_example_Ca_',num2str(n),'.txt'],'wt');
tr=fopen(['tri_example_Ca_',num2str(n),'.txt'],'wt');
for t=1:100000
fprintf(A,'% .4f\t',twoAca_rand_cumulative(:,t));
fprintf(A,'\n');
fprintf(sB,'% .4f\t',syn_twoBca_rand_cumulative(:,t));
fprintf(sB,'\n');
fprintf(eB,'% .4f\t',ex_twoBca_rand_cumulative(:,t));
fprintf(eB,'\n');
fprintf(tr,'% .4f\t',trica_rand_cumulative(:,t));
fprintf(tr,'\n');
end
fclose(A);
fclose(sB);
fclose(eB);
fclose(tr);

```

```

    [i,j]=find(twoAca>0);
    twoAdata=[];
    for loop=1:length(i)

twoAdata=[twoAdata;smoldtime(j(loop))*1000,floor(twoAca_rand(i(loop),j(
loop))),twoAsets(i(loop),:)]];
    end

    fid=fopen(['twoA_example_Ca_smoldyn_',num2str(n),'.txt'],'wt');
    if isempty(twoAdata)<1
    fprintf(fid,'cmd @ %4.2f pointsource ca %1.0f %8.4f %8.4f
8.4f\n',twoAdata');
    end
    fclose(fid);

    [i,j]=find(trica>0);
    tridata=[];
    for loop=1:length(i)

tridata=[tridata;smoldtime(j(loop))*1000,floor(trica_rand(i(loop),j(lo
op))),trisets(i(loop),:)]];
    end
    fid=fopen(['tri_example_Ca_smoldyn_',num2str(n),'.txt'],'wt');
    if isempty(tridata)<1
    fprintf(fid,'cmd @ %4.2f pointsource ca %1.0f %8.4f %8.4f
8.4f\n',tridata');
    end
    fclose(fid);

    [i,j]=find(syn_twoBca>0);
    syn_twoBdata=[];
    for loop=1:length(i)

syn_twoBdata=[syn_twoBdata;smoldtime(j(loop))*1000,floor(syn_twoBca_ran
d(i(loop),j(loop))),syn_twoBsets(i(loop),:)]];
    end
    fid=fopen(['syn_twoB_example_Ca_smoldyn_',num2str(n),'.txt'],'wt');
    if isempty(syn_twoBdata)<1
    fprintf(fid,'cmd @ %4.2f pointsource ca %1.0f %8.4f %8.4f
8.4f\n',syn_twoBdata');
    end
    fclose(fid);

    [i,j]=find(ex_twoBca>0);
    ex_twoBdata=[];
    for loop=1:length(i)

ex_twoBdata=[ex_twoBdata;smoldtime(j(loop))*1000,floor(ex_twoBca_rand(i
(loop),j(loop))),ex_twoBsets(i(loop),:)]];
    end
    fid=fopen(['ex_twoB_example_Ca_smoldyn_',num2str(n),'.txt'],'wt');

```

```
if isempty(ex_twoBdata)<1
    fprintf(fid,'cmd @ %4.2f pointsource ca %1.0f %8.4f %8.4f
8.4f\n',ex_twoBdata');
end
fclose(fid);

end
avg_all_twoAca=avg_all_twoAca./n;
avg_all_trica=avg_all_trica./n;
avg_all_ex_twoBca=avg_all_ex_twoBca./n;
avg_all_syn_twoBca=avg_all_syn_twoBca./n;
avg_all_ca=avg_all_ca./n;
avg_allVmem=avg_allVmem./n;

avg_Inmda=avg_Inmda./n;

%Plots average cumulative calcium entry for all simulations

figure(1)
plot(smoldtime(1:100000),avg_all_ca(1:100000),'r','LineWidth',2)
hold on
figure(2)
subplot(2,2,1)
plot(smoldtime(1:100000),avg_all_twoAca(1:100000),'r','LineWidth',2)
hold on
subplot(2,2,2)
plot(smoldtime(1:100000),avg_all_trica(1:100000),'r','LineWidth',2)
hold on
subplot(2,2,3)

plot(smoldtime(1:100000),avg_all_syn_twoBca(1:100000),'r','LineWidth',2
)
hold on
subplot(2,2,4)

plot(smoldtime(1:100000),avg_all_ex_twoBca(1:100000),'r','LineWidth',2)
hold on
figure(3)
plot(0.001e-3:0.001e-3:1000e-3,avg_allVmem(1:1000000),'r')
```

Appendix C: Smoldyn code: Modeling of Calmodulin – Calcium binding within the dendritic spine

```
##EXAMPLE SMOLDYN CODE FOR THE INTRACELLULAR ACTIVATION OF  
##CALMODULIN
```

```
graphics none  
graphic_iter 10  
dim 3
```

```
#Define names of molecular species  
names gl ca Cam CamN1 CamC1 CamN2 CamC2 CamN1C1 CamN2C1 CamN1C2  
CamN2C2 CBP CBP1 CB CBM1 CBH1 CBM2 CBH2 CBM1H1 CBM2H1 CBM1H2  
CBM2H2
```

```
max_mol 2000000
```

```
#Define color and size of molecules
```

```
color gl(all) 1 0 0 #red  
color ca(all) 0 1 0 #green  
color Cam(all) 0 0 1 #blue  
color CamN1(all) 1 0 0  
color CamC1(all) 1 0 0  
color CamN2(all) 1 0 0  
color CamC2(all) 1 0 0  
color CamN1C1(all) 1 0 0  
color CamN2C1(all) 1 0 0  
color CamN1C2(all) 1 0 0  
color CamN2C2(all) 1 0 0  
color CBP(all) 1 0 0  
color CBP1(all) 1 0 0  
color CB(all) 1 0 0  
color CBM1(all) 1 0 0  
color CBH1(all) 1 0 0  
color CBM2(all) 1 0 0  
color CBH2(all) 1 0 0  
color CBM1H1(all) 1 0 0  
color CBM2H1(all) 1 0 0  
color CBM1H2(all) 1 0 0  
color CBM2H2(all) 1 0 0
```

```
display_size gl(all) 2  
display_size ca(all) 2
```

```
display_size Cam(all) 2
display_size CamN1(all) 2
display_size CamC1(all) 2
display_size CamN2(all) 2
display_size CamC2(all) 2
display_size CamN1C1(all) 2
display_size CamN2C1(all) 2
display_size CamN1C2(all) 2
display_size CamN2C2(all) 2
display_size CBP(all) 2
display_size CBP1(all) 2
display_size CB(all) 2
display_size CBM1(all) 2
display_size CBH1(all) 2
display_size CBM2(all) 2
display_size CBH2(all) 2
display_size CBM1H1(all) 2
display_size CBM2H1(all) 2
display_size CBM1H2(all) 2
display_size CBM2H2(all) 2
```

```
#Define diffusion constant for molecules
```

```
difc ca(all) 220000
difc Cam(all) 22000
difc CamN1(all) 10000
difc CamC1(all) 10000
difc CamN2(all) 10000
difc CamC2(all) 10000
difc CamN1C1(all) 10000
difc CamN2C1(all) 10000
difc CamN1C2(all) 10000
difc CamN2C2(all) 10000
difc CBP(all) 0
difc CBP1(all) 0
difc CB(all) 28000
difc CBM1(all) 28000
difc CBH1(all) 28000
difc CBM2(all) 28000
difc CBH2(all) 28000
difc CBM1H1(all) 28000
difc CBM2H1(all) 28000
difc CBM1H2(all) 28000
```

```
difc CBM2H2(all) 28000
```

```
low_wall 0 -2000 r
high_wall 0 2000 r
low_wall 1 -2000 r
high_wall 1 2000 r
low_wall 2 -2000 r
high_wall 2 2000 r
```

```
#Define start time, end time, and time step
time_start 0
time_stop 1200
time_step 0.01
```

```
#Defined pointsources of calcium entry at distinct receptor locations as defined by
previous #model outputs of receptor activation and calcium entry
```

```
cmd @ 31.72 pointsource ca 12 -9.8040 249.9000 -26.1099
cmd @ 82.23 pointsource ca 5 -9.8040 249.9000 -26.1099
cmd @ 82.54 pointsource ca 11 -9.8040 249.9000 -26.1099
cmd @ 84.66 pointsource ca 9 -9.8040 249.9000 -26.1099
cmd @ 87.64 pointsource ca 9 -9.8040 249.9000 -26.1099
cmd @ 91.63 pointsource ca 11 -9.8040 249.9000 -26.1099
cmd @ 108.18 pointsource ca 5 -9.8040 249.9000 -26.1099
cmd @ 108.45 pointsource ca 10 -9.8040 249.9000 -26.1099
cmd @ 159.25 pointsource ca 11 -9.8040 249.9000 -26.1099
cmd @ 161.17 pointsource ca 12 -9.8040 249.9000 -26.1099
cmd @ 162.25 pointsource ca 10 -9.8040 249.9000 -26.1099
cmd @ 162.36 pointsource ca 8 -9.8040 249.9000 -26.1099
cmd @ 196.71 pointsource ca 9 -9.8040 249.9000 -26.1099
cmd @ 199.40 pointsource ca 8 -9.8040 249.9000 -26.1099
cmd @ 199.51 pointsource ca 6 -9.8040 249.9000 -26.1099
cmd @ 254.10 pointsource ca 7 -9.8040 249.9000 -26.1099
cmd @ 254.99 pointsource ca 11 -9.8040 249.9000 -26.1099
cmd @ 2.38 pointsource ca 10 -63.7896 249.9000 124.9730
cmd @ 4.76 pointsource ca 9 -63.7896 249.9000 124.9730
cmd @ 6.43 pointsource ca 5 -63.7896 249.9000 124.9730
cmd @ 7.41 pointsource ca 8 -63.7896 249.9000 124.9730
```

cmd @ 8.06 pointsource ca 6 -63.7896 249.9000 124.9730
cmd @ 8.23 pointsource ca 5 -63.7896 249.9000 124.9730
cmd @ 8.48 pointsource ca 6 -63.7896 249.9000 124.9730
cmd @ 10.41 pointsource ca 9 -63.7896 249.9000 124.9730
cmd @ 12.44 pointsource ca 3 -63.7896 249.9000 124.9730
cmd @ 23.51 pointsource ca 7 -63.7896 249.9000 124.9730
cmd @ 24.77 pointsource ca 5 -63.7896 249.9000 124.9730
cmd @ 25.98 pointsource ca 13 -63.7896 249.9000 124.9730
cmd @ 26.91 pointsource ca 3 -63.7896 249.9000 124.9730
cmd @ 27.86 pointsource ca 4 -63.7896 249.9000 124.9730
cmd @ 28.59 pointsource ca 5 -63.7896 249.9000 124.9730
cmd @ 30.42 pointsource ca 6 -63.7896 249.9000 124.9730
cmd @ 30.43 pointsource ca 4 -63.7896 249.9000 124.9730
cmd @ 31.13 pointsource ca 5 -63.7896 249.9000 124.9730
cmd @ 31.73 pointsource ca 9 -63.7896 249.9000 124.9730
cmd @ 32.22 pointsource ca 3 -63.7896 249.9000 124.9730
cmd @ 33.77 pointsource ca 10 -63.7896 249.9000 124.9730
cmd @ 35.75 pointsource ca 9 -63.7896 249.9000 124.9730
cmd @ 36.15 pointsource ca 10 -63.7896 249.9000 124.9730
cmd @ 36.18 pointsource ca 8 -63.7896 249.9000 124.9730
cmd @ 36.85 pointsource ca 13 -63.7896 249.9000 124.9730
cmd @ 37.61 pointsource ca 9 -63.7896 249.9000 124.9730
cmd @ 41.92 pointsource ca 7 -63.7896 249.9000 124.9730
cmd @ 42.89 pointsource ca 6 -63.7896 249.9000 124.9730
cmd @ 43.85 pointsource ca 10 -63.7896 249.9000 124.9730
cmd @ 44.01 pointsource ca 8 -63.7896 249.9000 124.9730
cmd @ 44.23 pointsource ca 5 -63.7896 249.9000 124.9730
cmd @ 47.01 pointsource ca 10 -63.7896 249.9000 124.9730
cmd @ 57.64 pointsource ca 12 -63.7896 249.9000 124.9730
cmd @ 58.19 pointsource ca 8 -63.7896 249.9000 124.9730
cmd @ 58.56 pointsource ca 10 -63.7896 249.9000 124.9730
cmd @ 0.36 pointsource ca 8 -77.7054 249.9000 11.5564
cmd @ 0.73 pointsource ca 12 -77.7054 249.9000 11.5564
cmd @ 0.77 pointsource ca 8 -77.7054 249.9000 11.5564
cmd @ 2.24 pointsource ca 8 -77.7054 249.9000 11.5564
cmd @ 3.97 pointsource ca 6 -21.0092 249.9000 -18.9144
cmd @ 4.12 pointsource ca 11 -77.7054 249.9000 11.5564
cmd @ 4.43 pointsource ca 7 -21.0092 249.9000 -18.9144
cmd @ 4.92 pointsource ca 7 -44.4056 249.9000 -33.4383
cmd @ 7.03 pointsource ca 10 -77.7054 249.9000 11.5564
cmd @ 7.11 pointsource ca 10 -21.0092 249.9000 -18.9144
cmd @ 7.37 pointsource ca 13 -21.0092 249.9000 -18.9144

cmd @ 7.43 pointsource ca 12 -44.4056 249.9000 -33.4383
cmd @ 7.61 pointsource ca 9 -44.4056 249.9000 -33.4383
cmd @ 8.49 pointsource ca 8 -44.4056 249.9000 -33.4383
cmd @ 8.90 pointsource ca 5 -44.4056 249.9000 -33.4383
cmd @ 9.06 pointsource ca 5 -77.7054 249.9000 11.5564
cmd @ 9.47 pointsource ca 9 -77.7054 249.9000 11.5564
cmd @ 9.52 pointsource ca 10 -77.7054 249.9000 11.5564
cmd @ 10.11 pointsource ca 11 -77.7054 249.9000 11.5564
cmd @ 10.58 pointsource ca 12 -44.4056 249.9000 -33.4383
cmd @ 11.23 pointsource ca 14 -77.7054 249.9000 11.5564
cmd @ 12.24 pointsource ca 16 -77.7054 249.9000 11.5564
cmd @ 12.38 pointsource ca 6 -77.7054 249.9000 11.5564
cmd @ 13.18 pointsource ca 4 -77.7054 249.9000 11.5564
cmd @ 13.28 pointsource ca 4 -44.4056 249.9000 -33.4383
cmd @ 13.71 pointsource ca 8 -77.7054 249.9000 11.5564
cmd @ 13.87 pointsource ca 4 -77.7054 249.9000 11.5564
cmd @ 14.65 pointsource ca 7 -77.7054 249.9000 11.5564
cmd @ 15.85 pointsource ca 10 -21.0092 249.9000 -18.9144
cmd @ 16.47 pointsource ca 6 -77.7054 249.9000 11.5564
cmd @ 17.02 pointsource ca 9 -21.0092 249.9000 -18.9144
cmd @ 18.01 pointsource ca 13 -77.7054 249.9000 11.5564
cmd @ 18.48 pointsource ca 6 -21.0092 249.9000 -18.9144
cmd @ 19.58 pointsource ca 10 -21.0092 249.9000 -18.9144
cmd @ 21.38 pointsource ca 10 -21.0092 249.9000 -18.9144
cmd @ 23.52 pointsource ca 8 -21.0092 249.9000 -18.9144
cmd @ 24.01 pointsource ca 5 -21.0092 249.9000 -18.9144
cmd @ 28.18 pointsource ca 10 -21.0092 249.9000 -18.9144
cmd @ 28.44 pointsource ca 7 -21.0092 249.9000 -18.9144
cmd @ 29.05 pointsource ca 9 -21.0092 249.9000 -18.9144
cmd @ 29.13 pointsource ca 8 -21.0092 249.9000 -18.9144
cmd @ 29.33 pointsource ca 5 -21.0092 249.9000 -18.9144
cmd @ 29.34 pointsource ca 9 -21.0092 249.9000 -18.9144
cmd @ 30.93 pointsource ca 10 -21.0092 249.9000 -18.9144
cmd @ 31.47 pointsource ca 12 -21.0092 249.9000 -18.9144
cmd @ 31.58 pointsource ca 7 -21.0092 249.9000 -18.9144
cmd @ 31.76 pointsource ca 6 -21.0092 249.9000 -18.9144
cmd @ 33.58 pointsource ca 9 -21.0092 249.9000 -18.9144
cmd @ 34.74 pointsource ca 5 -21.0092 249.9000 -18.9144
cmd @ 34.84 pointsource ca 11 -21.0092 249.9000 -18.9144
cmd @ 35.03 pointsource ca 6 -21.0092 249.9000 -18.9144
cmd @ 35.25 pointsource ca 5 -21.0092 249.9000 -18.9144
cmd @ 39.37 pointsource ca 9 -21.0092 249.9000 -18.9144

```
cmd @ 40.31 pointsource ca 11 -21.0092 249.9000 -18.9144  
cmd @ 40.34 pointsource ca 10 -21.0092 249.9000 -18.9144
```

#DEFINE SURFACES

```
max_surface 20
```

```
start_surface  
name absorbingbound  
action both all absorb  
polygon front face  
polygon back edge  
max_panels r 10
```

```
panel r -1 -400 1000 -400 800 800  
panel r +1 -400 -1000 -400 800 800  
panel r +0 -400 1000 -400 -2000 800  
panel r -0 400 1000 -400 -2000 800  
panel r -2 -400 -1000 -400 800 2000  
panel r -2 -400 -1000 400 800 2000  
end_surface
```

```
start_surface  
name synapticface  
action both all r  
#color all 1 0 0 0.5  
max_panels r 30  
max_panels tri 50  
polygon both edge  
panel r -1 -150 250 -150 300 300 synapticface  
end_surface
```

```
start_surface  
name perisynaptic  
action both all r  
#color all 1 0 0 0.5  
max_panels r 30  
max_panels tri 50  
polygon both edge
```

```
panel tri -150 250 150 -250 150 150 -250 150 -150 peri1
panel tri -150 250 150 -250 150 -150 -150 250 -150 peri2
panel tri -150 250 150 -150 150 250 -250 150 150 peri3
panel tri -150 250 150 -150 150 250 150 150 250 peri4
panel tri -150 250 150 150 250 150 150 150 250 peri5
panel tri 150 250 150 150 150 250 250 150 150 peri6
panel tri 150 250 150 250 150 150 250 150 -150 peri7
panel tri 150 250 150 150 250 -150 250 150 -150 peri8
panel tri 150 250 -150 250 150 -150 150 150 -250 peri9
panel tri 150 250 -150 150 150 -250 -150 150 -250 peri10
panel tri 150 250 -150 -150 250 -150 -150 150 -250 peri11
panel tri -150 250 -150 -150 150 -250 -250 150 -150 peri12
end_surface
```

```
start_surface
name extrasynaptic
action both all r
#color all 0 1 0 0.5
max_panels r 30
max_panels tri 50
polygon both edge
```

```
panel r +0 -250 150 -150 -300 300 extra1
panel r -0 250 150 -150 -300 300 extra2
panel r -2 -150 -150 -250 300 300 extra3
panel r -2 -150 -150 250 300 300 extra4
panel tri -150 150 250 -250 150 150 -250 -150 150 extra5
panel tri -150 150 250 -150 -150 250 -250 -150 150 extra6
```

```
panel tri 150 150 250 250 150 150 250 -150 150 extra7
panel tri 150 150 250 150 -150 250 250 -150 150 extra8
panel tri 250 150 -150 150 150 -250 150 -150 -250 extra9
panel tri 250 150 -150 250 -150 -150 150 -150 -250 extra10
panel tri -150 150 -250 -250 150 -150 -250 -150 -150 extra11
panel tri -150 150 -250 -150 -150 -250 -250 -150 -150 extra12
end_surface
```

```
start_surface
name spinebottom
#color all 1 0 0 0.5
```

```
max_panels r 30
```

```
max_panels tri 50
polygon both edge

panel tri -250 -150 150 -250 -150 -150 -150 -250 150
panel tri -150 -250 150 -150 -250 -150 -250 -150 -150
panel tri -250 -150 150 -150 -150 250 -150 -250 150
panel tri -150 -250 150 -150 -150 250 150 -150 250
panel tri -150 -250 150 150 -250 150 150 -150 250
panel tri 150 -250 150 150 -150 250 250 -150 150
panel tri 250 -150 150 150 -250 150 150 -250 -150
panel tri 250 -150 150 250 -150 -150 150 -250 -150
panel tri 150 -250 -150 250 -150 -150 150 -150 -250
panel tri 150 -150 -250 -150 -150 -250 -150 -250 -150
panel tri 150 -150 -250 150 -250 -150 -150 -250 -150
panel tri -150 -250 -150 -250 -150 -150 -150 -150 -250
panel r +1 -150 -250 -150 50 300
panel r +1 100 -250 -150 50 300
panel r +1 -100 -250 -150 200 50
panel r +1 -100 -250 100 200 50
panel tri -100 -250 -100 -50 -250 -100 -100 -250 -50
panel tri 50 -250 -100 100 -250 -100 100 -250 -50
panel tri -100 -250 50 -100 -250 100 -50 -250 100
panel tri 50 -250 100 100 -250 100 100 -250 50
panel r +0 -100 -250 -50 -500 100
panel r -0 100 -250 -50 -500 100
panel r -2 -50 -750 -100 100 500
panel r -2 -50 -750 100 100 500
panel tri -50 -250 100 -50 -750 100 -100 -750 50
panel tri -50 -250 100 -100 -250 50 -100 -750 50
panel tri 50 -250 100 50 -750 100 100 -750 50
panel tri 50 -250 100 100 -250 50 100 -750 50
panel tri -50 -250 -100 -50 -750 -100 -100 -750 -50
panel tri -50 -250 -100 -100 -250 -50 -100 -750 -50
panel tri 50 -250 -100 50 -750 -100 100 -750 -50
panel tri 50 -250 -100 100 -250 -50 100 -750 -50
end_surface

start_surface
name transparent_spine_bottom
action both ca t
action both Cam r
action both CamN1 r
```

```
action both CamC1 r
action both CamN2 r
action both CamC2 r
action both CamN1C1 r
action both CamN2C1 r
action both CamN1C2 r
action both CamN2C2 r
action both CBP r
action both CBP1 r
action both CB r
action both CBM1 r
action both CBH1 r
action both CBM2 r
action both CBH2 r
action both CBM1H1 r
action both CBM2H1 r
action both CBM1H2 r
action both CBM2H2 r

color both 0 0 1 0
polygon both edge
max_panels r 5
panel r -1 -175 -249 -175 350 350
end_surface

start_surface
name PSD
action both all t
color both 0 0 1 0.5
polygon both edge
max_panels r 10
panel r -1 -150 220 -150 300 300
panel r +1 -150 249 -150 300 300
panel r +0 -150 220 -150 29 300
panel r -0 150 220 -150 29 300
panel r -2 -150 220 -150 300 29
panel r -2 -150 220 150 300 29
end_surface

max_compartment 5
start_compartment
```

```
name PSD
surface PSD
point 0 220 0
end_compartment
```

```
start_compartment
name spinehead
surface synapticface
surface extrasynaptic
surface perisynaptic
surface spinebottom
surface transparent_spine_bottom
point 0 0 0
end_compartment
```

```
#Define initial number of intracellular molecules within spine head
compartment_mol 1200 Cam spinehead
compartment_mol 300 CBP spinehead
compartment_mol 2700 CB spinehead
```

```
#Define reactions – REACTANTS -> PRODUCTS RATE
reaction CamN1bind Cam + ca -> CamN1 179280
reaction CamN1unbind CamN1 -> Cam + ca 4.15
reaction CamC1bind Cam + ca -> CamC1 11288
reaction CamC1unbind CamC1 -> Cam + ca 0.068
reaction CamN2bind CamN1 + ca -> CamN2 179280
reaction CamN2unbind CamN2 -> CamN1 + ca 0.8
reaction CamC2bind CamC1 + ca -> CamC2 11288
reaction CamC2unbind CamC2 -> CamC1 + ca 0.010
reaction CamN1C1bind1 CamN1 + ca -> CamN1C1 11288
reaction CamN1C1unbind1 CamN1C1 -> CamN1 + ca 0.068
reaction CamN1C1bind2 CamC1 + ca -> CamN1C1 179280
reaction CamN1C1unbind2 CamN1C1 -> CamC1 + ca 4.15
reaction CamN2C1bind1 CamN2 + ca -> CamN2C1 11288
reaction CamN2C1unbind1 CamN2C1 -> CamN2 + ca 0.068
reaction CamN2C1bind2 CamN1C1 + ca -> CamN2C1 179280
reaction CamN2C1unbind2 CamN2C1 -> CamN1C1 + ca 0.8
reaction CamN1C2bind1 CamN1C1 + ca -> CamN1C2 11288
reaction CamN1C2unbind1 CamN1C2 -> CamN1C1 + ca 0.010
reaction CamN1C2bind2 CamC2 + ca -> CamN1C2 179280
reaction CamN1C2unbind2 CamN1C2 -> CamC2 + ca 4.15
reaction CamN2C2bind1 CamN2C1 + ca -> CamN2C2 11288
```

```
reaction CamN2C2unbind1 CamN2C2 -> CamN2C1 + ca 0.010
reaction CamN2C2bind2 CamN1C2 + ca -> CamN2C2 179280
reaction CamN2C2unbind2 CamN2C2 -> CamN1C2 + ca 0.8
reaction CBPbind CBP + ca -> CBP1 99600
reaction CBPunbind CBP1 -> CBP + ca 1.2
reaction CBM1bind CB + ca -> CBM1 72210
reaction CBM1unbind CBM1 -> CB + ca 0.0358
reaction CBH1bind CB + ca -> CBH1 9130
reaction CBH1unbind CBH1 -> CB + ca 0.0026
reaction CBM2bind CBM1 + ca -> CBM2 72210
reaction CBM2unbind CBM2 -> CBM1 + ca 0.0358
reaction CBH2bind CBH1 + ca -> CBH2 9130
reaction CBH2unbind CBH2 -> CBH1 + ca 0.0026
reaction CBM1H1bind1 CBM1 + ca -> CBM1H1 9130
reaction CBM1H1unbind1 CBM1H1 -> CBM1 + ca 0.0026
reaction CBM1H1bind2 CBH1 + ca -> CBM1H1 72210
reaction CBM1H1unbind2 CBM1H1 -> CBH1 + ca 0.0358
reaction CBM2H1bind1 CBM2 + ca -> CBM2H1 9130
reaction CBM2H1unbind1 CBM2H1 -> CBM2 + ca 0.0026
reaction CBM2H1bind2 CBM1H1 + ca -> CBM2H1 72210
reaction CBM2H1unbind2 CBM2H1 -> CBM1H1 + ca 0.0358
reaction CBM1H2bind1 CBM1H1 + ca -> CBM1H2 9130
reaction CBM1H2unbind1 CBM1H2 -> CBM1H1 + ca 0.0026
reaction CBM1H2bind2 CBH2 + ca -> CBM1H2 72210
reaction CBM1H2unbind2 CBM1H2 -> CBH2 + ca 0.0358
reaction CBM2H2bind1 CBM2H1 + ca -> CBM2H2 9130
reaction CBM2H2unbind1 CBM2H2 -> CBM2H1 + ca 0.0026
reaction CBM2H2bind2 CBM1H2 + ca -> CBM2H2 72210
reaction CBM2H2unbind2 CBM2H2 -> CBM1H2 + ca 0.0358
```

```
output_files phys_CaM_example CaM example_ca
```

```
#Define the output files
```

```
output_file_number phys_noloss_Cam_new 35
```

```
output_file_number phys_noloss_Cam_new_ca 35
```

```
#Define the writing of output files
```

```
cmd e molcount Cam_example
```

```
cmd e molcountincmpt spinehead Cam_example_ca
```